The role of T cell receptor affinity in CD4+ T cell differentiation

A DISSERTATION

SUBMITTED TO THE FACULTY OF

THE UNIVERSITY OF MINNESOTA

By

Dmitri Ivanovich Kotov

IN PARTIAL FULFILLMENT OF THE REQUIERMENTS

FOR THE DEGREE OF

DOCTOR OF PHILOSOPHY

Marc K. Jenkins, Ph.D., Advisor

February 2019

Acknowledgements

I would like to thank my mentor Dr. Marc Jenkins for his guidance in the lab, in his office, and at Stub and Herb's. I received a lot of great advice and tasty beer, for which I am eternally gratefully. I thank my thesis committee: Drs. Dan Mueller, Dave Masopust, and Mike Farrar for all of their excellent insight and advice. My Jenkins lab colleagues have been indispensable for technical support and brain storming sessions, thank you all. Lastly, thank you to all my friends and colleagues at the Center for Immunology, who made the center an incredibly collaborative and fun environment to grow as a scientist and human.

Dedication

To my Minnesota-made family, Jessica and Mikhail.

Abstract

Naïve helper T cells become activated when their T cell receptor (TCR) recognizes a microbial peptide presented on MHCII (p:MHCII) by dendritic cells (DCs). During this interaction, DCs provide polarizing cues to guide T cell differentiation towards specific fates, like T follicular helper cells which help B cells. The affinity of TCR for its cognate p:MHCII is known to influence the fate adopted by $CD4^+$ T cells, but the mechanisms responsible for this effect are not completely understood. The mechanism could be T cell extrinsic, by affecting the DC subset a T cell contacts thereby influencing the polarizing factors received, or T cell intrinsic, by modulating TCR signal strength thus regulating genes involved in T cell differentiation.

The T cell extrinsic hypothesis was tested with a quantitative, imaging approach called histo-cytometry to analyze the T cell-DC interactions. This technique involves time-consuming manual image analysis. Therefore, we wrote software to automate histo-cytometry analysis, reducing hands-on analysis time by up to 90%. With histo-cytometry, we determined that TCR affinity did not affect the DC subset contacted by $CD4^+$ T cells, rendering the cell extrinsic hypothesis unlikely.

We therefore focused on the T cell intrinsic hypothesis by performing a CRISPR/Cas9 screen to identify TCR regulated genes that influence T cell differentiation. This screen revealed two novel regulators of helper T cell differentiation, *Eef1e1* and *Gbp2*, which are expressed at a higher level in high affinity than low affinity T cells. These results suggest that TCR affinity influences helper T cell differentiation intrinsically by regulating genes that control the differentiation process.

We next explored the relationship between $CD4^+$ T cell differentiation and cytotoxic activity. This study determined that cytotoxic function of helper T cells was dependent on the Fas pathway and Fas was upregulated on target cells proportional to the TCR affinity of the responding T cells. Additionally, we identified that many different helper T cell subsets express FasL and have cytotoxic potential. Thus, my work could benefit future vaccines by providing greater understanding of how helper T cell fate decisions occur and how these decisions influence cytotoxic function.

Table of Contents

List of Figures

Chapter 5

Chapter 1

Background and Introduction

The 1950s and 60s were a golden age of immunological discovery that defined the lay of the land in cellular immunology, with one of the earliest discoveries being that small lymphocytes initiate immune responses (1). Once the function of lymphocytes was identified, the next logical question was: Where do they come from? Contrary to the thinking at the time, Jacques Miller identified that the thymus had immunological function and suggested that it produces the small lymphocytes (2). While these findings demonstrated lymphocytes play a role in immunity, there was still no separation between T cells and B cells. The possibility of lymphocyte heterogeneity was illuminated upon the discovery that the thymus and bursa of chickens provided different kinds of immunity, with the thymus involved in immune recognition while the bursa is involved in antibody generation (3). This work was furthered by the mouse studies of Miller and colleagues, which solidified that antigen-reactive cells stemming from the thymus helped antibody generating cells that developed from the bone marrow (4-6).

Strikingly, the explanation for thymic T cell development was postulated prior to discovery of the immune function associated with thymus or lymphocytes. In 1957, Sir Frank MacFarlane Burnet published the concept of clonal selection in which he proposed each clone or cell has a genetically encoded unique receptor that defines the cell's antigen specificity. If a cell encounters its antigen then it will proliferate allowing for a rapid, stronger response to secondary exposure with the same antigen. Additionally, clonal

specificity provided an explanation for immunological tolerance, with self-specific clones being eliminated. Thus, the clonal selection hypothesis provided a blueprint for how the adaptive immune system develops and functions.

T cell receptor

In time, immunologists filled in the details of the framework provided by the clonal selection hypothesis. One of these initial discoveries was the identification of antigen presentation, the foundation of which was appreciating that T cells must recognize foreign antigens and self-antigens simultaneously to become activated (7-9). So what are T cells using to detect antigen presentation? Generation of anti-CD3 monoclonal antibody opened the door for identifying the T cell receptor (TCR). Incubating T cell clones with this antibody blocked their recognition of antigen demonstrating that CD3 is involved in the antigen receptor on T cells (10). Next, antibodies were generated that stained specific TCRs and were used to demonstrate that the TCR is closely associated with CD3 (11-13). Further studies demonstrated that the TCR is a heterodimer and compared different TCRs (13-15). Within a year after the TCR was identified, numerous manuscripts were published describing the cloning of various TCRs and demonstrating the homology between TCRs and immunoglobulins (16-24).

TCRs are encoded by variable, diverse, and joining (VDJ) gene segments which are cleaved by Rag1 and Rag2 enzymes (25). The terminal deoxynucleotidyl transferase enzyme adds nucleotides to cleaved gene segments that are then recombined. This somatic recombination occurs for the TCRα and TCRβ loci resulting in proteins that are able to interact. This somatic recombination of gene segments allows for a potential pool

of over 10^{15} TCRs that can be utilized by T cells to provide the diversity necessary to mount a response to any pathogen a host might encounter (26).

$CD4^+$ T cell development

Understanding T cell development required identification of the receptor and ligand mediating selective pressure as well as the location in which this selection occurs. As predicted by Burnet's hypothesis, the TCR is a genetically encoded molecule responsible for antigen specificity. Antigen presentation provides the ligand, which consists of a peptide presented on major histocompatibility complex (MHC). The location is the thymus, as demonstrated by Jacques Miller (2). However, there is added complexity that was not envisioned by Burnet's theory because cells in the thymus not only undergo selection but also lineage commitment. In the thymus, T cells either become helper cells or cytotoxic cells, which can be distinguished based on their expression of CD4 and CD8, respectively (27, 28).

T cell precursors arrive in the thymus from the bone marrow as $CD4^-$ $CD8^-$ cells, termed double negative thymocytes (29). Upon reaching the double negative 3 stage, defined by cells expressing CD25 but not CD44, the progenitor cells rearrange their TCR γ, δ, and β loci. The TCRβ pairs with an invariant pre-TCRα chain and if this pairing is functional, then the precursor cell becomes a double positive thymocyte, a cell that expresses CD4 and CD8, and undergoes rearrangement of its TCRα locus. Approximately 90% of double positive cells undergo death by neglect due their lack of a functional TCR (30). The 10% that survive are maintained because they underwent positive selection by utilizing their TCR to recognize antigen displayed in the cortex of

the thymus, likely by a cortical thymic epithelial cell. Classic models of T cell development state that positively selected thymocytes commit to the helper T cell or cytotoxic T cell lineage, indicated by their expression of CD4 or CD8, respectively, and then travel to thymic medulla where they undergo negative selection.

Negative selection was another aspect of immunology that was correctly predicted by Burnet's clonal selection hypothesis. During negative selection, thymocytes interact with antigen-presenting dendritic cells (DCs), B cells, and medullary epithelial cells (30). The antigen-presenting cells primarily display self-antigens, with some being tissue-restricted antigens whose expression is induced by *Aire* (31). If the thymocytes undergo strong TCR signaling in response to these self-antigens, they will undergo apoptosis or develop into regulatory T cells. While the traditional model states that these interactions occur in the medulla, more recent data suggests that the majority of negative selection occurs in the cortex by double positive thymocytes (32). The end result of thymic selection is as Burnet hypothesized, cells with autoreactivity are culled leaving MHC-restricted T cells that are ready to respond to invading pathogens.

Helper T cell activation and differentiation

DCs are a bridge between the innate and adaptive immune systems, because they are innate cells that drive the activation of adaptive cells. In the 1970s, Steinman and colleagues first identified DCs and demonstrated their activation of T cells (33, 34). This ability to induce T cell responses is due to the DCs' capacity to process and present antigens on MHC and their expression of co-stimulatory molecules. DCs express two classes of MHC molecules, MHC class I presents peptides that are recognized by TCRs

on $CD8^+$ T cells and MHC class II presents peptides that are recognized by TCRs on $CD4^+$ T cells. The ability to process and present antigen is critical for DCs to interact with and activate T cells, however it is the DCs' expression of co-stimulatory molecules that dictates whether the interactions lead to activation or tolerance. If T cells do not receive this second signal of co-stimulation they will adopt an anergic phenotype (35, 36).

This balancing act between activation and tolerance requires tight regulation of co-stimulatory molecule expression. To provide a context for when DCs should be activated, DCs can undergo maturation by detecting cytokines, like TNF-α, co-stimulatory molecules, like CD40L, and direct sensing of pathogens via toll-like receptors (37). This maturation enhances DC antigen uptake, presentation, and co-stimulatory molecule expression, thereby greatly enhancing their capability to activate T cells. Another aspect of DCs that controls their ability to activate T cells is the unique properties of each DC subset.

Human, mouse, and macaque classical DCs are classified as cDC1 and cDC2, with each subset having unique properties that are conserved across the different genus (38). cDC1 are *Batf3*-dependent, express the transcription factor IRF8, and express XCR1 and CD8α on their surface. cDC2 express IRF4 and can be identified by their surface expression of SIRPα and CD4. A critical functional difference between these subsets is their ability to process and present antigen to T cells. While both are able to activate $CD4^+$ and $CD8^+$ T cells, cDC1 cross-present antigens and have higher expression of molecules involved in MHC class I presentation rendering them better at priming $CD8^+$ T cell responses (39). Conversely, cDC2 are specialized for activating $CD4^+$ T cells by their

higher expression of genes involved in antigen processing for presentation on MHC class II. In line with these results, $CD4^+$ T cells were activated by cDC2 and $CD8^+$ T cells were activated by cDC1 in response to skin infection with herpes simplex virus (40).

Another way that DC subsets are specialized is the cytokines and co-stimulatory molecules that they express. During helper T cell activation, DCs produce polarizing factors, like cytokines and co-stimulatory molecules that drive their differentiation into specialized lineages. For example, IL-12 induces Type 1 helper (Th1) T cells, which secrete cytokines like IFNγ in response to their cognate antigen thereby helping macrophages clear intracellular infections (41). Interestingly, IL-12 is produced by cDC1 but not cDC2 (42, 43). Therefore, both DC subsets can activate helper T cells but the fate adopted by the T cell may differ depending on which type of DC it contacts.

There are other options for helper T cells beyond Th1 differentiation, with each lineage expressing a defining transcription factor. T-bet is the master transcription for Th1s, Gata3 for Type 2 helpers (Th2), Rorγt for T helper 17s (Th17), Bcl6 for T follicular helpers (Tfh), and Foxp3 for T regulatory (Treg) cells (44-50). Each of these lineages also has a specialized function. Tfh cells help B cells generate high affinity, class switched antibodies, Th17 cells aid in clearing extracellular infections via neutrophils, Th2 cells protect against helminth infections, and Tregs inhibit autoimmunity (51-55). During T cell differentiation, all of these lineages are an option but the environment in which antigen presentation occurs influences which fate is adopted. For example, oral inoculation with *Listeria monocytogenes* (*Lm*) induces Th17 cells while intravenous infection with the same pathogen does not (56). This result may stem from a difference in

the type of cytokines produced by the dendritic cells, with the oral infection potentially inducing IL-6 production, a cytokine that promotes Th17 differentiation (57).

The cytokine milieu influences T cell differentiation by regulating localization and expression of transcription factors. For example, IL-2 signaling induces Blimp1, a transcription factor that regulates the bifurcation of Th1 and Tfh differentiation by inhibiting the Tfh fate through repression of Bcl6 (48). Interestingly, Bcl6 is itself a repressor that can directly inhibit T-bet expression (54, 58-60). Thus, it is a balance between two repressors that regulates the bifurcation, but what are the signals that dictate the balance between these repressors? A major contributor is IL-2, which signals through the IL-2 receptor inducing signal transducer and activator of transcription 5 (STAT5) phosphorylation (61, 62). Phosphorylated STAT5 forms a homodimer that traffics to the nucleus and drives Blimp1 expression, thereby inhibiting Tfh differentiation (63). The source of the IL-2 appears to be cells slated to adopt the Tfh fate, indicating that IL-2 acts in a paracrine manner to regulate T cell differentiation (64). Thus, helper T cell differentiation is influenced by route of infection, interactions with specific DC subsets, and cytokine milieu present during T cell activation.

Influence of TCR signaling on helper T cell differentiation

In a classic in vitro experiment, T cells activated with a low amount of antigen and presumably TCR signaling became Th2 cells while higher amounts of antigen drove the Th1 fate (65). This study was one of the first to demonstrate that TCR signaling can influence T cell differentiation. This initial study varied antigen concentration, but TCR signaling could also be altered by modulating the TCR affinity for antigen (66). In a

normal repertoire, each T cell with a given specificity has a unique TCR and a distinct affinity for its cognate peptide presented on MHC class II (p:MHCII) (67). By examining single cells from a conventional T cell repertoire, it is therefore possible to determine whether TCR biases differentiation during a physiological response to infection. In fact, this is exactly the case with some TCRs heavily favoring the Th1 fate while others strongly induce Tfh differentiation after *Lm* infection (68). Therefore, the antigen-specific helper T cell response is an amalgamation of each of these clones.

If TCR signal strength influences T cell differentiation, then which fates are promoted by greater signaling? When comparing Th1 and Th2 differentiation, the in vitro results of O'Garra and colleagues were recapitulated in vivo, with Th1 favored at higher antigen concentrations and Th2 adopted at lower concentrations independent of the type of adjuvant injected alongside the peptide (69). Using p:MHCII tetramers as a read-out of TCR affinity, which correlates with TCR signaling, a study determined that high TCR affinity T cells primarily adopted the Tfh fate (70). However, TCR is internalized upon signaling, which was not controlled for in this study. Accordingly, the highest affinity cells might be incorrectly identified as low affinity cells skewing the results.

An alternative strategy for examining the role of TCR signaling in T cell differentiation that avoids the complication presented by TCR internalization is TCR transgenic T cells, which are genetically engineered to express a specific TCR. The optimal experimental setup is two populations of TCR transgenic T cells with TCRs specific for the same p:MHCII but at different affinities. Such a setup was used to demonstrate that high affinity TCR-bearing cells adopt the Th1 fate more than medium affinity cells, with the inverse being true for Tfh lineage commitment in response to *Lm*

infection (68). These results were corroborated at high and low antigen doses as well as in response to a viral infection (71, 72).

A possible explanation for why greater TCR signaling may drive Th1 differentiation is expression of CD25, the high affinity IL-2 receptor. Naïve T cells do not express CD25 but signaling through the TCR rapidly induces CD25 expression (73). This signaling event also drives expression of IL-2, thereby providing the ligand and receptor. Signaling through the IL-2 receptor induces Blimp1, repressing Tfh differentiation and allowing adoption of non-Tfh fates (63). Thus, TCR affinity biases helper T cell differentiation potentially by regulating IL-2 signaling.

Cytotoxic T cells

Upon activation, T cells can acquire cytotoxic capabilities that act through a variety of pathways, like Fas as well as perforin and granzymes. TCR signaling induces expression of Fas ligand which can interact with Fas on target cells inducing apoptosis via caspase 8 (74). Similar to the Fas pathway, TCR signaling is required to express perforin and granzyme B in T cells. Perforin and granzyme B are stored in granules that are released upon TCR signaling in the direction of the T cell contact (75). Perforin forms pores in the target cell allowing granzyme B to enter the cell and cleave proteins including caspases, thereby inducing apoptosis. Additional cell-mediated cytotoxic pathways exist, like TNF and TRAIL, with these pathways triggering apoptosis in a similar manner to Fas signaling (75).

Cytotoxic function has traditionally been associated with $CD8^+$ T cells. However, cytotoxic $CD4^+$ T cells were initially identified over 40 years ago, but this discovery was

discounted as an in vitro culture artifact (76). More recent studies have identified cytotoxic $CD4^+$ T cells in mice and humans, with these cells arising in response to viral and bacterial infections and cancer (77-82). Cytotoxic $CD4^+$ T cell responses even correlate with early control of HIV and protection against influenza infection (77, 81, 83). The signals driving cytotoxic $CD4^+$ T cell differentiation are not entirely understood, but IL-15, TGF-β, 4-1BB and OX40 have been suggested to play a role (82, 84). Additionally, Eomes has been proposed as a master transcription for cytotoxic $CD4^+$ T cells, which is supported by over-expression of Eomes inducing cytotoxic function in $CD4^+$ T cells (78, 82, 85, 86). It is still unclear whether cytotoxic $CD4^+$ T cells are a unique lineage or a basic property of helper T cells.

Statement of thesis

My thesis is that TCR affinity controls T cell differentiation in a T cell intrinsic manner by regulating expression of genes that bias differentiation, like *Il2ra*, *Eef1e1*, and *Gbp2,* and dictates cytotoxic effector function via control of the Fas pathway.

Chapter 2

Materials and Methods

Mice

Six- to eight-wk old C57BL/6 (B6), B6.SJL-*Ptprc*^{a} *Pepc*^{b}/BoyJ (CD45.1), B6.129S-*Tnfrsf1a*^{tm1Imx} *Tnfrsf1b*^{tm1Imx}/J (TNFR I & II KO), B6.129P2-*Cd40*^{tm1Kik}/J (CD40 KO), C57BL/6-*Prf1*^{tm1Sdz}/J (Perforin KO), B6.MRL-*Fas*^{lpr}/J (Fas KO), B6.129S6-*Tbx21*^{tm1Glm}/J (T-bet KO), and *Cd25*$^{-/-}$ female mice were purchased from the Jackson Laboratory or the National Cancer Institute Mouse Repository (Frederick, MD, USA). B6 IFN-ɣR1-deficient mice were a gift from M. Farrar (University of Minnesota). B6 *Cd4-Cre* *Eomes*$^{fl/fl}$ and B6 *Eomes*^{GFP} mice were a gift from S. L. Reiner (Columbia University). B6 DR5 (TRAIL-R KO) deficient mice were a gift from T. S. Griffith (University of Minnesota). *Itgax*^{YFP} (87) and *Rag1*$^{-/-}$ *Ubc*^{GFP} (88) TEa TCR transgenic (89) female mice were a gift from B.T. Fife (University of Minnesota). *Rag1*$^{-/-}$ B3K506 TCR transgenic (90), *Rag1*$^{-/-}$ B3K508 TCR transgenic mice (90), *Rag1*$^{-/-}$ *Ubc*^{GFP} TEa TCR, and *Rag1*$^{-/-}$ SM1 *Tbx21*^{ZsGreen} TCR transgenic mice were bred and housed in specific pathogen–free conditions in accordance with guidelines of the University Institutional Animal Care and Use Committee and National Institutes of Health. *Clec4a4*^{DTR} mice (42) were backcrossed onto the B6 background and used as bone marrow donors. The University Institutional Animal Care and Use Committee approved all animal experiments.

Infections and immunizations

For bacterial intranasal and intravenous infections, mice were injected with 10^7 colony-forming units of ActA-deficient *Listeria monocytogenes* (*Lm*)-3K, *Lm*-P5R, *Lm*-P2A, or *Lm*-Flic bacteria as described previously (56, 68, 91). *Lm*-3K, *Lm*-P5R, and *Lm*-P2A strains were generated by inserting sequences encoding each peptide in frame with the Listeriolysin-O signal sequence and promoter that drives maximal production under *in vivo* infection conditions, as described previously (91). The P5R epitope was inserted into the PR8 influenza A virus genome as previously described (92, 93). Mice were infected intranasally with 40 plaque-forming units of PR8 influenza A virus expressing P5R. Some mice were injected intraperitoneally with $2x10^5$ plaque-forming units of the LCMV Armstrong strain. For immunizations, mice were injected intraperitoneally with 10 μg of peptide mixed with 20 μg Poly I:C or 100 μL CFA. In some experiments mice received 10 μg of peptide mixed with 20 μg Poly I:C subcutaneously, intravenously, or intramuscularly. In some experiments, peptide/Poly I:C-immunized animals were challenged with an i.v. injection of 100 μg of 2W peptide and sacrificed 2 h later for analysis of IFN-γ production.

Tetramers

Biotin-labeled soluble I-A^b molecules containing 2W, 3K, or LCMV glycoprotein (GP)66–77 peptides covalently attached to the I-A^b beta chain were produced with the I-A^b alpha chain in Drosophila melanogaster S2 cells, then purified and made into tetramers with streptavidin (SA)-phycoerythrin (PE) or (SA)-allophycocyanin (Prozyme, San Leandro, CA, USA) as described previously (94, 95).

Cell transfer

Lymph nodes were collected from *Rag1*$^{-/-}$ B3K506 TCR transgenic, *Rag1*$^{-/-}$ B3K508 TCR transgenic, and *Rag1*$^{-/-}$ *Ubc*^{GFP} TEa TCR transgenic mice and hand-mashed into a single cell suspension. Aliquots were stained with allophycocyanin- or eFluor 450-labeled CD4 (RM4–5; Tonbo biosciences) antibody and analyzed with Fluorescent AccuCheck counting beads (Invitrogen) to assess CD4^{+} T cell numbers and purity using a LSR II (BD biosciences) flow cytometer. For imaging experiments, 10^6 TCR transgenic cells were transferred into B6 mice 24 h before infection. 10^5 TCR transgenic cells were transferred into B6 mice for flow cytometry experiments examining the initial three d following *Lm* infection, while $3x10^3$ TCR transgenic cells were transferred for experiments examining the response at seven d post-infection with *Lm* or influenza. In some cases, the T cells from the *Rag1*$^{-/-}$ B3K506 and *Rag1*$^{-/-}$ B3K508 TCR transgenic mice were also labelled with CellTracker Orange (ThermoFisher Scientific) or CellTraceViolet (ThermoFisher Scientific), respectively (96). For some experiments, twenty-thousand *Rag1*$^{-/-}$ B3K508 TCR transgenic cells were injected intravenously into C57BL/6 (B6) 24 h before infection with *Lm*-3K.

Cell enrichment and flow cytometry

Single cell suspensions were generated by dissociating spleens with the GentleMACS dissociator (Miltenyi Biotec) or hand-mashed in a petri dish. Single cell suspensions were stained for one h at room temperature with allophycocyanin-conjugated tetramers or 0.1 µg of FITC-labeled CD90.1 antibody (HIS51; ThermoFisher Scientific) and 2 µg of

BV650-labeled (L138D7; Biolegend) or BUV395-labeled (2G8; BD biosciences) CXCR5 antibody. Biotinylated anti-FasL or FasL-PE antibody (MFL3; eBioscience) was also added to the staining cocktail for some of the experiments. Samples were then enriched for p:MHCII tetramer-bound or CD90.1 antibody-bound cells using magnetic bead-based enrichment as described previously (97) with the minor modification that EasySep Mouse APC or FITC Positive Selection Kits (Stemcell Technologies) and EasySep magnets (Stemcell Technologies) were used.

For identification of surface markers, the sample was stained on ice with various combinations of the following antibodies: PE-Cy7 or APC-ef780-labeled B220 (RA3–6B2; ThermoFisher Scientific), APC-ef780-labeled CD11b (M1-70; ThermoFisher Scientific), APC-ef780-labeled CD11c (N418; ThermoFisher Scientific), PE-Cy7-labeled PD-1 (J43; eBioscience), PE-labeled CD3ε (145-2C11; eBioscience), BV786- or eFluor 450-labeled CD4 (GK1.5; BD biosciences), AF700-labeled CD44 (IM7; ThermoFisher Scientific), BV510- or FITC-labeled CD45.1 (A20; Biolegend), BUV395-labeled CD45.2 (104; BD biosciences), PE- or V500- or BV510-labeled CD8α (53-6.7; eBioscience or Becton-Dickinson), FITC-labeled Fas (Jo2; Becton-Dickinson), AF700-labeled MHC Class II (I-A/I-E; M5/114.15.2; eBioscience), BUV395-labeled CD25 (PC61; BD biosciences), PE-labeled CD69 (H1.2F3; ThermoFisher Scientific) and FITC-labeled CD90.1 (HIS51; ThermoFisher Scientific). All samples were also stained with a fixable viability dye (Ghost Dye Red 780; Tonbo Biosciences). For transcription factor staining, samples were fixed with the eBioscience Foxp3/transcription factor staining kit (ThermoFisher Scientific) and then stained with BV421-labeled RORɣt (Q31-378; BD

biosciences), PE-labeled Eomes (Dan11mag; eBioscience), Percp-Cy5.5-labeled Foxp3 (FJK-16s; eBioscience), BV605-labeled or BV421-labeled T-bet (4B10; Biolegend), and AF488-labeled Bcl-6 (K112-91; BD biosciences) antibodies. For cytokine staining, samples were fixed with the BD Biosciences Fixation/Permeabilization Solution Kit (BD biosciences) and then stained with BV650-labeled IFN-ɣ (XMG1.2; Biolegend). In experiments using biotinylated anti-FasL antibodies, PE-conjugated streptavidin (eBioscience) was included in the staining cocktail. When analyzing T cell differentiation, intracellular transcription factors, or IFN-γ production after peptide challenge, staining was performed as described previously (95). To calculate cell numbers, Fluorescent AccuCheck counting beads (Invitrogen) were added to each sample after the final wash step. Cells were then analyzed on an LSR II or Fortessa (BD biosciences) flow cytometer. Data were analyzed with FlowJo (TreeStar).

Cell sorting and co-culture

Spleens were harvested from mice 48 h after intravenous infection with *Lm*-P5R bacteria. The spleens were chopped into small pieces and digested with collagenase P (Millipore Sigma) for 20 min at 37°C prior to hand-mashing in a petri dish to generate a single cell suspension. The single cell suspension was enriched for CD11c expressing cells using a CD11c positive selection kit (Miltenyi Biotec). The enriched samples were stained for 30 min at room temperature with BV421-labeled XCR1 (ZET; Biolegend), PE-labeled CD64 (X54-5/7.1; Biolegend), APC-labeled SIRPα (P84; Biolegend), APC-Cy7-labeled Ly-6G (1A8; Biolegend), APC-Cy7-labeled Siglec F (E50-2440; BD biosciences), APC-eF780-labeled NKp46 (29A1.4; ThermoFisher Scientific), APC-eF780-labeled CD90.2

(53-2.1; ThermoFisher Scientific), PE-Cy7-labeled Ly-6C (HK1.4; ThermoFisher Scientific), FITC-labeled CD11c (N418; ThermoFisher Scientific) antibodies, and a fixable viability dye (Ghost Dye Red 780; Tonbo Biosciences). The cells were sorted with a FACS Aria II (BD biosciences) to isolate live XCR1$^+$ (CD64$^-$ NKp46$^-$ Ly-6C$^-$ CD90.2$^-$ Ly-6G$^-$ SIRPα$^-$ CD11c$^+$ XCR1$^+$) and SIRPα$^+$ (CD64$^-$ NKp46$^-$ Ly-6C$^-$ CD90.2$^-$ Ly-6G$^-$ XCR1$^-$ CD11c$^+$ SIRPα$^+$) DCs.

For co-culture, naïve B3K508 CD4$^+$ T cells were isolated from *Rag1*$^{-/-}$ B3K508 TCR transgenic mice as described in the cell transfer section. B3K508 cells were co-cultured with the sort-purified XCR1$^+$ or SIRPα$^+$ DCs at 1 to 1, 1 to 3, and 1 to 10 ratios of DCs to T cells in complete IMDM for 24 h at 37°C. Some T cells were also cultured without DCs to serve as negative staining controls for markers of activation. After culture, T cells were stained with antibody and analyzed on a flow cytometry as described in the cell enrichment and flow cytometry section.

In vivo cytotoxicity assay

The target cells for the *in vivo* cytotoxicity assays were prepared by labeling bulk splenocytes from CD45.1 mice with CellTrace Violet (CTV; Life Technologies). Briefly, spleen cells were suspended in PBS at 3x10^7 cells/ml and incubated at 37°C for 10 minutes in 2 μM (hi) or 0.4 μM (lo) CTV. The CTV was quenched by adding RPMI with 10% FBS. The CTV^{lo} cells received 100 μg of 2W or GP66 peptide in the RPMI with 10% FBS for a final peptide concentration of 10 μg/ml. The CTV^{hi} and CTV^{lo} cells were then incubated for 1 h at 37°C before being washed twice with PBS. The CTV^{hi} and

CTV^{lo} cells were mixed at a 1:1 ratio and transferred into mice, with each mouse receiving $2x10^7$ total cells. The mice were sacrificed 20 h after the cell transfer and the spleens were processed for cell enrichment as previously described (94). The unbound fraction from the cell enrichment was collected and 5% of this fraction was assayed by flow cytometry to determine the CTV^{lo}/CTV^{hi} ratio of the B cells in the target cell population in addition to their expression of Fas and MHC II. Specific Lysis = 100 - (CTV ratio in experimental mice/CTV ratio in naive mice) X 100.

In vitro cytotoxicity assay

B cells were isolated from CD45.1 mice using a B cell negative selection kit (Stemcell Technologies) and cultured overnight at $1x10^7$ cells/ml at 37°C in complete IMDM media and 10 μg/ml of Pam3CSK4 (Invivogen). The cells then were labelled with 0.2 μM CTV or 0.2 μM CFSE (Life Technologies) for 10 minutes at 37°C in PBS. The labelling reactions were quenched by 1 h incubation at 37°C in complete IMDM media. FliC peptide was added to the CFSE-labeled samples during the quenching period. 10 μg/ml. CFSE- and CTV-labelled cells were washed twice with complete IMDM media, mixed at a 1:1 ratio, and added to 96 well cell culture plates. To obtain cytotoxic T cells for the culture, $1x10^5$ SM1 $Tbx21^{ZsGreen}$ TCR transgenic $CD4^+$ T cells were transferred into B6 mice, which were immunized with FliC/CFA. Secondary lymphoid organs were harvested 7 d post-immunization and SM1 cells were isolated by allophycocyanin-labelled CD90.1 antibody-based magnetic enrichment (Stemcell Technologies). The SM1 cells were then stained with CCR6-PE (FAB590P; R and D biosystems), CXCR5-BUV395, and CD4-eFluor 450 antibodies at room temperature for 1 h before sorting on a

FACS Aria (Becton Dickinson) cell sorter. Sorted SM1 T cells expressing CCR6, *Tbx21*^{ZsGreen}, CXCR5, or lacking all three markers were added to B cell-containing wells for a final ratio of 10 T cells to 1 CFSE labelled B cell. Some wells received B cells alone to determine the baseline CFSE/CTV ratio. The cells were cultured for 20 h and assayed by flow cytometry to determine the CFSE/CTV ratio of the B cells. Specific lysis = 100 – (CFSE/CTV ratio for T cell containing well / CFSE/CTV ratio for B cell alone well) X 100.

Cell depletion with mAbs

Monoclonal antibodies were used to deplete CD4 or CD8α expressing cells in mice immunized with 2W peptide and PolyI:C. Each mouse was intravenously injected with 500 µg of CD4, CD8α, or isotype control antibody (GK1.5, 53-6.72, or 2A3 respectively; BioXcell) at the time of injection of target cells.

Confocal microscopy

Twenty µm splenic sections from naive or *Lm*-P5R infected mice were stained with Brilliant Violet (BV) 421-conjugated F4/80 (BM8, BioLegend), Pacific Blue-conjugated B220 (RA3-6B2, BioLegend), CF405L-conjugated CD8α (53-6.7, BioLegend), AF488-conjugated pS6 (2F9,Cell Signaling Technologies), CF555-conjugated CD86 (GL-1, BioLegend), AF647-conjugated CD45.2 (104, BioLegend), AF700-conjugated MHC II (M5/114.15.2, BioLegend), CF514-conjugated CD11c (N418, BioLegend), BV480-conjugated CD3 (17A2, BD biosciences), and AF594-conjugated SIRPα (P84, BioLegend) antibodies. Certain purified antibodies from BioLegend were conjugated

with CF405L, CF514, or CF555 with Biotium Mix-n-Stain labelling kits. Confocal microscopy was performed with a Leica SP5 confocal microscope with two HyD detectors; two PMT detectors; 405, 458, 488, 514, 543, 594 and 633 laser lines; and a 63X oil objective with a 1.4 numerical aperture. The mark and find feature in the Leica Application Suite was used to image 12 T cell zones in each spleen with each image consisting of a 20 μm z-stack acquired at a 0.5 μm step size. Additionally, the Leica SP5 microscope was used to image single color stained Ultracomp eBeads (ThermoFisher Scientific) for generating a compensation matrix.

Epi-fluorescence microscopy

Spleens from B6 mice infected 48 h earlier with *Lm*-P5R were fixed with paraformaldehyde, dehydrated with sucrose, and embedded in OCT. Seven μm sections of these spleens were stained with BV421-conjugated F4/80, AF488-conjugated B220 (RA3-6B2, BioLegend), AF647-conjugated CD45.2 (104, BioLegend), and AF594-conjugated CD3 (17A2, BioLegend) antibodies. The samples were imaged with a Leica DM6000B epi-fluorescence microscope equipped with a dry 20X objective with 0.5 numerical aperture and a Leica DFC 9000 camera with custom filter cubes. The tiling feature in the Leica Application Suite (Leica Microsystems) software was used to image the entire splenic section. The images were analyzed in Imaris 8.4 (Bitplane), which was used to create surfaces to identify TCR Tg cells. For quantifying T cell localization by signal absorption, statistics for the TCR Tg cell surfaces were exported with the XTStatisticsExport Xtension and imported into Flowjo v10.3 (Treestar) for analysis. To quantify T cell localization by distance measurement, surfaces were also created for B

cell follicles based on B220 staining. The Distance Transformation Xtension was then used to calculate the distance of T cells from the follicle edge toward the follicle center. Statistics for TCR Tg cells were exported with the XTStatisticsExport Xtension and imported into Flowjo v10.3 (Treestar) for quantification. With the distance method, T cells were considered to reside in a B cell follicle if they were greater than 0 μm into a B cell follicle. For a detailed protocol, refer to the Histo-cytometry Protocol and Documentation file available at https://histo-cytometry.github.io/Chrysalis/.

Two-Photon microscopy

Rag1$^{-/-}$ *Ubc*^{GFP} TEa TCR transgenic CD4^{+} T cells, CMTMR-labelled B3K506 TCR transgenic T cells, and CTV labelled B3K508 TCR transgenic T cells were transferred into *Itgax*^{YFP} mice that were then infected with *Lm*-P5R bacteria 24 h after cell transfer. Recipient spleens were immobilized on plastic coverslips, sliced longitudinally with a vibratome, and perfused with 37° C DMEM media bubbled with 95% O_2 and 5% CO_2. Samples were imaged with a 4-channel Leica TCS MP microscope with a resonant-scanner containing two NDD- and two HyD- photomultiplier tubes operating at video rate. The objective was a water dipping 25X with 0.95 numerical aperture. Samples were excited with a MaiTai TiSaphire DeepSee HP laser (15 W; Spectra-Physics) at 870 nm, and emissions at 440-480 (CTV), 500–520 (GFP), 520-560 (YFP) and 560-630 (CMTMR) nm were collected. Images acquired were 20–250 μm below the cut surface of the spleen slice and 512x512 XY frames were collected at 3.0 μm steps every 30 s for 30 min.

Image processing and histo-cytometry analysis

For automated histo-cytometry analysis, a compensation matrix was created in ImageJ (NIH) by using the GenerateCompensationMatrix script on images of single color stained Ultracomp eBeads. This compensation matrix was applied to 3D images and movies in Chrysalis to compensate for the spillover of each fluorescent signal from its channel into other channels. Chrysalis was also used for further automated image processing as described in Fig. 1A and Fig. 5A. Imaris 8.3, 8.4, 9.0, and 9.1 (Bitplane) were used for image analysis, including surface creation to identify cells in images. The Sortomato V2.0, XTChrysalis, and XTChrysalis2phtn Xtensions were used in Imaris for identifying cellular subsets based on protein expression, quantifying cell-cell interactions, and exporting cell surface statistics. Statistics were exported from these applications and imported into FlowJo v10.3 (Treestar) for quantitative image analysis. Details of these steps are described in the Histo-cytometry Protocol and Documentation file that is available at https://histo-cytometry.github.io/Chrysalis/.

For the traditional histo-cytometry analysis, a compensation matrix was generated and applied to the 3D images with the Leica Application Suite (Leica Microsystems) software. Imaris 8.4 (Bitplane) was used to merge images from a single spleen together by stacking them in the z-plane. The DC channel was generated in in Imaris 8.4 (Bitplane) using the Channel Arithmetics Xtension prior to running surface creation to identify DCs and TCR Tg cells in images. DCs were categorized as XCR1 or SIRPα DCs using the Sortomato Xtension and the distance to each DC subset was calculated with the

Distance Transformation Xtension. Statistics were exported for each surface and imported into FlowJo v10.3 (Treestar) for quantitative image analysis.

Quantitative PCR

10^6 B3K506 or B3K508 TCR transgenic cells were transferred into B6 mice 24 h before intravenous infection with *Lm*-P5R bacteria. The spleen and lymph nodes were harvested 48 h after infection and stained with FITC-labeled CD90.1 (HIS51; ThermoFisher Scientific), APC-ef780-labeled B220 (RA3–6B2; ThermoFisher Scientific), APC-ef780-labeled CD11b (M1-70; ThermoFisher Scientific), APC-ef780-labeled CD11c (N418; ThermoFisher Scientific), BV786-labeled CD4 (GK1.5; BD biosciences), AF700-labeled CD44 (IM7; ThermoFisher Scientific), and a fixable viability dye (Ghost Dye Red 780; Tonbo Biosciences). The TCR transgenic cells were then enriched with the EasySep Mouse FITC Positive Selection Kit (Stemcell Technologies) and EasySep magnets (Stemcell Technologies). Live TCR transgenic $CD4^+$ T cells were sorted from the enriched sample into Trizol (ThermoFisher Scientific) using a FACS Aria II (BD biosciences). RNA was extracted using chloroform (ThermoFisher Scientific) and purified with the RNeasy micro kit (Qiagen). RNA quantities were measured with a Qubit 2.0 (ThermoFisher Scientific) and 41 ng RNA of each sample was converted to cDNA with SuperScript IV reverse transcriptase (ThermoFisher Scientific). Primers were designed with the NCBI Primer-Blast tool (98) and quantitative PCR was performed with FastStart SYBR Green (Millipore Sigma) in a thermocycler (Eppendorf). The resulting data was analyzed by normalizing to the housekeeping gene *Gapdh* and then calculating

fold change in gene expression for B3K506 cells relative to B3K508 cells with the comparative C_T method (99).

CRISPR/Cas9 screen

A CRISPR/Cas9 system utilizing two MSCV-based gamma retroviral vectors was used to target genes of interest. One virus encoded Cas9 and the fluorescent protein mNeongreen (100) and the other encoded gRNAs and the fluorescent protein mAmetrine (101). These vectors were created by modifying the LMP-Amt vector (102), which was a gift from S. Crotty (La Jolla Institute). The vector encoding Cas9 and mNeongreen was generated by replacing the shRNA-encoding segment, PGK promoter, and mAmetrine gene with Cas9-P2A and mNeongreen (Allele Biotechnology) through In-Fusion cloning (Takara Bio USA). The Cas9-P2A fragment was cloned from the lentiCRISPRv2 puro plasmid which was a gift from B. Stringer (Addgene plasmid # 98290).

To generate the gRNA vector, the LMP-Amt vector (102) was modified by removing the SapI site and replacing the shRNA-encoding segment with the bacterial toxin gene CCDB flanked by AarI sites using In-Fusion cloning (Takara Bio USA). This CCDB containing fragment was cloned from the pMOD_B2303 plasmid, which was a gift from D. Voytas (University of Minnesota). This modified LMP-Amt plasmid served as the recipient for Golden Gate cloning reactions that replaced the CCDB gene with a tRNA-gRNA array (103-105) using AarI (ThermoFisher Scientific), SapI (New England BioLabs), and T4 (New England BioLabs) enzymes. The gRNAs used in the tRNA-gRNA arrays were designed in Benchling (Benchling) to target functional motifs

identified in InterPro (106) with two gRNA designed for each target gene. Primers encoding the gRNAs were then generated using the Voytas laboratory toolkit (107) and the cloning of the tRNA-gRNA array was performed as described previously (107).

Retrovirus was prepared as described previously (108), with minor alterations. In brief, Platinum-E cells (Cell Biolabs) were grown in complete DMEM media (Gibco) prior to transfection with Polyethylenimine, Linear, MW 25,000 (Polysciences), pCL-Eco and retroviral plasmids encoding Cas9 or tRNA-gRNA arrays. After transfection, the media was supplemented with ViralBoost (Alstem Cell Advancements) and 30 μM water soluble cholesterol (Millipore Sigma). The virus containing supernatant was collected 24 and 48 h after transfection and filtered with a 0.45 μm Nylon 25 mm Syringe Filter (Fisher). Aliquots were stored at -80°C for up to three mo.

Retroviral transduction was performed as described previously (108), with minor alterations. Specifically, naïve B3K508 $CD4^+$ T cells or naïve $Cas9^+$ B3K508 $CD4^+$ T cells were isolated from *Rag1*$^{-/-}$ B3K508 TCR transgenic or *Rag1*$^{-/-}$ $Cas9^+$ B3K508 TCR transgenic mice, respectively, as described in the cell transfer section. These B3K508 T cells were grown in a 96 well plate with complete IMDM media (Millipore Sigma) containing IL-7 (Tonbo biosciences). Cells were activated in plates coated with anti-CD3 (2C11; BioXcell) and anti-CD28 (37.51; BioXcell). The cells were transduced with retroviral supernatant and polybrene (Millipore Sigma) 24 and 40 h after activation. B3K508 T cells were transduced with retrovirus encoding Cas9 and retrovirus encoding tRNA-gRNA arrays, while the $Cas9^+$ B3K508 T cells were only transduced with tRNA-

gRNA array encoding retrovirus. For transductions, plates were spun at 1500 rpm for two h at 37°C and then the media was exchanged for complete IMDM media containing IL-2 (Peprotech). After three d of culture, the cells were moved to plates that were not coated with anti-CD3 or anti-CD28 and two d later the media was switched to complete IMDM media containing IL-7 (Tonbo biosciences). After 24 h, cells were either directly transferred into B6 mice or stained with BV786-labeled CD4 (RM4-5; BD biosciences) antibody and a fixable viability dye (Ghost Dye Red 780; Tonbo Biosciences). The stained cells were sorted with a FACS Aria II (BD biosciences) to isolate live $Cas9^+$ $gRNA^+$ $CD4^+$ T cells, which were then transferred into B6 mice. Each B6 mouse received 2500 T cells. Four d after transfer, mice were infected with *Lm*-3K bacteria and the spleens were harvested seven d post-infection for flow cytometric analysis.

Statistical analysis

Statistical significance was determined using Prism (Graphpad) software for unpaired two-tailed Student's t test, one-way and two-way ANOVA tests. Prism (Graphpad) was also used to calculate linear correlations and R squared.

Code availability

All of the code generated for image processing or analysis can be downloaded at https://histo-cytometry.github.io/Chrysalis/, including compiled versions of Chrysalis for Windows and Mac OSX with a Linux version available upon request due to Github limitations on file size. Additionally, all of the Imaris Xtensions are compatible with

Windows and Mac OSX. The documentation for the code as well as a detailed protocol for image acquisition and analysis is also provided at this github link.

Chapter 3

Chrysalis: A new method for high-throughput histo-cytometry analysis of images and movies

3.1 Introduction

Imaging of biological samples has traditionally been used to resolve anatomic structures (109) or identify specific cells in tissues (110). Recent advances in image analysis, like histo-cytometry (111) and dynamic in situ cytometry (112) have expanded the depth of analysis by increasing characterization of cell types and objective quantification of cells in images. These new techniques combine multispectral image analysis with a quantitative workflow. The image quantification is performed by analyzing image-derived statistics in flow cytometry analysis software (111, 112). These approaches can quantify the number and location of cells throughout a tissue (113), identify cell-cell interactions (114), and correlate protein expression to cellular localization (51). Histo-cytometry and dynamic in situ cytometry have been applied to a variety of imaging systems including confocal (115-117), epi-fluorescence (118, 119), and two-photon microscopy (112). However, these approaches are time consuming due to the need for extensive hands-on image processing. We addressed this issue by creating the software Chrysalis and a suite of Imaris Xtensions to batch image processing and analysis (https://histo-cytometry.github.io/Chrysalis/). This automation reduced hands-on analysis time for confocal, epi-fluorescence, and two-photon microscopy images. The

broad applicability of this protocol was confirmed by quantifying cell localization and cell-cell interactions in the spleen using multiple imaging platforms. Automation should facilitate the use of the powerful histo-cytometry technique.

3.2 Results

Automated Processing of 3D images

Image acquisition, processing, and analysis with histo-cytometry consists of eight steps (Fig. 1A). We developed a stand-alone software called Chrysalis for automating the three image processing steps (steps 2-4) as well as a suite of Imaris Xtensions that automate two of the image analysis steps (steps 6 and 7; Fig. 1A). For processing 3D images, Chrysalis spectrally unmixes images, merges images, and generates new channels prior to image analysis in Imaris (Fig. 1A). Each of these features addresses existing issues with standard image analysis workflows and expedites image analysis. For example, spectral unmixing accounts for spectral overlap between different fluorophores and fluorescent proteins (120). To aid in this step, we wrote a script that automatically generates a compensation matrix from user-provided single-color control images. Chrysalis uses this compensation matrix to spectrally unmix an image with a linear unmixing algorithm (Fig. 1B) (121).

Another issue addressed by Chrysalis is the image processing required for efficiently analyzing cell-cell interactions in 3D images. When analyzing cell-cell interactions, high magnification images need to be taken to observe the interaction event. Analysis of interactions in large tissues like spleen or lymph node can be performed by

tiling images of the entire tissue together. However, this process is extremely time intensive for image acquisition and analysis due to the high magnification and large number of images required. This approach is also inefficient in cases where the interaction event occurs only in a small percentage of the tissue. Rare interactions within 3D images can instead be identified at the microscope allowing for the acquisition of only the images that depict the relevant interactions at high magnification prior to manually merging the images together for analysis. Such a process was previously applied to analyze T regulatory cell-dendritic cell (DC) clusters (51). To make it easier to study rare interaction events, Chrysalis can automatically merge multiple images from one tissue through stacking images in the z plane (Fig. 1C), which allows for time-efficient and consistent analysis of the relevant cell-cell interaction event.

Some cell types require identification based on expression of multiple proteins. For example, DCs are identified by their expression of CD11c and MHC class II (MHCII), but not B220, F4/80, or CD3 (38, 87, 122). To address this issue, Chrysalis creates new channels consisting of voxels that are above a computer-generated threshold (123) for user-selected "include" channels and below a computer-generated threshold for user-selected "exclude" channels, a process called voxel gating (111). A user-selected base channel expressed by the cell type dictates the signal intensity in this new channel. For a new DC channel, CD11c and MHCII would be the include channels, while B220, F4/80, and CD3 would be the exclude channel and the base channel would be CD11c (Fig. 1D). In effect, this new channel provides better DC resolution than the CD11c channel alone.

Automated histo-cytometry analysis of 3D images

For histo-cytometry analysis, Chrysalis processed images are imported into the image analysis software Imaris, which creates surfaces to identify cells based on the image's channels (111, 115, 117, 124). These surfaces are created based on user-specified fluorescence intensity thresholds for the cell population of interest and the expected diameter of the cell. For example, non-proliferating adoptively transferred TCR Tg T cells can be identified based on the fluorescence intensity of a congenic marker antibody and a six μm diameter cell size. Once the surface creation parameters are set for one image, they can be automatically applied to other images that were acquired with the same microscope settings. However, it is important to visually inspect the quality of surface generation for each image by checking for potential issues, such as whether a group of cells is classified as a single cell. This step is necessary because differences in cell state, e.g. resting versus proliferating cells, can impact the accuracy of surface creation.

Traditionally, the steps required to analyze surfaces requires extensive hands-on time. Thus, we created the Xtension XTChrysalis, which automates this process. XTChrysalis 1) separates existing surfaces into new surfaces based on a gating scheme defined in a Xtension called Sortomato, 2) calculates distances to each new surface, 3) rescales signal intensities for any images, and 4) exports statistics for any surface (Fig. 1A). The exported statistics contains each channel's intensity mean and minimum values as well as each cell's volume, sphericity, and position. All values have 0.1 added to them to enable logarithmic display of each parameter. This data can be directly imported into quantitative analysis software, like Flowjo or XiT (125), for further analysis.

Analyzing T cell activation and T cell-DC interactions in 3D images

To demonstrate 3D image analysis with Chrysalis and XTChrysalis, we analyzed images of T cells, DCs, and their interactions captured by confocal microscopy. Following infection, DCs interact with T cells by presenting MHCII-bound peptides derived from the invading pathogen, leading to TCR signaling (126, 127). To analyze this type of interaction, splenic tissue from *Lm* infected mice was analyzed by 10 color confocal microscopy. T cell responses were examined using a system involving adoptive transfer of B3K506 TCR transgenic (Tg) $CD4^+$ T cells that express P5R peptide:MHCII-specific TCRs. B3K506 TCR Tg T cells were injected into B6 recipient that were then infected with *Lm*-P5R bacteria. Twenty-four h after infection, 12 T cell zones were imaged per spleen to obtain sufficient cells for analysis (128). We used Chrysalis to spectrally unmix, rescale, and merge images, and generate a new channel representing DC voxels before image analysis in Imaris (Fig. 2A). TCR Tg cell surfaces were then created based on CD45.2 fluorescence (Fig. 2B). Staining for the phosphorylated form of S6 kinase (pS6), an indicator of TCR signaling (129), was examined within those surfaces to identify cells undergoing TCR signaling (Fig. 2B). DC surfaces were generated based on the DC voxel channel, thereby identifying hundreds of DCs (Fig. 2C). The Sortomato Xtension was used to identify a gating strategy to subset the DCs based on expression of CD8α or SIRPα (Fig. 2D) (38, 130-132). XTChrysalis was then applied to the processed images and the resulting data was analyzed in Flowjo.

This automated workflow was compared to the traditional histo-cytometry protocol to determine the reduction in hands-on anaylsis time as a result of automation.

For this experiment, 12 splenic T cell zone images were acquired by confocal microscopy, as described in Fig. 2A. These images were analyzed to quantify T cell-DC interactions. The automated approach was performed as in Fig. 2A-D, while the traditional approach utilized the Leica Application Suite for image processing (steps 2-4) and Imaris for image analysis (steps 5-7; Fig. 1A). For the image processing, the traditional approach required 47 min of hands-on time while Chrysalis only required 4 min, yielding a 91% reduction in hands-on time (Fig. 2E). Automation of the image analysis performed in Imaris provided a 74% reduction in hands-on time, requiring 80 min with the traditional technique and 21 min with the automated protocol (Fig. 2E). These results demonstrate that the Chrysalis automated workflow confers a significant reduction in hands-on time required for histo-cytometry analysis of confocal images.

Identifying T cell-DC interactions by signal absorption

As expected, B3K506 TCR Tg cells in confocal images contained CD45.2 signal, while DCs had CD11c and MHCII signals (Fig. 3A). Surprisingly, however, there were two populations of TCR Tg cells, one lacking CD11c and MHCII signals and one with these signals (Fig. 3B). The populations were similar in cell size but the $MHCII^{high}$ $CD11c^{high}$ population had greater TCR signaling based on pS6 expression (Fig. 3B). Since MHCII and CD11c are not expressed by T cells (133), we hypothesized that the TCR Tg cell surfaces "absorbed" MHCII and CD11c signals by being in close proximity to DCs. This hypothesis was tested by comparing the frequency of T cell-DC interactions for the $MHCII^{high}$ $CD11c^{high}$ and the $MHCII^{low}$ $CD11c^{low}$ T cells. The $MHCII^{high}$ $CD11c^{high}$ T cells interacted with $XCR1^{+}$ and $SIRP\alpha^{+}$ DCs 10 times as often as the

MHCII^{low} CD11c^{low} T cells, suggesting that the DC signal absorption hypothesis was correct (Fig. 3C).

Quantifying cellular localization in epi-fluorescence microscopy images

The experimental approach described above was also used to assess the locations of B3K506 TCR Tg cells by epi-fluorescence microscopy. Spleens from B6 recipients of B3K506 T cells infected three d earlier with *Lm*-P5R bacteria were stained for F4/80, B220, and CD4 to identify the red pulp, B cell zones, and T cell zones, respectively (Fig. 3D) (134, 135). Spleens were also stained for CD45.2 to identify the TCR Tg cells. Macrophages in the red pulp express F4/80 (135) and B cells in the B cell zone express B220 (136), but neither protein is expressed by T cells (137-139). Therefore, TCR Tg surfaces that have B220 signal should be in close proximity to B cells and reside in B cell follicles while those with F4/80 signal should be near macrophages and localize to the red pulp. Indeed, although most of the B3K506 T cells were in the T cell zones, some were in the B cell follicles and absorbed B220 signal, while others were in the red pulp and absorbed F4/80 signal (Fig. 3D). Thus, the location of a cell can be determined based on 'absorption' of fluorescent signal from proteins expressed by nearby cells.

The 'signal absorption' strategy was further validated by comparing this strategy to a different counting method. Epi-fluorescence microscopy images were acquired and analyzed as described in Fig. 3D and the localization of the TCR Tg cells to B cell follicles was analyzed. For the 'signal absorption' strategy, follicular TCR Tg cells were defined based on their absorption of B220 fluorescent signal (Fig. 3E). In the other method, Imaris was used to determine the distance of each T cell from a follicle edge to

the center of that follicle. A distance greater than 0 μm indicated that a T cell resided in the follicle (Fig. 3E). There was no significant difference in the percentages of T cells found in B cell follicles based on the signal absorption or distance quantification methods (Fig. 3F). These results demonstrate that signal absorption can determine cellular localization as accurately as a more traditional counting technique.

The effect of TCR affinity on T cell localization

The capacity of the signal absorption strategy to identify cell location was also employed to validate the concept that TCR signal strength influences Th cell differentiation (71). It has been shown that naïve T cells with high TCR affinity for peptide:MHCII tend to differentiate into Type 1 helper (Th1) cells while cells with lower affinity TCRs primarily adopt the T follicular helper (Tfh) fate (68, 72). These differences in T cell differentiation would be expected to modulate T cell localization because different Th subsets express different chemokine receptors. For example, Th1 cells express CXCR3 (140, 141) driving them towards sites of inflammation such as the splenic red pulp, while Tfh cells express CXCR5 allowing them to traffic into B cell follicles (142, 143). Thus, Tfh-biased low TCR affinity T cells would localize to B cell follicles at a higher frequency than Th1-biased high TCR affinity T cells.

B3K506 T cells were compared to B3K508 TCR Tg T cells, which express TCRs with lower affinity for P5R:I-A^b complexes, to test this hypothesis (90, 144). The TCR Tg populations were transferred into B6 mice, which were infected with *Lm*-P5R bacteria. Spleen sections were stained, imaged by epi-fluorescence microscopy, and analyzed with Chrysalis one, two, and three d after infection. As in the previous

experiment (Fig. 3D), B220 identified B cell follicles, CD4 defined T cell zones, F4/80 delineated red pulp, and CD45.2 specified TCR Tg T cells (Fig. 4A). T cell localization in the follicles or red pulp was identified based on T cell absorption of B220 or F4/80 signal, respectively (Fig. 4B). As expected, TCR Tg cells were primarily situated in T cell zones in naive mice and during the initial three d following *Lm*-P5R infection (Fig. 4C-E). However, the signal absorption assay revealed a greater proportion of low TCR affinity B3K508 T cells localized to B cell follicles than high TCR affinity B3K506 T cells, in line with B3K508 T cells favoring the B cell follicle-homing Tfh cell fate (Fig. 4D) (68). This result demonstrates the ability of the improved histo-cytometry workflow to quantify cellular localization in epi-fluorescence microscopy images with a novel signal absorption strategy.

Automated processing and histo-cytometry analysis of two-photon microscopy images

Previously, histo-cytometry has been applied to 3D images, however this same methodology can be applied to two-photon time-lapse data (movies) (51, 115). Chrysalis can aid in this application because it can spectrally unmix, generate new channels, and rescale movies (Fig. 5A). Additionally, Chrysalis expedites two-photon movie analysis by simplifying existing workflows. For example, two-photon movies can have variable image quality due to poor tissue health stemming from a lack of oxygenation or low tissue temperature (145, 146). Tissue health can be assessed by examining the motility of a control population within the tissue, like fluorescently labeled polyclonal T cells (147). By reviewing the motility of a control cell population across several movies, movies that

depict healthy tissue can be identified prior to conducting in-depth analysis. To optimize this process, Chrysalis processes movies by Gaussian filtering and rescales each channel to maximize signal intensity and movie clarity. The processed movies are saved as AVI files, which can be quickly examined for tissue health prior to performing more time-consuming analysis.

We have also written an Imaris Xtension called XTChrysalis2phtn that batches histo-cytometry analysis of two-photon movies. For each movie, XTChrysalis2phtn will 1) calculate distances between cell surfaces and define cell-cell interactions at each time point, 2) rescale signal intensities, and 3) export statistics for each surface (e.g. average velocity, displacement, volume, and cell-cell interactions) (Fig. 5A). The data generated can be directly imported into Flowjo for further analysis. Thus, Chrysalis and XTChrysalis2phtn automate histo-cytometry analysis of cell-cell interactions and protein expression in two-photon movies thereby reducing the required hands-on analysis time. To demonstrate this improved workflow, T cell-DC interactions were quantified in two-photon microscopy movies depicting spleens from B6 recipients of B3K506, B3K508, and TEa TCR Tg cells infected 16 h earlier with *Lm*-P5R bacteria. The two-photon movies had 4 colors, which identified DCs and the three different TCR Tg populations (Fig. 5B) (96). Chrysalis spectrally unmixed and rescaled the movies, as well as generated AVI files to determine tissue health. For further analysis, the processed movies were opened in Imaris and surfaces were generated for the DCs and TCR Tg populations (Fig. 5B). XTChrysalis2phtn then generated cell statistics for analysis in Flowjo, which provided a way to compare B3K506 and B3K508 T cells recognizing P5R:I-A^b on DCs. TEa TCR Tg cells served as control cells because they do not respond to the infection

(68, 90). The B3K506 and B3K508 cells had lower mean velocity than the TEa cells, suggesting that B3K506 and B3K508 cells interacted with DCs after infection while TEa cells did not (Fig. 5C). In line with this hypothesis, B3K506 cells had a lower confinement correlate value and greater contact time with DCs than TEa cells (Fig. 5D). Histo-cytometry analysis of these T cell-DC interactions allowed for a more granular view of these interactions by quantifying the duration of the longest contact event as well as the number of prolonged contact events for each T cell (Fig. 5D). As expected, T cells with the longest contact events with DCs made fewer total contacts with DCs (Fig. 5D). This example demonstrates a powerful and streamlined workflow for analyzing two-photon movies.

3.3 Discussion

The Chrysalis software and Imaris Xtensions described in this thesis can be applied to a broad range of biological questions, while reducing analysis time and empowering quantitative image analysis. We demonstrated the power of this workflow by quantifying T cell localization within splenic tissue in epi-fluorescence images, T cell-DC interactions in confocal microscopy images, and T cell motility and T cell-DC interactions in two-photon microscopy images. These same approaches can answer other immunological questions that require the quantification of cell localization, cell-cell interactions, or the ability to subset cells in images.

To extend the capabilities of this workflow beyond the applications described here, we also generated separate Imaris Xtensions for each of the major steps performed

by XTChrysalis, like batched statistics export. With these additional Xtensions, users can daisy chain Xtensions to batch image analysis in a manner that specifically addresses their research question. To further facilitate the use of this quantitative imaging approach in immunological research, we provide a step-by-step protocol that incorporates the automation steps detailed in this manuscript to streamline acquisition and analysis of confocal, epi-fluorescence, and two-photon microscopy images.

While our protocol utilizes the commercial image analysis software Imaris, it can also be paired with free, publically available software such as CellProfiler and ilastik (148-151). While these programs do not have all of the features of Imaris, these programs are able to perform cell segmentation to identify cells within images, an essential step in the histo-cytometry workflow that is performed by Imaris in our protocol. Additionally, although our protocol utilizes the commercial software Flowjo for comparing and quantifying image-derived statistics for each identified cell population, publicly available software such as XiT and FACSanadu (125, 152) can be used within our workflow in place of Flowjo for quantifying images.

To further reduce analysis time, we developed a signal absorption technique that expedites the quantification of cellular localization. The premise of this method is that a cell near other cells will absorb the nearby cell's fluorescence. For example, a T cell residing in a B cell follicle will absorb B220 signal from nearby B cells. Signal absorption can then be used as a readout of cell location. This strategy is favorable over directly quantifying cell distance to a tissue structure because signal absorption only requires creating surfaces for cells and measuring their fluorescent signal. Conversely, the distance quantification approach involves creating surfaces for cells and tissue

structures before quantifying the cells distance to the tissue structure. While the distance quantification approach provides a more definitive determination of localization, the extra steps of this approach require greater hands-on analysis time and computational power. This problem is exacerbated when the distance quantification approach is applied to the analysis of large tissues, like the spleen, or to many biological samples. Therefore, the signal absorption strategy is a simpler and more time-efficient approach for quantifying cellular localization in certain cases.

While we demonstrated that the signal absorption technique works with a variety of image resolutions, it might not be compatible with very high-resolution microscopy techniques, like super-resolution microscopy, because signal overlap will not occur. An additional limitation of the signal absorption technique is the fluorescence intensity of the signal being absorbed. For example, B220 is highly expressed by B cells and they are abundant in B cell follicles. Therefore, it was possible to use signal absorption of B220 to accurately quantify T cell localization to B cell follicles. If B cells had low florescence intensity for their identifying marker or were extremely rare in the follicles, then the signal absorption method could not be used to quantify follicular T cells.

In summary, Chrysalis and the suite of Imaris Xtensions provide a high-throughput image processing workflow for confocal, epi-fluorescence, and two-photon microscopy images. This approach identifies subtle differences in cell phenotype and cell-cell interactions, while also offering up to a 90% reduction in hands-on analysis time. This time-savings reduces the barrier of entry for conducting quantitative, multispectral image analysis. Accessibility to this image analysis pipeline is further enhanced by the accompanying step-by-step protocol describing how to prepare samples, acquire images,

and analyze images using the novel Chrysalis software and Imaris Xtensions for confocal, epi-fluorescence, and two-photon microscopy images. An increase in the widespread adoption of these powerful, quantitative image analysis approaches will allow for novel and counterintuitive discoveries about the function and maintenance of the immune system.

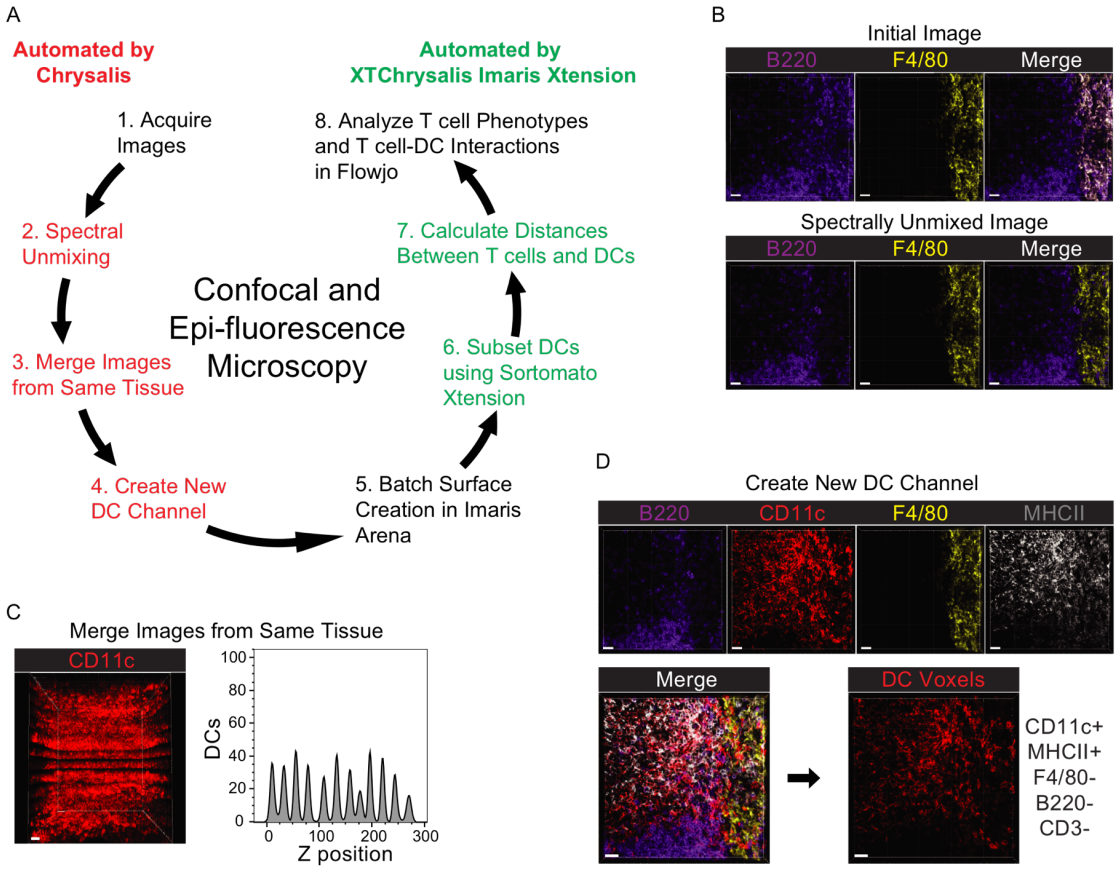

Figure 1. Image Processing with Chrysalis.

(A) Diagram of the histo-cytometry workflow on 3D images when automated by Chrysalis and XTChrysalis. (B) B220 and F4/80 staining of splenic tissue before and after spectral unmixing in Chrysalis. (C) CD11c staining and histogram of DCs in 12 confocal microscopy images merged together in the z plane. (D) Generation of a DC voxel channel with Chrysalis' new channel feature by utilizing the fluorescence of existing channels including B220, CD11c, F4/80 and MHCII, which are depicted for a splenic tissue section. Scale bar, 20 µm. Data representing two to three independent experiments are shown.

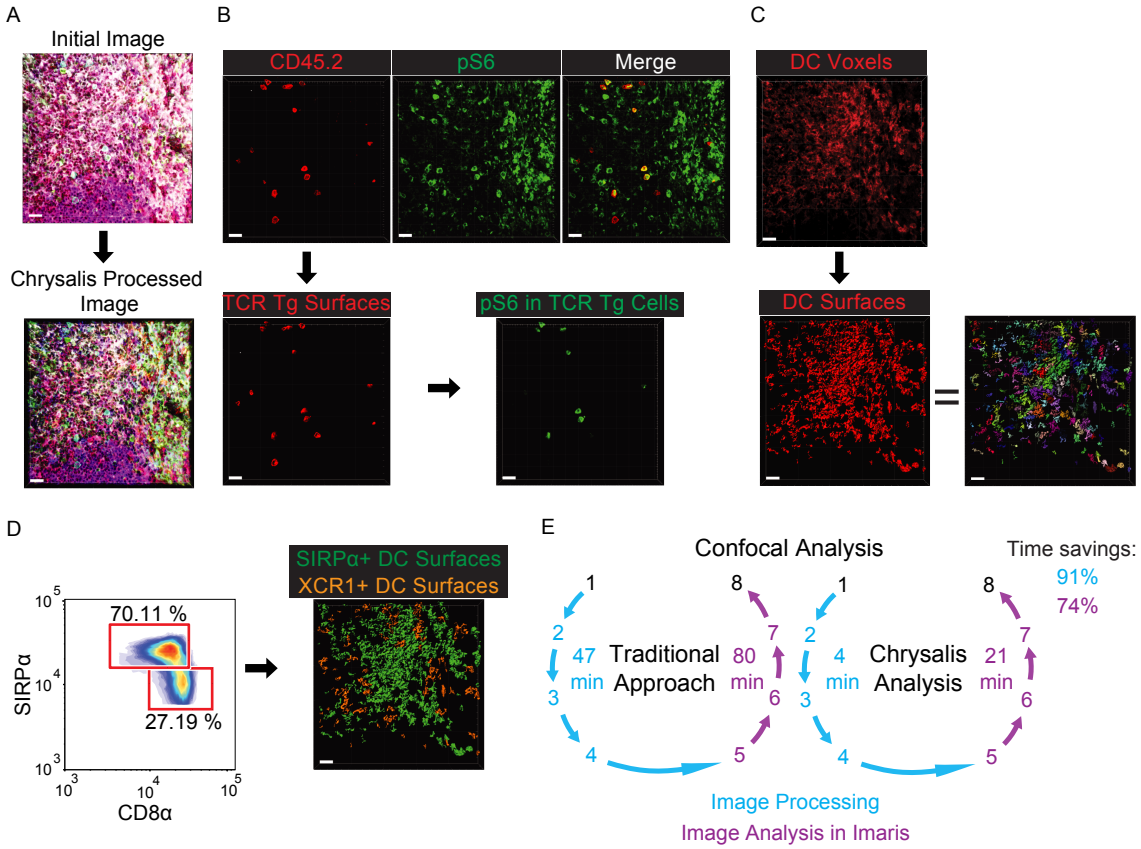

Figure 2. Chrysalis and XTChrysalis analysis of a 3D image.

(A) Confocal microscopy 10 color image before and after Chrysalis processing. (B) Identifying TCR Tg cells with CD45.2 staining and TCR signaling based on pS6 expression. (C) DC voxels ($CD11c^+$ $MHCII^+$ $B220^-$ $CD3^-$ $F4/80^-$) that were used to identify DCs by surface creation in Imaris. (D) 2D plot generated with Sortomato for subsetting DC surfaces into $SIRP\alpha^+$ or $XCR1^+$ DCs based on SIRPα and CD8α expression. (E) Comparison of the hands-on time required for histo-cytometry analysis of a set of confocal microscopy images of a spleen using the traditional or Chrysalis automated workflow depicted in reference to the diagram in Fig. 1A. Scale bar, 20 µm. Data representing two to three independent experiments are shown.

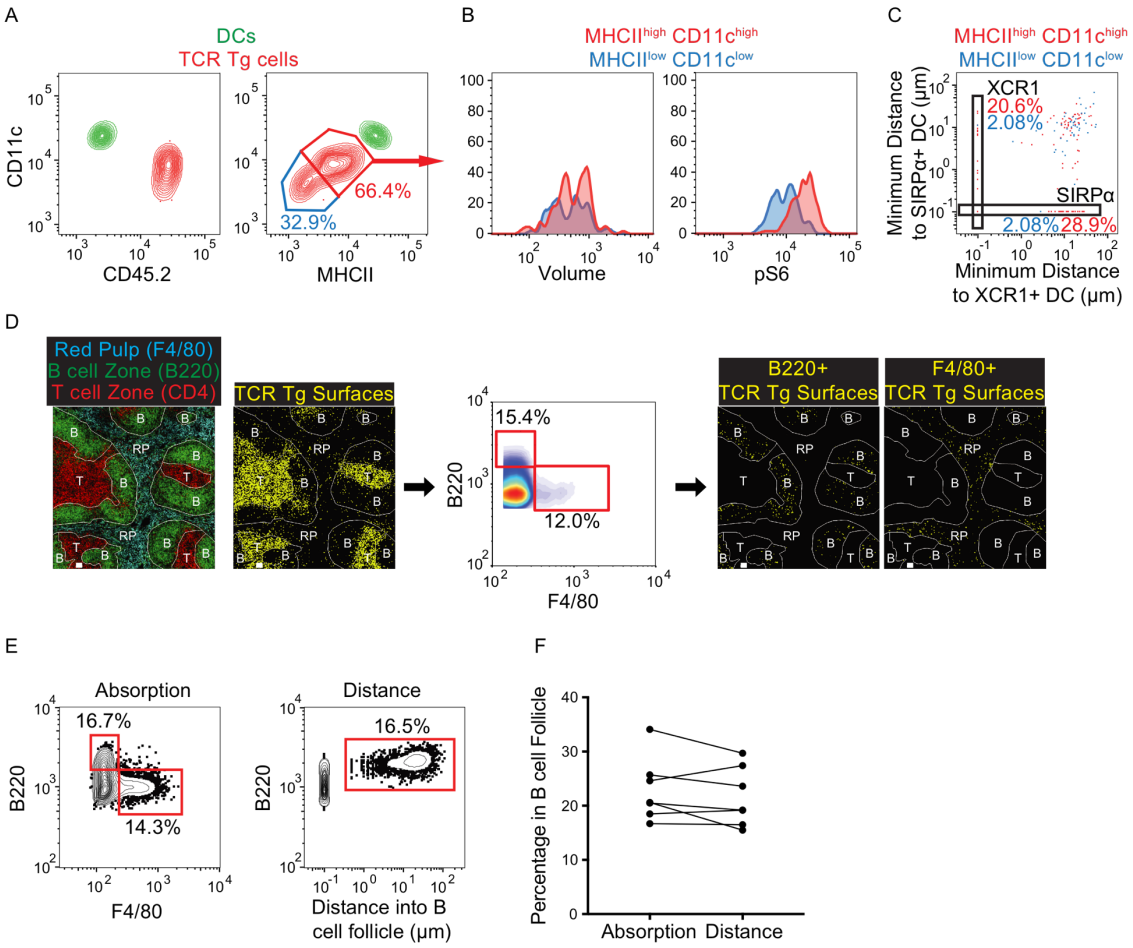

Figure 3. The 'signal absorption' strategy can accurately quantify cell-cell interactions and cellular localization.

(A) Flowjo analysis of CD11c, CD45.2, and MHCII expression on DCs (green) and B3K506 TCR Tg T cells (red) identified in confocal microscopy images. (B) Histogram of volume and pS6 expression for MHCII^{high} CD11c^{high} (red) and MHCII^{low} CD11c^{low} (blue) TCR Tg T cells. (C) Quantifying T cell-DC interactions for MHCII^{high} CD11c^{high} (red) and MHCII^{low} CD11c^{low} (blue) TCR Tg T cells with SIRPα^{+} and XCR1^{+} DCs. (D) Epi-fluorescence image of splenic tissue stained for F4/80, B220, CD4, and CD45.2, with TCR Tg cell surfaces created based on CD45.2 fluorescence. TCR Tg surfaces were

subsetted into cells that absorbed B220 or F4/80 thereby allowing for the characterization of TCR Tg cell localization. (E) Representative gating scheme with 10^{-1} μm added to each cell for logarithmic visualization and (F) quantification of the percent of TCR Tg cells in B cell follicles three d after *Lm*-P5R infection when analyzed by B220 absorption or T cell distance into B cell follicles (n=7). Scale bar, 20 μm. Data representing two to three independent experiments are shown. A paired t test was used to determine significance for F. No significant difference was detected.

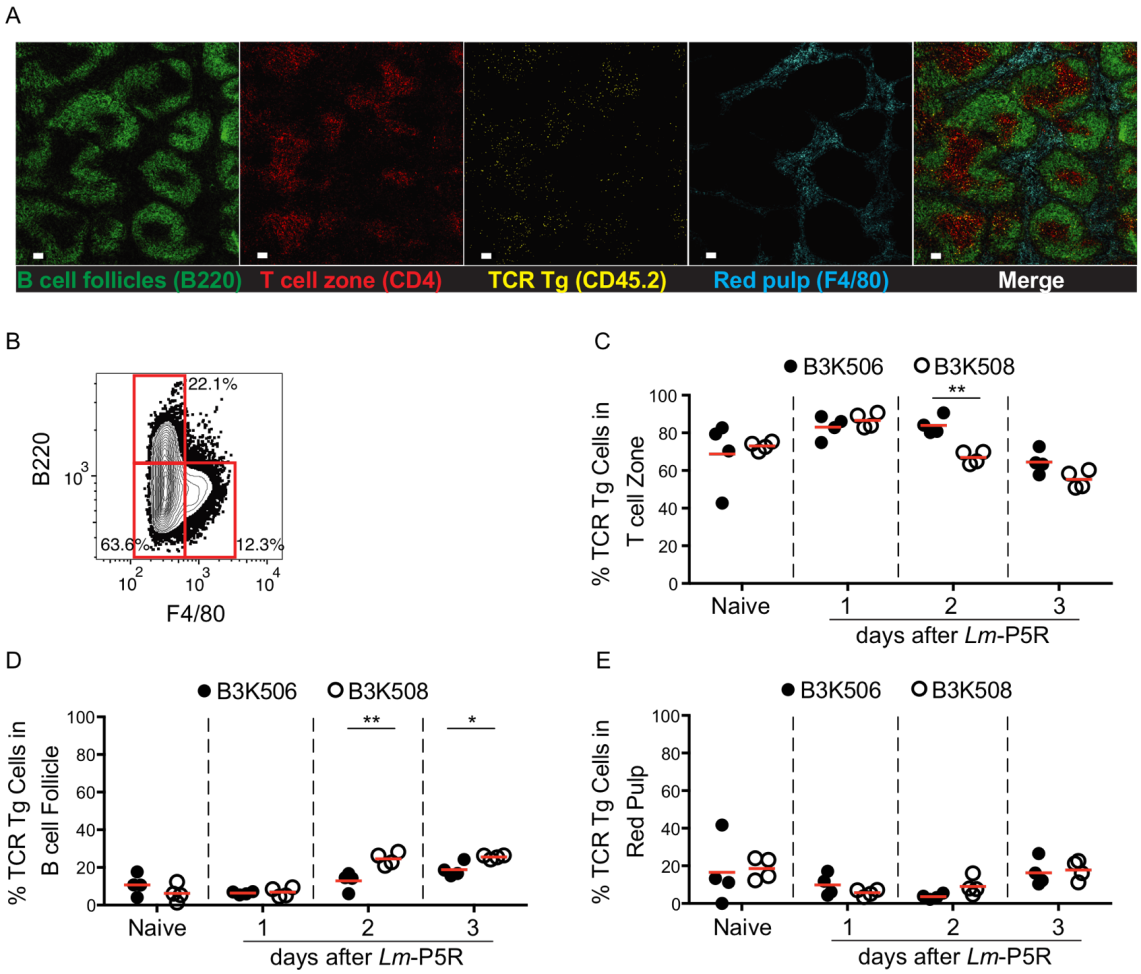

Figure 4. T cells primarily reside in T cell zones following *Listeria* infection, and low affinity T cells traffic into B cell follicles more than high affinity T cells.

(A) Representative images of B220, CD4, CD45.2, and F4/80 staining of a splenic tissue section acquired by epi-fluorescence microscopy. (B) Gating strategy for using 'signal absorption' to identify B cell follicle ($B220^{+}$) or red pulp ($F4/80^{+}$) residing TCR Tg T cells in epi-fluorescence microscopy images. (C-E) Quantification of epi-fluorescence microscopy images that determine B3K506 (filled circle, n=4) and B3K508 (empty circle, n=4) cell localization in (C) T cell zone, (D) B cell follicle, or (E) red pulp in spleens of naïve mice and mice one, two, or, three d after *Lm*-P5R infection. Scale bar,

100 μm. Pooled data from three independent experiments are shown. One-way ANOVA was used to determine significance for D. * = $p < 0.05$, ** = $p < 0.01$.

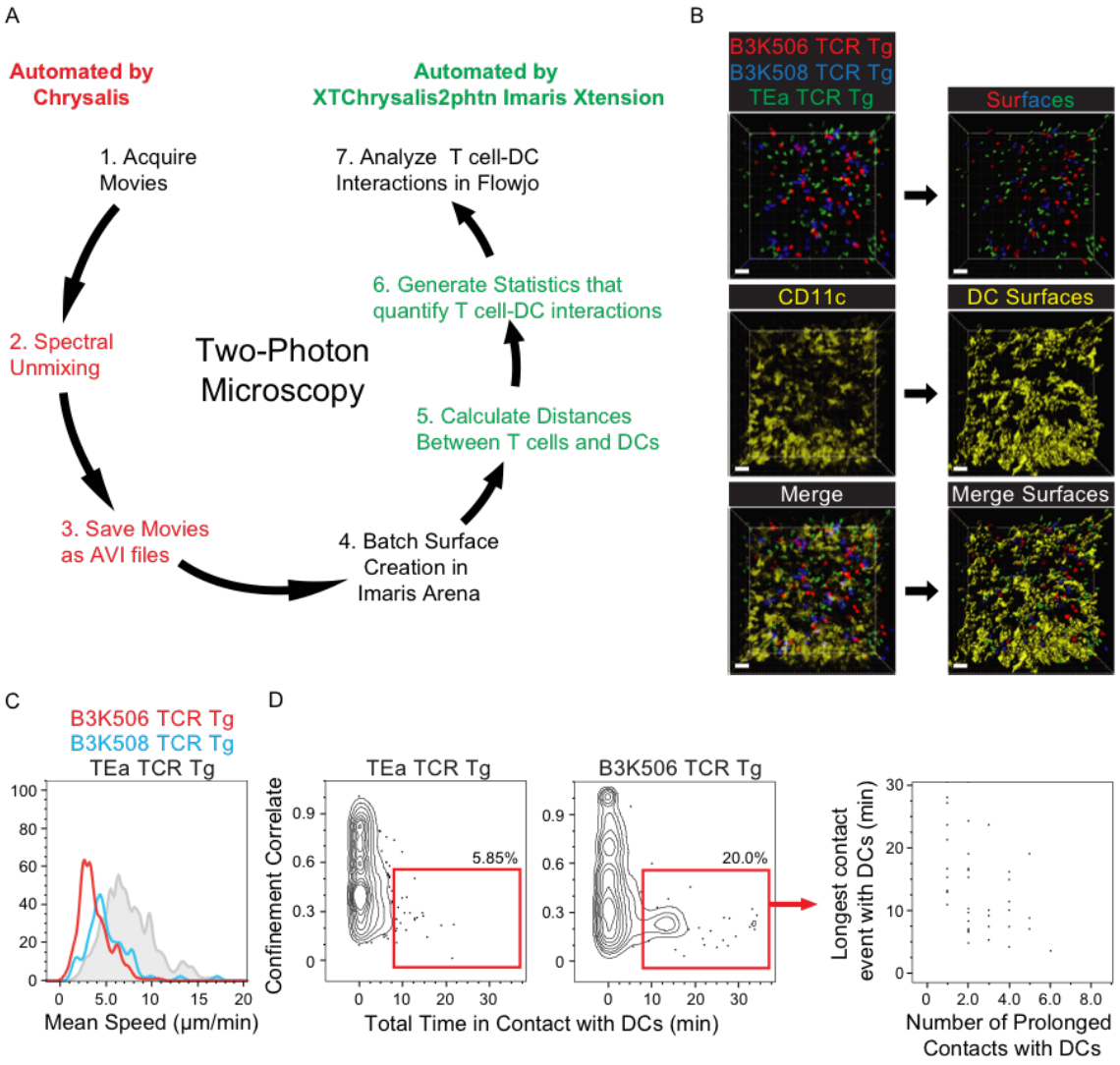

Figure 5. Chrysalis and XTChrysalis2phtn analysis of a two-photon microscopy movie.

(A) Diagram of the histo-cytometry workflow on two-photon movies when automated by Chrysalis and XTChrysalis2phtn. (B) Surface-mediated identification of B3K506, B3K508, and TEa TCR Tg cells as well as DCs in two-photon movies. (C) Quantifying cellular velocity in a two-photon movie with Flowjo for B3K506 (red), B3K508 (blue), and TEa (grey) TCR Tg T cells. (D) Flowjo analysis of B3K506 and TEa TCR Tg cells in a two-photon movie, with quantification of track straightness, total contact time with

DCs, longest contact with a DC, and number of prolonged contacts with DCs. Scale bar, 20 μm. Data representing two to three independent experiments are shown.

Chapter 4

TCR affinity biases Th cell differentiation by regulating CD25, Eef1e1, and Gbp2

4.1 Introduction

$CD4^+$ T lymphocytes are critical for controlling infections through their ability to provide help to B cells, cytotoxic T cells, or myeloid cells (153). $CD4^+$ T cells provide these diverse functions by differentiating into specialized subsets following TCR recognition of p:MHCII complexes on the surface of DCs and in the context of cytokines from the innate immune system (128, 153, 154). Work by our group and others has shown that TCR dwell time on p:MHCII, which strongly correlates with TCR affinity, also influences Th cell differentiation (68, 69, 71). In our experiments, increases in TCR affinity corresponding to p:MHCII dwell times of 0.9 to 2.3 s correlated with increased differentiation of macrophage-helping Th1 cells and decreased formation of B cell-helping Tfh cells (68, 71, 72). Although Th1 differentiation fostered by high affinity TCR interactions is related to strong induction of the IRF4 transcription factor (155), additional aspects of the mechanism by which TCR affinity affects T cell differentiation have yet to be determined.

IL-2 receptor signaling promotes Th1 and suppresses Tfh differentiation by driving STAT5 activation and induction of Blimp1, a repressor for the Tfh promoting transcription factor Bcl-6 (63, 66, 95, 156-159). Potentially, TCR affinity regulates Th cell differentiation, in part, by influencing IL-2 signaling. We therefore tested two TCR

affinity-regulated IL-2 signaling-based mechanisms, one rooted in dendritic cell Ag presentation and another focused on IL-2 receptor alpha chain (CD25) expression. The two major classical dendritic cells (DCs) in the spleen differ in p:MHCII presentation and IL-2 consumption potential (38, 39, 43). $XCR1^+$ DCs are potent producers of the Th1-inducing cytokine IL-12 (43), but are relatively poor producers of p:MHCII complexes, whereas $SIRP\alpha^+$ DCs consume IL-2 and are weak IL-12 producers, but are strong producers of p:MHCII complexes (39). Thus, it is possible that high TCR affinity could bias toward Th1 differentiation because only Th cells with high affinity TCRs cells could access the small number of p:MHCII complexes displayed on $XCR1^+$ DCs, while low affinity cells could access the abundant p:MHCII complexes on $SIRP\alpha^+$ DCs favoring Tfh differentiation (160). Alternatively, since IL-2 receptor expression is proportional to the strength of TCR signaling and drives Th1-promoting STAT5 activation (63, 66, 95, 156-159), Th cells with high affinity TCRs may be intrinsically more likely to become Th1 cells than Th cells with low affinity TCRs.

We tested these models by examining the influence of TCR affinity on differentiation and T cell-DC interactions using two TCR transgenic (Tg) strains that contain T cells with differing TCR affinities for the same p:MHCII ligand (90). We found that Th cells with low, medium, or high affinity TCRs T cells tended to adopt uncommitted, Tfh, or non-Tfh fates, respectively, after exposure to bacteria or virus expressing the relevant peptide. In all cases, Th cells interacted more frequently with $SIRP\alpha^+$ DCs than with $XCR1^+$ DCs, indicating that differential interactions with DCs did not account for TCR affinity-based differences in Th1/Tfh formation. Rather, TCR affinity influenced Th differentiation by controlling the expression of the IL-2 receptor

and eukaryotic translation elongation factor 1 epsilon 1 (Eef1e1), which promoted Th1 cells, and guanylate binding protein 2 (Gbp2), which promoted Tfh cells. Our results suggest that TCR affinity-based effects on Th differentiation are related to the capacity of the TCR to induce different genetic programs at different affinity levels.

4.2 Results

TCR affinity biases Th cell differentiation

We utilized B3K506 and B3K508 TCR Tg strains (90) to examine the relationship between TCR affinity and T cell differentiation. B3K506 and B3K508 mice contain monoclonal populations of $CD4^+$ T cells with TCRs that bind to a peptide called P5R complexed with the I-A^b MHCII molecule of C57BL/6 (B6) mice. The B3K506 TCR, however, binds more strongly to this ligand than B3K508 TCR (K_Ds of 11 and 93 μM) while the B3K508 TCR binds to a related ligand P2A:I-A^b more strongly than the B3K506 TCR (K_Ds of 175 and 278 μM). The K_Ds of 11 and 93 μM will be considered high and medium affinities, respectively, while K_Ds of 175 and 278 μM will be considered to be low affinities. The effect of these affinity differences on differentiation was examined by adoptive transfer of $CD90.1^+$ B3K506 or B3K508 T cells into $CD90.2^+$ mice (161) that were then infected intravenously with *Lm* bacteria engineered to express P5R (*Lm*-P5R) or P2A (*Lm*-P2A) peptide.

As expected from the work of Huseby and colleagues (90), the expansion of B3K506 and B3K508 T cells in response to *Lm*-P5R and *Lm*-P2A infection correlated positively with TCR affinity (Fig. 6A). Previous work (53) indicated that *Lm* infection

drives the differentiation of Th1 cells, which express the T-bet transcription factor (46), and Tfh cells, which express the CXCR5 chemokine receptor (162-164). B3K506 and B3K508 cells also adopted these fates (Fig. 6B), although high TCR affinity (lower K_D) biased differentiation to the Th1 fate and medium affinity towards the Tfh fate as we reported previously (68), while lower affinity T cells predominantly remained uncommitted as defined by a lack of T-bet or CXCR5 (Fig. 6C). This result was recapitulated in mice infected with influenza expressing P5R (PR8-P5R). After PR8-P5R infection, T cells with a higher TCR affinity were again biased towards the Th1 fate while lower TCR affinity biased cells towards the Tfh fate, demonstrating that the influence of TCR affinity on T cell differentiation is not restricted to *Lm* infection (Fig. 6D).

The effect of TCR affinity on T cell differentiation was also tested after intranasal *Lm*-P5R infection, which induces Th17 cells along with Th1 and Tfh cells (56). Th17 differentiation was identified by expression of the lineage-defining transcription factor RORγt (47). B3K506 cells generated larger fractions of Th17 and Th1 cells, an equal fraction of Tfh cells, and a lower fraction of uncommitted cells than B3K508 cells (Fig. 6E), suggesting that high TCR affinity also promotes the Th17 fate. The large percentage of uncommitted Th cells observed after this infection was likely a consequence of low Ag presentation due to poor adaptation of this enteric bacterium to the intranasal route.

XCR1$^+$ and SIRPα$^+$ DCs differ in Ag presentation and effect on T cell differentiation

Before testing the differential Ag presentation hypothesis, we first examined the kinetics of Th differentiation to identify the time when critical T-DC interactions occur. B3K506 and B3K508 cell differentiation was examined over the first three d after *Lm* infection because Th1/Tfh bifurcation occurred in this time frame in another system (108, 156). A larger fraction of the B3K508 effector T cell population consisted of $CXCR5^+$ cells than the B3K506 population on d one, two, and three after infection (Fig. 7A) and did not change after d three (Fig. 6C, 7A). These results suggest that the Th1/Tfh cell bifurcation occurs within the first three d following *Lm* infection.

We also confirmed that $SIRP\alpha^+$ DCs produce more p:MHCII complexes than $XCR1^+$ DCs after *Lm* infection as reported in another system (39). The amount of p:MHCII presentation was determined by measuring the capacity of purified splenic DCs from d two intravenously *Lm*-P5R-infected mice to stimulate CD69 and CD25 expression by cognate Th cells *in vitro* (39, 66) (Fig. 7B). $SIRP\alpha^+$ DCs were more potent activators of B3K508 cells than $XCR1^+$ DCs in this assay (Fig. 7B), indicating that $SIRP\alpha^+$ DCs display more P5R:I-A^b complexes than $XCR1^+$ DCs as expected.

We then tested how the different DC types affected Th differentiation using a cell ablation strategy. The majority of $SIRP\alpha^+$ DCs, which express Clec4a4 (DCIR2), were ablated by administering diphtheria toxin (DT) to radiation chimeras generated with *Clec4a4*^{DTR} bone marrow (42). The effect of $XCR1^+$ DCs was studied with *Batf3*$^{-/-}$ mice, which lack these cells (165). A 60% reduction in $SIRP\alpha^+$ DCs led to an increase in Th1 and a decrease in Tfh differentiation by B3K506 and B3K508 cells following *Lm*-P5R infection irrespective of TCR affinity (Fig. 7C). Ablation of $XCR1^+$ DCs had the opposite effect - increased Tfh and decreased Th1 formation for high and medium affinity TCR T

cells (Fig. 7D). These results indicate that XCR1$^+$ DCs are critical for optimal Th1 and SIRPα$^+$ DCs for optimal Tfh differentiation after *Lm* infection for high and low affinity T cells. Thus, this approach indicated that differential Ag presentation by XCR1$^+$ and SIRPα$^+$ DCs cannot explain the tendency of high affinity cells to produce Th1 cells and low affinity cells to produce Tfh cells.

TCR affinity does not influence T cell-DC interactions following Listeria infection

Because cell ablation can result in compensatory effects (166), we also tested the DC preference model by direct observation of T-DC interactions in mice with a normal complement of DCs. Histo-cytometry was used to assess B3K506 and B3K508 T cell interactions with XCR1$^+$ and SIRPα$^+$ DC because two-photon microscopy cannot simultaneously resolve all the T cell and DC populations of interest. The analysis focused on T cell zones of splenic sections from *Lm*-P5R infected and naive CD45.1$^+$ mice that received CD45.2$^+$ B3K506 or B3K508 cells because the T cells were primarily located in this location (161). TCR Tg cells were identified based on the congenic marker, CD45.2, which was used to generate digital surfaces corresponding to these cells (Fig. 8A and 8B). TCR Tg Th cells receiving acute TCR signals and thus likely engaged in productive interactions with DCs were identified by staining the phosphorylated form of S6 kinase (pS6) (129) (Fig. 8B, 8C). Although B3K506 and B3K508 cells had equal pS6 levels one d after infection, B3K508 cells had significantly lower values one d later (Fig. 8D). This result suggests that higher TCR affinity B3K506 cells had more prolonged TCR signaling than lower TCR affinity B3K508 cells.

Th cell interactions with the DCs subsets were then assessed. DCs were identified by generating surfaces on a DC channel that contained voxels with strong MHCII and CD11c, but weak B220, CD3, F4/80, and CD45.2 signal (Fig. 9A). $XCR1^+$ DCs and $SIRP\alpha^+$ DCs were identified based on CD8α and SIRPα expression, respectively (38, 43, 167, 168) (Fig. 9B). Identification of $XCR1^+$ and $SIRP\alpha^+$ DCs was validated by comparing the DC gating strategy in WT and *Batf3*$^{-/-}$ mice, which lack $XCR1^+$ DCs, 1 d after *Lm*-P5R infection (Fig. 9B). DCs in the WT mice consisted of approximately 30% $XCR1^+$ DCs and 70% $SIRP\alpha^+$ DCs, while over 90% of the DCs were $XCR1^+$ DCs in *Batf3*$^{-/-}$ mice (Fig. 9B). Productive T cell-DC interactions were identified as T cells undergoing TCR signaling ($pS6^+$) and touching a DC(s) (Fig. 9C). B3K506 and B3K508 cells interacted equally with DCs one and two d after *Lm*-P5R infection (Fig. 9D). The ratio of T cell contacts with $SIRP\alpha^+$ or $XCR1^+$ DCs was analyzed to determine whether low or high affinity T cells interacted preferentially with one DC subset or the other. The analysis revealed that high affinity B3K506 and medium affinity B3K508 cells interacted 1.5 times more frequently with $SIRP\alpha^+$ than with $XCR1^+$ DCs one and two d after infection (Fig. 9E). Thus, TCR affinity-mediated bias in T cell differentiation was not associated with preferential access of low or high affinity T cells to a particular DC subset.

CD25, Eef1e1, and Gbp2 are TCR regulated proteins that bias helper T cell differentiation

The lack of impact on T cell-DC interactions suggested that TCR affinity regulates differentiation in a T cell intrinsic manner. We, therefore, tested a model in

which increasing TCR affinity for p:MHCII drives greater IL-2 receptor expression, STAT5 signaling, and Th1 differentiation. As described previously (71), B3K506 and B3K508 cells expressed CD25 (IL-2 receptor α) in a TCR affinity dependent manner two d after infection with *Lm*-P5R, with higher TCR affinity correlating with higher CD25 expression (Fig. 10A). This difference in CD25 expression inversely correlated with Tfh differentiation for high and medium TCR affinity T cells, in line with IL-2 receptor signal transduction suppressing Tfh differentiation (63) (Fig. 10A). T cells with a low affinity TCR had the lowest CD25 expression, but less Tfh differentiation than T cells with a medium affinity TCR, which could be attributed to a larger proportion of uncommitted cells (Fig. 10A). These results suggest that high affinity TCR-p:MHCII interactions promote Th1 differentiation by maintaining CD25, which represses the Tfh fate.

TCR signaling induces many proteins in addition to CD25, some of which could be mediators of TCR affinity-based effects on Th differentiation. We focused on nine candidates from a published list of genes induced in naïve TCR transgenic T cells in vitro to a greater extent by a large amount of agonist peptide than by a lower amount (66). The candidate genes were identified by excluding genes with less than 10 Reads Per Kilobase of transcript, per Million mapped for the no peptide condition, less than a 4-fold increase in expression in the high versus no peptide conditions, and less than a 2-fold increase in expression in the high versus low peptide conditions. Of the 12 most abundantly expressed genes, Nr4a1 and Irf4 were excluded from further analysis due to their well-established roles in T cell differentiation (155, 169-174), while CD25 was used as a positive control.

Expression of the candidate genes was validated by quantitative PCR (qPCR) analysis of B3K506 and B3K508 T cells two d after *Lm*-P5R infection. Of the nine genes analyzed, seven were induced to a greater extent in B3K506 than B3K508 T cells indicating a dependence on TCR signaling (Fig. 10B). The role of these seven genes in Th cell differentiation was determined by disrupting each gene in B3K508 cells using CRISPR/Cas9-mediated gene targeting. Cas9-expressing B3K508 cells were transduced with a retrovirus encoding the fluorescent protein mAmetrine and guide RNAs (gRNA) targeting the candidate genes or the bacterial gene LacZ as a control. The transduced T cells were then transferred into B6 mice before intravenous infection of the mice with *Lm* bacteria expressing 3K peptide (*Lm*-3K). The transferred $gRNA^+$ T cells were identified based on CD90.1 and mAmetrine expression and evaluated for adoption of the Th1, Tfh, and uncommitted cell lineages (Fig. 10C, 10D). The expansion of $gRNA^+$ B3K508 cells in the recipient mice was unaffected in the majority of cases, with the exceptions of *Eef1e1* and *Srm*, loss of which resulted in reduced or enhanced expansion, respectively (Fig. 10E). As expected, targeting the *Il2ra* gene encoding CD25 reduced Th1 differentiation relative to the LacZ control population (Fig. 10F). Of the candidate genes, only *Eef1e1* (encoding eukaryotic translation elongation factor 1 epsilon-1 (Eef1e1), also known as AIMP3 and p18) and *Gbp2* (encoding GTP-binding protein 2 (Gbp2)) had significant effects on T cell differentiation. Ablation of *Eef1e1* reduced Th1 differentiation (Fig. 10F) while targeting *Gbp2* led to enhanced Th1 differentiation. These results demonstrate that TCR-driven Eef1e1 promotes Th1 differentiation whereas Gbp2 inhibits this process.

4.3 Discussion

Our results indicate that uncommitted effector Th cells are induced by low affinity TCR-p:MHCII interactions. Tfh cells then become the preferred effector cells as TCR affinity increases, until Th1 and Th17 cells become predominant at higher affinities. The facts that $XCR1^+$ DCs are potent producers of IL-12 (43) but relatively poor producers of p:MHCII complexes, while IL-2 consuming $SIRP\alpha^+$ DCs have the opposite properties suggested an extrinsic explanation of these TCR affinity-based effects on Th cell differentiation. $XCR1^+$ DCs could display fewer p:MHCII complexes than $SIRP\alpha^+$ DCs creating a situation where Th cells with low affinity TCRs would be unable to interact with $XCR1^+$ DCs thereby receive IL-12 and become Th1 cells, but could still interact with $SIRP\alpha^+$ DCs to become Tfh cells. There was potential for this model to be correct because we confirmed that $XCR1^+$ DCs present fewer P5R:I-A^b complexes than $SIRP\alpha^+$ DCs two d after *Lm*-P5R infection, the time frame when Tfh differentiation is initiated. However, we found medium and high affinity Th cells equally interacted with each DC subset, 20% with $SIRP\alpha^+$ DCs and 15% with $XCR1^+$ DCs. Thus, the frequency of interaction with $XCR1^+$ DCs cannot explain the greater tendency of high affinity Th cells to produce non-Tfh cells in this system.

We found better evidence in favor of a Th cell intrinsic mechanism. The CD25 component of the IL-2 receptor was an attractive mediator of such an effect because its expression is proportional to TCR signaling (66, 72, 157, 158) and biases differentiation by inhibiting Tfh formation (63). We found that high TCR affinity positively correlated with stronger TCR signaling and maintenance of CD25 expression. Longer expression of

the IL-2 receptor would provide more time for induction of the STAT5-regulated Tfh repressor Blimp1 (63, 156). A similar situation may exist for Type 2 immune responses since the population of house dust mite allergen p:MHCII-specific Th cells induced by allergen inhalation is comprised of Th2 and Tfh cells (175) and Th2 cells are CD25-dependent (176-178).

Our results indicate that the Eef1e1 is another TCR signal strength responsive driver of the Th1 fate. Eef1e1 binds to Lamin A (179) and overexpression studies performed in cell lines demonstrated that Eef1e1 facilitates Lamin A ubiquitination and degradation via the ubiquitin ligase, Siah1 (180). Interestingly, Lamin A-deficient T cells have reduced *in vivo* Th1 differentiation (181), while Siah1 promotes Th17 cell differentiation *in vitro* (182). Thus, strong TCR signaling may favor the differentiation of non-Tfh cells by engaging a pathway involving Eef1e1, Lamin A, and Siah1. The Th1-promoting effects of Eef1e1 may also be related to the role that we identified for this molecule in proliferation. Craft and colleagues showed that IL-2-mediated activation pathways associated with cellular proliferation promote Th1 over Tfh cell differentiation (183). Eef1e1, which interacts with ATM (184), a protein critical for TCR signaling-induced proliferation (185) may contribute to this non-Tfh-promoting process.

Increased expression of Eef1e1, CD25, and IRF4 and induction of downstream pathways is a plausible explanation for the increase in Th1 formation that occurs as TCR affinity increases from moderate to high levels. This mechanism, however, cannot explain the increase in Tfh formation that occurs as TCR affinity increases from low to moderate levels. Our results indicate that Gbp2, a TCR-induced protein that promoted Tfh cell formation, could be involved in this transition. Gbp2 is associated with reduced

mitochondrial fission (186), which is important for aerobic glycolysis (187-189) and operates at low levels in Tfh cells (183, 190). Therefore, Gbp2 may promote Tfh formation by keeping aerobic glycolysis in check.

Together, our results suggest a general model in which low TCR affinity and signaling induces Gbp2 thereby promoting Tfh differentiation, while high TCR affinity and signaling drives Eef1e1 and CD25, which represses the Tfh fate and promotes non-Tfh cell formation. The type of non-Tfh cells would then depend on the type of cytokines produced by the innate immune system. For example, intranasal infection, which elicits IL-6 and TGF-β production by cervical lymph node DCs (52), would favor Th17 differentiation, while intravenous infection, which stimulates IL-12 production by splenic $XCR1^+$ DCs (43), would bias towards Th1 differentiation. This mechanism would ensure that polyclonal populations of epitope-specific naïve Th cells, which always contain a spectrum TCR affinities (97), generate effector cells capable of promoting humoral and cellular immunity suited to clearance of the microbe. The tendency of moderate affinity T cells to become Tfh cells may foster affinity maturation by only allowing B cells with the highest affinity immunoglobulins to garner T cell help, while diversion of high affinity T cells to become myeloid cell-helpers would ensure that the helped cells achieve the optimal state of microbicidal activity.

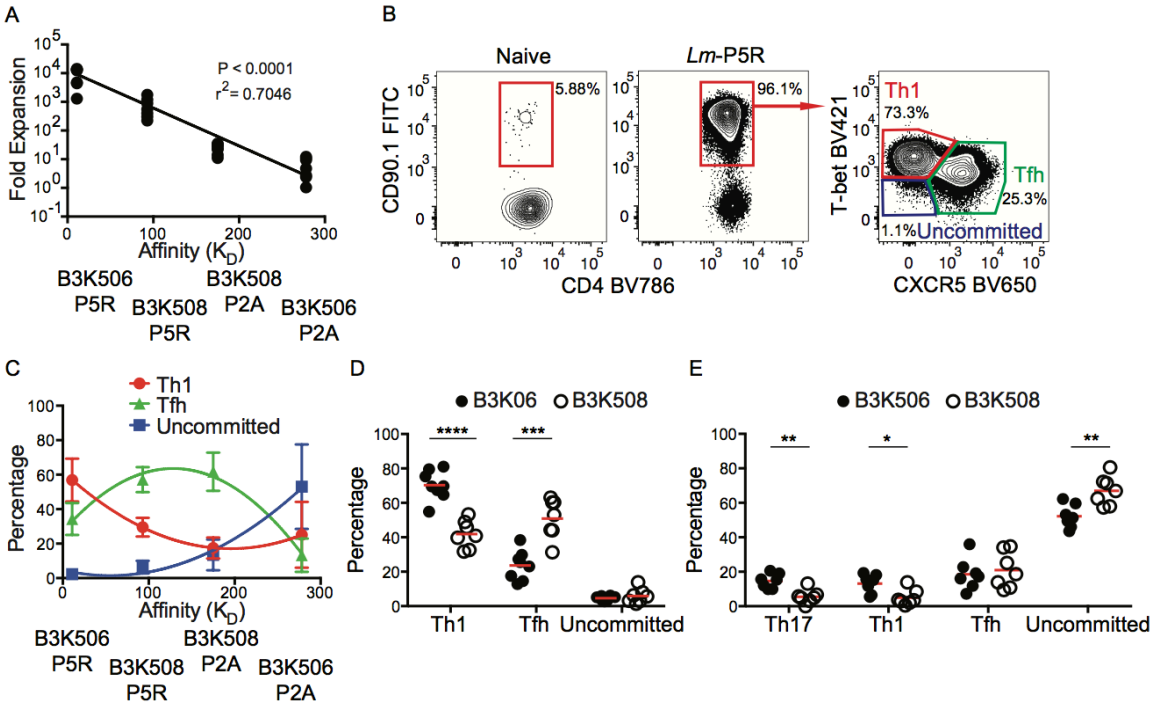

Figure 6. TCR affinity differences between B3K506 and B3K508 cells influence T cell expansion and bias T cell differentiation.

(A) Fold expansion of B3K506 or B3K508 cells seven d after *Lm*-P5R (n=7) or *Lm*-P2A (B3K506 n=7, B3K508 n=8) infection plotted in relation to the affinity of the relevant TCR-p:MHCII interaction. (B) Representative flow cytometric identification of TCR Tg cells (red gates in the left and middle panels) in naive or *Lm-P5R* infected mice. Th1 (T-bet^{+}), Tfh (CXCR5^{+}), or uncommitted (T-bet^{-} CXCR5^{-}) cells were identified in the right panel in the red, green and purple gates, respectively. (C) Differentiation (Th1 in red, Tfh in green, and uncommitted in blue) of B3K506 or B3K508 cells seven d after *Lm*-P5R (n=7) or *Lm*-P2A (B3K506 n=7, B3K508 n=8) infection plotted in relation to the affinity of the relevant TCR-p:MHCII interaction. (D) Frequency of Th1, Tfh, or uncommitted cells among B3K506 (filled circle, n=8) or B3K508 (empty circle, n=7) effector cell populations seven d after infection with influenza PR8-P5R. (E) Frequency of Th17, Th1,

Tfh, or uncommitted cells among B3K506 (filled circle, n=7) or B3K508 (empty circle, n=7) cells seven d after intranasal infection with *Lm*-P5R. The bars in D and E represent the mean. Pooled data from two or three independent experiments are shown. Multiple t tests were used to determine significance for D and E. A linear regression was used to calculate significance for A and a nonlinear fit was used to calculate the r^2. * = $p < 0.05$, ** = $p < 0.01$, *** = $p < 0.001$, **** = $p < 0.0001$.

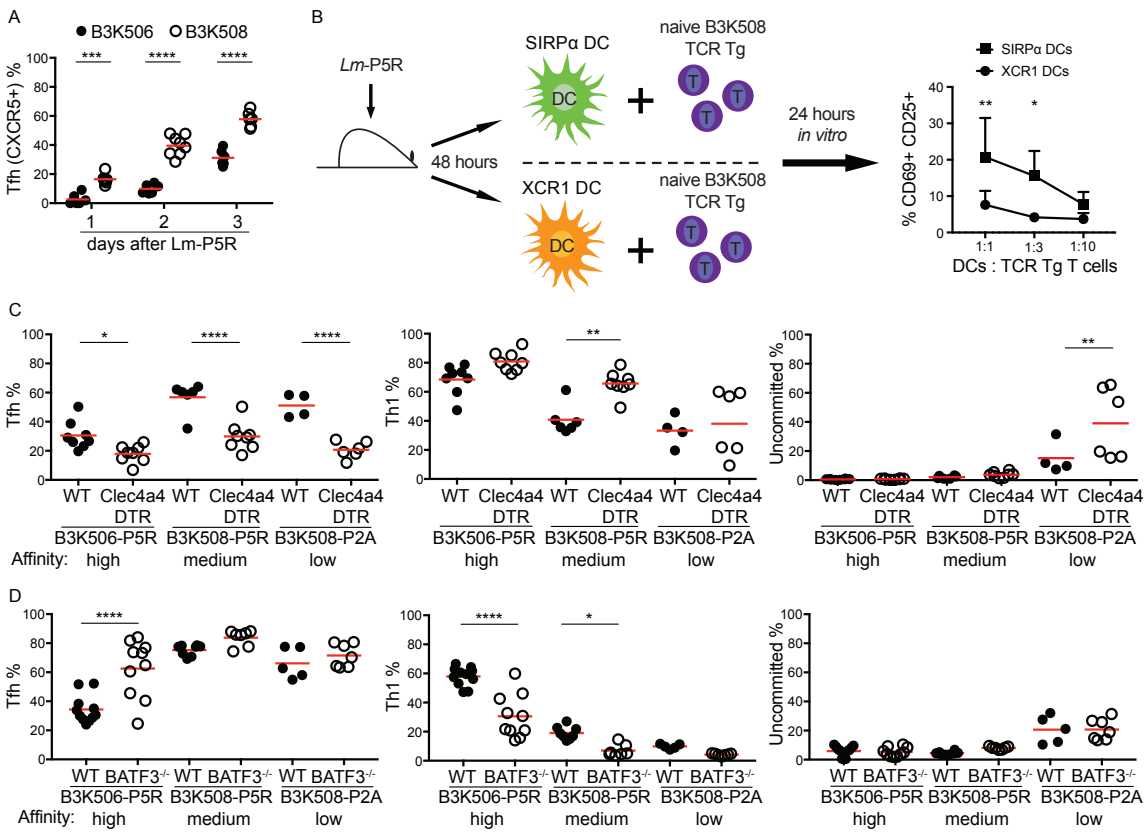

Figure 7. Effect of genetic ablation of XCR1$^+$ or SIRPα$^+$ DCs on Th differentiation.

(A) Tfh differentiation by B3K506 (filled circle, n=6) and B3K508 (empty circle, d 1 d 2 n=6, d 3 n=8) cells in the initial three d following *Lm*-P5R infection. (B) Experimental model and resulting mean frequencies ± SD of CD69$^+$ CD25$^+$ B3K508 cells after one d of co-culture with SIRPα$^+$ (square, n=3) or XCR1$^+$ (circle, n=3) DCs from *Lm*-P5R infected mice two d post-infection. (C) Frequency of Tfh, Th1, or uncommitted cells among B3K506 or B3K508 TCR Tg cells in DT-treated WT (filled circle) or *Clec4a4*^{DTR} (empty circle) mice three d after *Lm*-P5R (B3K506 WT n=8, *Clec4a4*^{DTR} n=8; B3K508 WT n=6, *Clec4a4*^{DTR} n=8) or *Lm*-P2A (B3K508 WT n=4, *Clec4a4*^{DTR} n=6) infection. (D) Frequency of Tfh, Th1, or uncommitted cells among B3K506 or B3K508 cells in WT (filled circle) or *Batf3*$^{-/-}$ (empty circle) mice three d after *Lm*-P5R (B3K506 WT n=11,

Batf3$^{-/-}$ n=7; B3K508 WT n=8, *Batf3*$^{-/-}$ n=7) or *Lm*-P2A (B3K508 WT n=5, *Batf3*$^{-/-}$ n=7) infection. The bars in A, C, and D represent the mean. Pooled data from two or three independent experiments are shown. Two-way ANOVA was used to determine significance for B and one-way ANOVA with Sidak's multiple comparison test was used to determine significance for A, C and D. * = $p < 0.05$, ** = $p < 0.01$, *** = $p < 0.001$, **** = $p < 0.0001$.

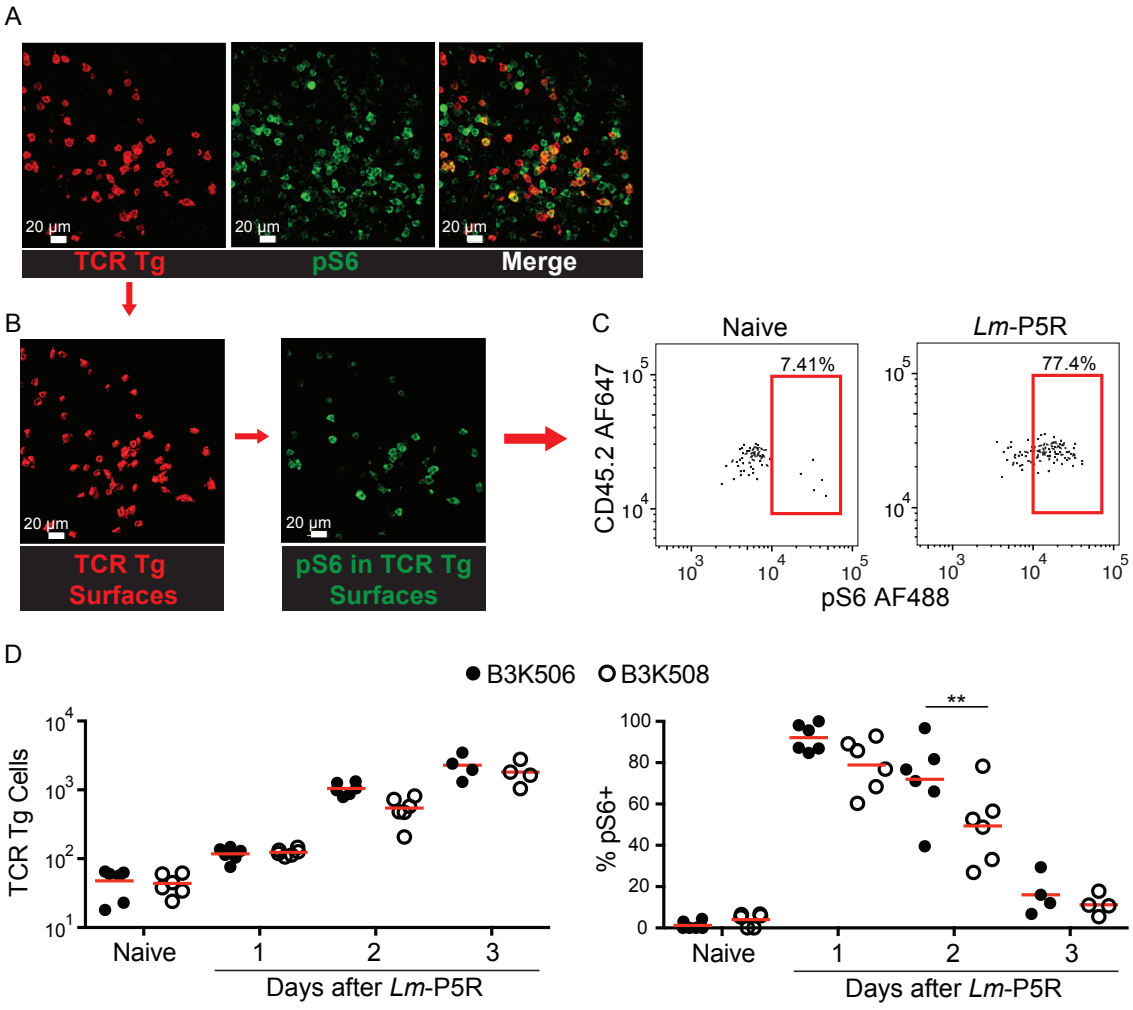

Figure 8. Histo-cytometry analysis of the effect of TCR affinity on T cell activation. (A) Representative images of TCR Tg cells identified with CD45.2 (red) and pS6 (green) in a spleen one d post-*Lm*-P5R infection. (B) Digital surfaces of the cells were created and analyzed with histo-cytometry. (C) TCR Tg cell expression of pS6 was then quantified in Flowjo. (D) Histo-cyotmetric quantification of B3K506 (filled circle) and B3K508 (empty circle) cell numbers and their pS6 expression in naïve mice and mice during the initial three d following *Lm*-P5R infection (naïve, d 1, d 2 n=6; d 3 n=4). The bars in B represent the mean. Scale bar, 20 µm. Pooled data from three independent

experiments are shown. One-way ANOVA was used to determine significance for D. ** = $p < 0.01$.

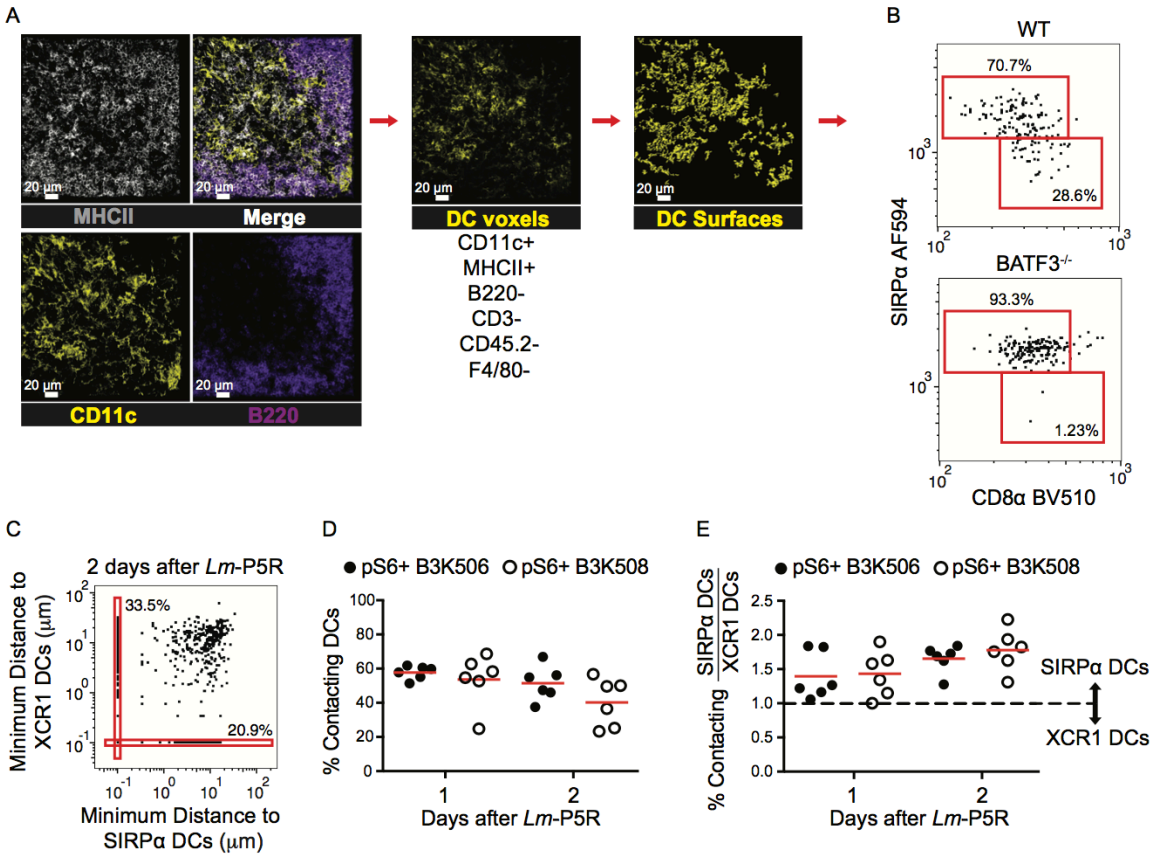

Figure 9. Histo-cytometry analysis of DCs and T cell-DC interactions.

(A) Representative images of MHCII (grey), CD11c (yellow), and B220 (purple) staining from a spleen one d post-*Lm*-P5R infection. Histo-cytometry was used to generate surfaces for DCs ($CD11c^+$ $MHCII^+$ $B220^-$ $CD3^-$ $CD45.2^-$ $F4/80^-$). $XCR1^+$ or $SIRP\alpha^+$ surfaces were identified among the DC surfaces based on the indicated gates. (B) Histo-cytometry identification of $XCR1^+$ and $SIRP\alpha^+$ DCs in WT and *Batf3*$^{-/-}$ mice infected with *Lm*-P5R for one d. (C) Representative histo-cytometry analysis displaying the percentage of $pS6^+$ TCR Tg cells interacting with $XCR1^+$ or $SIRP\alpha^+$ DCs in mice infected with *Lm*-P5R for one or two d. Interactions are defined as TCR Tg cells that are within 0 µm of either DC subset with 10^{-1} µm added to each cell for logarithmic visualization. (D) Histo-cytometry-identified interactions between $pS6^+$ B3K506 (filled

circle, n=6) or B3K508 (empty circle, n=6) T cells with $XCR1^+$ or $SIRP\alpha^+$ DCs in mice infected with *Lm*-P5R for one or two d. (E) Ratio of T cell interactions with $SIRP\alpha^+$ DC to $XCR1^+$ DC interactions by $pS6^+$ B3K506 (filled circle, n=6) or B3K508 (empty circle, n=6) T cells. The bars in D and E represent means. Scale bar, 20 μm. Pooled data from three independent experiments are shown. One-way ANOVA was used to determine significance for D and E. No significant differences were detected.

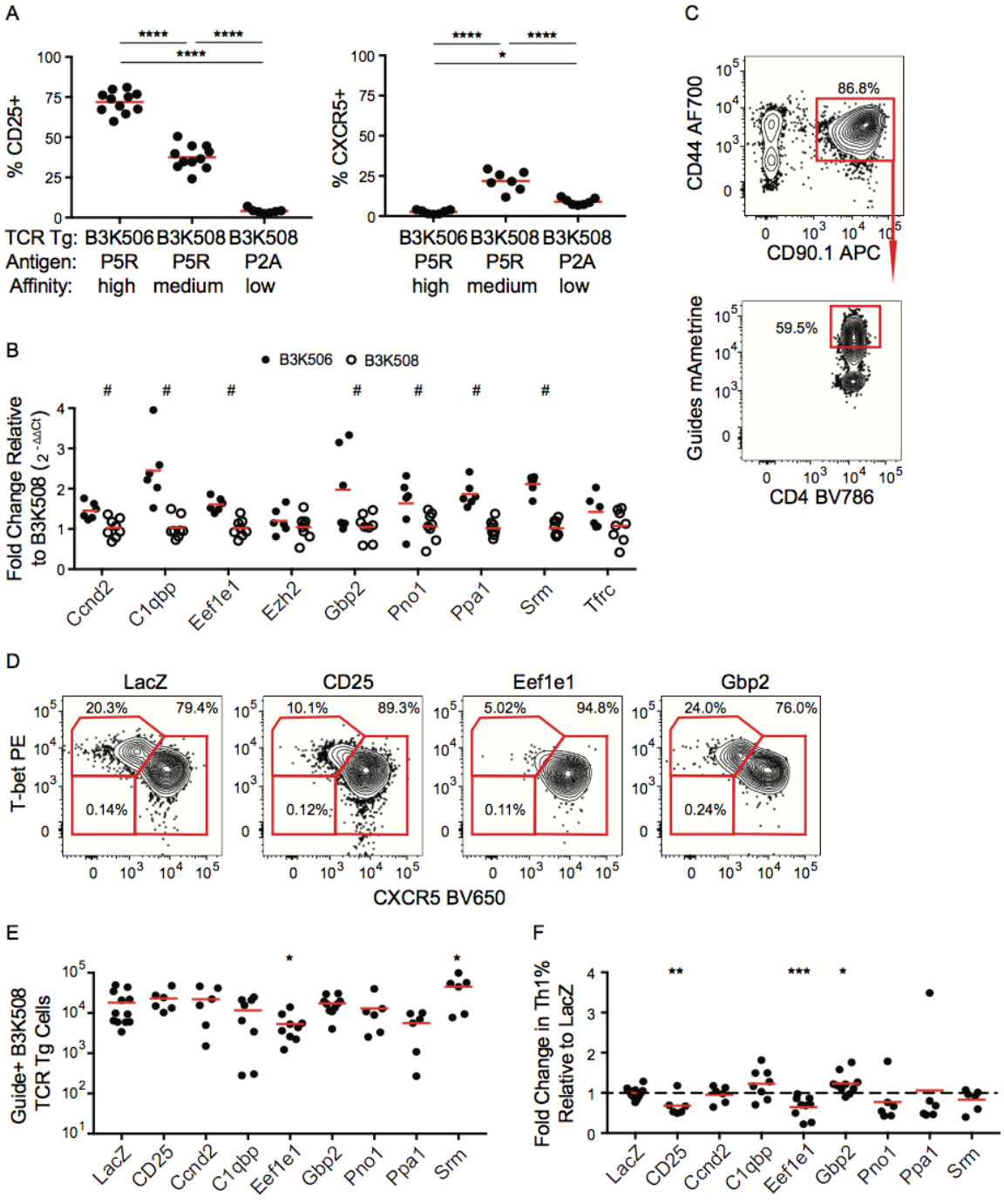

Figure 10. CD25, Eef1e1, and CD25 are upregulated by TCR signaling and bias helper T cell differentiation.

(A) Frequency of CD25^{+} and CXCR5^{+} B3K506 and B3K508 T cells two d after infection with *Lm*-P5R (CD25% n=11, CXCR5% n=7) or *Lm*-P2A (n=7). (B) Fold change in gene

expression relative to B3K508 T cells based on qPCR analysis for B3K506 (filled circle, n=6) and B3K508 (empty circle, n=8) T cells two d after infection with *Lm*-P5R. (C) Representative flow cytometric identification of $gRNA^+$ $Cas9^+$ B3K508 T cells (red squares) seven d after *Lm*-3K infection and (D) their differentiation into Th1 ($T\text{-}bet^+$), Tfh ($CXCR5^+$), or uncommitted ($T\text{-}bet^-$ $CXCR5^-$) lineages when targeting *LacZ*, *CD25*, *Eef1e*1, or *Gbp*2. (E) Quantification of $gRNA^+$ $Cas9^+$ B3K508 T cells and (F) their fold change in Th1% relative to the LacZ group seven d after *Lm*-3K infection. The bars in A, B, E, and F represent means. Pooled data from two or three independent experiments are shown. Multiple t tests were used to determine discoveries based on a false discovery rate of 5% for B and significance for A, E, and F. # = discovery, * = $p < 0.05$, ** = $p < 0.01$, *** = $p < 0.001$, **** = $p < 0.0001$.

Chapter 5

Many helper T cell subsets have Fas ligand-dependent cytotoxic potential

5.1 Introduction

T cells have traditionally been categorized as cytotoxic $CD8^+$ T cells and helper $CD4^+$ T cells. Both types exist as quiescent naïve cells in the pre-immune repertoire, but proliferate and differentiate into effector cells following TCR binding to the relevant MHC-bound peptides on APCs. $CD8^+$ effector T cells utilize Fas ligand (FasL), TNFα, perforin, and/or granzyme (191, 192) to kill cells displaying the relevant MHC-bound peptide. In contrast, $CD4^+$ effector T cells secrete cytokines after interaction with cells expressing the relevant MHCII-bound peptide and typically enhance the microbicidal functions of the interacting cells. For example, Th1 cells migrate to sites of infection where they produce TNFα, IFN-ɣ, and CD40L, which activate macrophages to clear intracellular infections (41, 193-196).

Recently, however, it has become clear that $CD4^+$ T cells, usually Th1 cells, can also have direct cytotoxic activity (197-202) *in vivo* following infections and cancer (203, 204). Cytotoxic Th cell frequency correlated with viral control in influenza- and HIV-infected humans indicating a role for these cells in immunity (77, 83). In mouse models, cytotoxic Th cells depend on perforin for cytotoxic function and express KLRG1 and Ly6C, which are also expressed preferentially on Th1 cells (78, 200, 205, 206). In addition, cytotoxic Th cells can express the Th1-associated transcription factors Blimp1,

T-bet, and Eomes, and Eomes has been proposed as a master regulator of cytotoxic Th cell formation (46, 63, 78, 85, 86, 207, 208). It is unclear, however, whether Th1 cells are the only Th cells with cytotoxic activity.

Here, we characterized p:MHCII-specific cytotoxic $CD4^+$ Th cell populations induced by immunization or acute infections. In these cases, cytotoxic Th formation did not require Eomes or perforin, was not limited to T-bet-expressing Th1 cells, and acted in part through a mechanism requiring Fas expression by target cells. Multiple Th subsets including T follicular helper (Tfh), regulatory T (Treg) cells, and Th17 cells expressed FasL, suggesting all could have cytotoxic potential. TCR-dependent interactions between p:MHCII-specific T cells and p:MHCII-bearing target cells induced Fas on the target cells. These results suggest that many different kinds of Th cells have the capacity to stimulate the target cell to express the surface protein that causes its demise.

5.2 Results

Generation of cytotoxic Th cells

We sought to identify an immunization regimen that drives a robust cytotoxic Th cell response. The 2W peptide was chosen as a model Ag because it is highly immunogenic in C57BL/6 (B6) mice and the TLR3 agonist Poly I:C was chosen as an adjuvant because it induces strong Th1 immunity of the kind thought to be associated with Th-mediated cytotoxicity (209, 210). A fluorochrome-labeled 2W:I-A^b tetramer and a magnetic bead-based cell enrichment method was used to track 2W:I-A^b-specific $CD4^+$ T cells (97). As reported previously, unimmunized B6 mice contained about 200 2W:I-

A^b-specific $CD4^+$ T cells in their spleens (94) (Fig. 11A, 11B). This naïve precursor population increased to 3,000 $CD44^{high}$ effector cells seven days after injection of 2W peptide alone, or 30,000 such cells after injection of 2W peptide and Poly I:C (Fig. 11A, 11B). The large increase in the number of 2W:I-A^b-specific $CD4^+$ effector T cells induced in the presence of Poly I:C confirmed the adjuvant activity of this molecule. As expected, these T cells expressed $CD4^+$ and not CD8α (67) (Fig. 11C).

$CD4^+$ T cell-mediated cytotoxicity was then assessed using an *in vivo* assay. Target cells were prepared by labeling splenocytes with CellTrace Violet (CTV) at two concentrations. Cells labeled with a lower concentration were incubated with 2W peptide while cells labeled with a higher concentration were incubated without peptide. These cells were mixed and injected into naive or 2W peptide/PolyI:C-immunized mice. The target cells displaying 2W:I-A^b complexes were preferentially lysed, as indicated by a decrease in the percentage of cells with low CTV labeling (Fig. 12A). CD4 or CD8α depleting antibodies were then administered at the same time as the target cells to identify the cytotoxic population. The specific lysis was then calculated by taking the ratio of 2W-incubated to no peptide-incubated target cells in 2W primed mice, and dividing this ratio by that in naïve mice (203). CD4 but not CD8α antibody treatment depleted 2W:I-A^b-specific $CD4^+$ T cells (Fig. 12B) and greatly reduced 2W-target cell lysis (Fig. 12C). These results demonstrate that 2W peptide/Poly I:C immunization generates a 2W:I-A^b-specific $CD4^+$ cytotoxic Th cell response.

Analysis of the cytotoxic pathways utilized by Cytotoxic Th cells

We sought to define the pathways utilized by cytotoxic Th cells to kill target cells. CTV-labeled target cells deficient in expression of CD40, IFN-γ receptor, TNF receptor I and II, TRAIL receptor, or Fas were injected into wild-type (WT) mice that were primed with 2W peptide/Poly I:C (203, 211-214). The perforin pathway was tested by injecting CTV-labeled WT target cells into 2W peptide/Poly I:C-immunized perforin-deficient mice (206). WT and perforin-deficient mice generated similar numbers of 2W:I-A^b-specific $CD4^+$ T cells after priming (Fig. 13A). Of the six pathways tested, only deficiency in the Fas pathway caused a significant decrease in specific target cell lysis (Fig. 13B). The dependence of target cell lysis on Fas correlated with induction of FasL expression on the 2W:I-A^b-specific $CD4^+$ effector T cells that formed in response to 2W peptide/Poly I:C immunization (Fig. 13C, 13D). These results suggest that peptide/Poly I:C-induced Th cells kill target cells by inducing FasL to engage Fas expressed on the target cells.

Cytotoxic Th cells have been shown to be protective against viral infections in humans and mice, and $CD4^+$ T cells expressing cytotoxic cell associated markers have been identified following bacterial infections (77, 78, 83, 206). Therefore, we determined whether the Fas pathway is important for cytotoxic Th cell-mediated killing under these conditions. Mice were infected with Lymphocytic Choriomeningitis Virus (LCMV) or *Listeria monocytogenes*-expressing 2W peptide (*Lm*-2W) and Ag-specific $CD4^+$ T cell responses were examined using LCMV GP66:I-A^b or 2W:I-A^b tetramers, respectively. Both infections induced expansion of the relevant $CD4^+$ T cell populations although LCMV induced more than *Lm*-2W (Fig. 14A). In both cases, the relevant $CD4^+$ T cell populations expressed FasL with *Lm*-2W infection driving significantly higher expression

(Fig. 14B). Both the LCMV and *Lm*-2W infected mice showed substantial specific target cell lysis *in vivo*, which was significantly but partially reduced in the case of Fas-deficient target cells (Fig. 14C, 14D). The *Lm*-2W infected mice did not exhibit as robust specific cell lysis as the LCMV infected mice in line with the sizes of their $CD4^+$ T cell responses (Fig. 14A, 14C, 14D). Taken together, these results suggest that the Fas pathway is involved in the killing of target cells by cytotoxic Th cells induced by acute viral and bacterial infections.

The relationship between different T helper subsets and cytotoxic function

The Th subsets induced by peptide/Poly I:C immunization were examined to determine which ones could have been responsible for cytotoxicity. Th1 and Treg cells were identified based on expression of the lineage defining transcription factors T-bet and Foxp3, respectively, while Tfh cells were identified based on expression of the chemokine receptor CXCR5 (Fig. 15A; (44-46, 143, 215). The 2W:I-A^b-specific naïve $CD4^+$ T population in unimmunized mice contains about 10% Treg cells, but no Th1 or Tfh cells (67, 68). In contrast, the 2W:I-A^b-specific effector cell population generated by 2W peptide/Poly I:C immunization consisted of 59% Th1, 3% Treg, 8% Tfh, and 30% cells of unknown lineage (Fig. 15B). T-bet-deficient mice, which do not generate Th1 cells, were then examined to test the cytotoxic potential of this subset (216). The clonal expansion of T-bet-deficient 2W:I-A^b-specific $CD4^+$ T cells was equivalent to their WT counterparts following immunization with 2W peptide/Poly I:C (Fig. 15C). As expected, T-bet-deficient 2W:I-A^b-specific $CD4^+$ T cells did not become Th1 cells (Fig. 15B) or produce IFN-γ after peptide challenge (Fig. 15D) and instead became unknown effector

cells distinct from Tfh or Treg cells (Fig. 15B). Remarkably, 2W-pulsed target cells were killed as efficiently in T-bet-deficient mice as they were in WT mice (Fig. 15E). These results demonstrate that although 2W peptide/Poly I:C immunization induces primarily Th1 cells, the function of these cells is not necessary for Th cell-mediated killing.

The surprising Th cell-mediated cytotoxicity in T-bet-deficient mice warranted investigation of the role of Eomes, another transcription that has been implicated in cytotoxic function (78). About 10% of the 2W:I-A^b-specific $CD4^+$ T cells in 2W/PolyI:C-immunized WT mice expressed Eomes (Fig. 16A, 16B), mainly in T-bet^+ Th1 cells (Fig. 6A). The 2W:I-A^b-specific $CD4^+$ T cells in *Cd4-Cre Eomes$^{fl/fl}$* mice did not express Eomes (Fig. 16A), proliferated (Fig. 16C) and differentiated normally into Th1 cells (Fig. 16A), and demonstrated normal cytotoxicity following 2W/PolyI:C immunization (Fig. 16D). These results demonstrate that Eomes is also not necessary for the generation of Th cell-mediated cytotoxicity after PolyI:C immunization.

The finding that cytotoxic Th function was not a unique property of Th1 cells prompted investigation of other Th subsets. Immunization with CFA was used for this purpose because it induces a diverse $CD4^+$ T cell response including Th17 cells, which were identified by expression of RORγt (47, 217). Mice primed with 2W peptide in CFA generated a large 2W:I-A^b-specific $CD4^+$ T population consisting of $CXCR5^+$ Tfh, T-bet^+ Th1, $Foxp3^+$ Treg, RORγt^+ Th17, or cells of unknown lineage (Fig. 17A) and displayed in vivo cytotoxic activity that was weaker than induced by peptide/Poly I:C immunization (Fig. 17B). Each of the subsets significantly upregulated FasL in comparison to naive $CD4^+$ T cells (Fig. 17C) suggesting that all subsets could be involved in Fas-dependent target cell lysis.

The cytotoxic function of the different T helper subsets was examined using an *in vitro* cytotoxicity assay. The various Th subsets were generated from congenically-marked naïve SM1 TCR transgenic cells (218) capable of expressing ZsGreen from the *Tbx21* promoter (219), after adoptive transfer into B6 recipients primed with CFA containing the Salmonella FliC peptide for which the SM1 TCR is specific. SM1 Th1, Th17, Tfh, and lineage$^-$ cells were sorted based on expression of ZsGreen, CCR6 (220), CXCR5, or lack of all three markers, respectively, and cultured with FliC-pulsed and unpulsed B cells *in vitro*. Each subset lysed target cells in an Ag-dependent manner (Fig. 17E). The lineage$^-$ cells, however, were the worst at inducing cell lysis, which is in line with their lower FasL expression relative to Th1 and Th17 cells (Fig. 17C, 17E). These results demonstrate that many helper T cell subsets have the ability to kill target cells, likely through the Fas pathway.

The role of TCR affinity in regulating cytotoxic Th cell-mediated killing

It was of interest to assess the amount of Fas expressed by target cells given that maximal Th-mediated cytotoxicity depended on this molecule. 2W peptide-pulsed and unpulsed splenocytes were injected into 2W/CFA-primed mice and assayed for Fas expression by flow cytometry after 20 h. B cells that remained in the target cell population that was pulsed with the 2W peptide expressed more Fas than comparable cells that were not pulsed with peptide (Fig. 18A, 18B). This result indicated that Fas was induced on the target cells via cognate interactions with 2W:I-A^b-specific CD4$^+$ T cells. This hypothesis was tested with CD4$^+$ T cells from the B3K508 transgenic strain, which express a TCR that is specific for I-A^b-binding peptides called 3K, P5R, and P2A with

11, 93, and 175 K_D affinities, respectively (Fig. 8C) (144). CD45.1$^+$ B3K508 T cells were transferred into CD45.2$^+$ B6 mice that were then infected with *Lm* expressing 3K peptide (Fig. 18C). By day 7 after infection, the approximately 20,000 transferred naïve B3K508 T cells produced 562,609 ± 388,270 effector cells. On this day, the mice received target cells pulsed with 3K, P5R, or P2A peptides for an *in vivo* cytotoxicity assay and Fas measurement on residual target cells (Fig. 18C). The specific lysis of the target cells correlated with B3K508 TCR affinity for the various peptide:I-A^b complexes, that is, 3K-pulsed target cells were killed more efficiently than P5R-pulsed target cells, which were killed more efficiently than P2A-pulsed target cells (Fig. 18D). Fas induction on the residual peptide-pulsed target cells showed the same positive correlation with TCR affinity for the cognate p:MHCII (Fig. 18E). These results suggest that CD4$^+$ T cells recognize target cells through their TCR and regulate Fas expression on the target cells in a manner that is proportional to their TCR affinity.

5.3 Discussion

Cytotoxic Th cells have been described as either Th1-like cells with cytotoxic function, notable for their high IFN-γ production, Eomes expression, and perforin-dependent cytotoxicity, or as cells that have undergone re-programming to express CD8α and CD8$^+$ T cell-like functions (78, 221-223). Initial studies used 4-1BB agonist antibodies to induce Eomes-expressing cytotoxic CD4$^+$ T cells, while CD4$^+$ T cell re-differentiation into CD8$^+$ T cell-like cells is associated with mucosal tissue (78, 84). In contrast, our studies of peptide:MHCII-specific effector T cells induced by peptide and

Poly I:C revealed a T-bet- and Eomes-independent pathway of cytotoxic Th cell formation that did not involve $CD8^+$ T cell-like re-differentiation. This cytotoxic pathway was also perforin-independent and instead partially relied on Fas expression by target cells. Since Th1, Th17, and Tfh cells expressed FasL and had cytotoxic function after immunization with peptide/CFA, each of these subsets could have been responsible for the cytotoxicity observed in this system. The broad expression of FasL could explain why the induction of Th cell-mediated cytotoxicity does not require the cytokines necessary for Th1, Th2, or Th17 polarization (208). It is important to note, however, that the Fas pathway only accounted for about half of the cytotoxic potential of the peptide/Poly I:C-induced Th cells. Thus, some pathway of cytotoxicity other than those mediated by IFN-γR, TNFRI and II, or TRAIL is also involved.

Our experiments suggest that a cognate T-B cell interaction-based amplification loop regulates Th cell-mediated cytotoxicity. Th cells induced Fas on target cells (194, 224, 225) in proportion to the affinity of their TCRs for the peptide:MHCII ligand displayed by the target cell. These T cells likely also expressed CD40L, which is a transient consequence of TCR signaling (226). Although Fas is induced on B cells by pattern recognition receptor signaling, expression could have been enhanced on the target B cells by signals from CD40 engaged by CD40L on the interacting Th cell (227-229). CD40 signaling enhances Fas-induced apoptosis in B cells that do not simultaneously receive signals through their surface Ig receptors (230). This could have occurred in our experiments since it is likely that very few of the 2W peptide-pulsed B cells that were used as target cells were specific for the 2W-peptide since they came from naïve mice.

The capacity of Th cells to induce Fas on their targets cells could improve the efficiency of their cytotoxicity.

Cytotoxic $CD4^+$ T cells are induced during persistent infections (106, 223, 231). The findings presented here and in work by others (232, 233) demonstrate that cytotoxic Th cells are also induced during acute viral and bacterial infections. Although there is no doubt that cytotoxic $CD8^+$ T cells play a major role in the control of these infections (232, 233), the surprising potency of cytotoxic Th cells (234, 235) indicates that they may also contribute. Future work will need to be carried out for a more complete understanding of cytotoxic Th cell activity in the context of different infections.

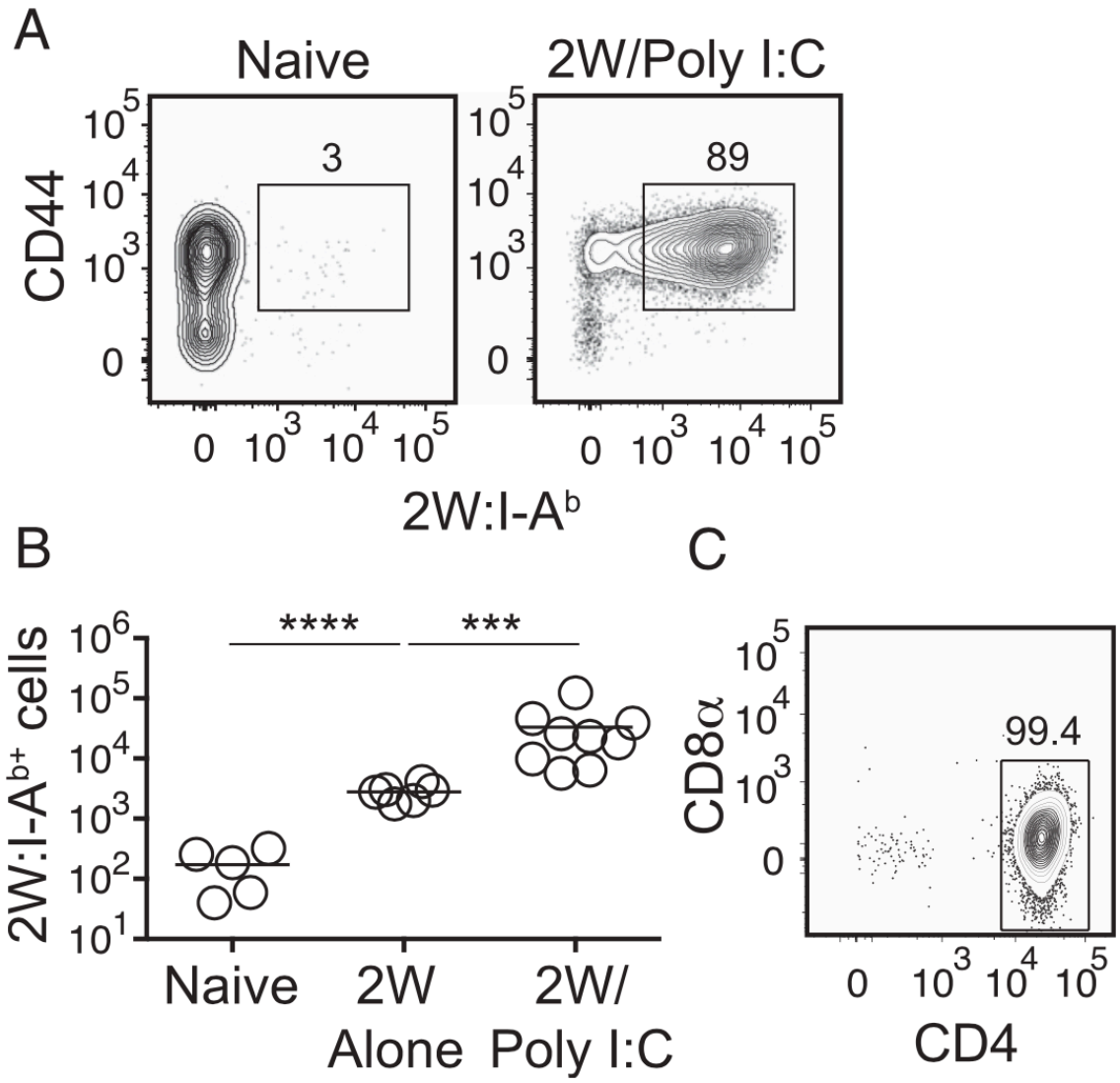

Figure 11. Poly I:C immunization induces robust CD4$^+$ T cell responses.

(A) Flow cytometric analysis of B220$^-$ CD11b$^-$ CD11c$^-$ 2W:I-A^b tetramer-enriched cells from a naïve mouse or a mouse 7 days after 2W peptide/Poly I:C immunization. (B) Number of 2W:I-A^{b+} CD4$^+$ T cells in individual naïve or immunized mice, 7 days post-immunization with 2W peptide alone or 2W peptide/Poly I:C (n=5-9/group). (C) Representative flow cytometric analysis of CD4 and CD8α expression by 2W:I-A^{b+} CD4$^+$ T cells from 2W peptide/Poly I:C immunized mice. The bars in B represent the mean for

each group. Pooled data from two independent experiments are shown. One-way ANOVA was used to determine significance. *** = $p < 0.001$, **** = $p < 0.0001$.

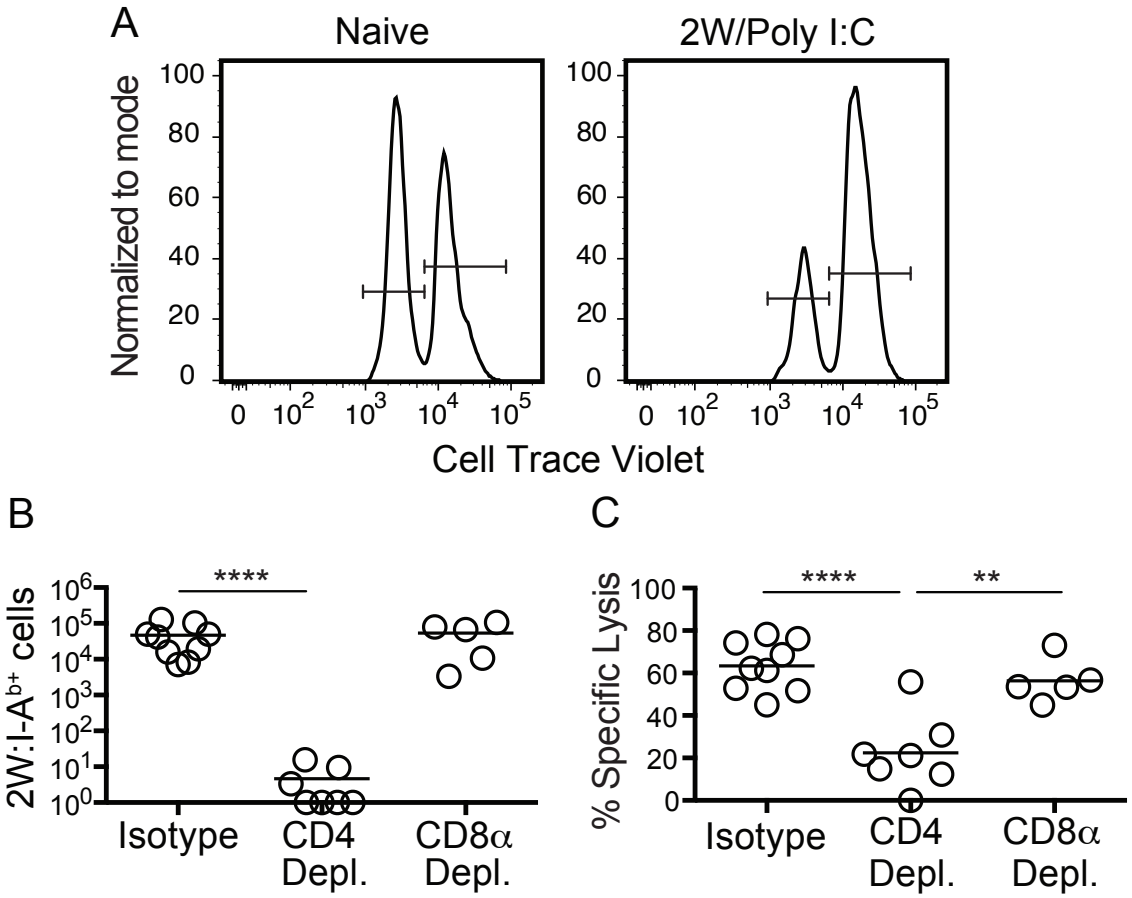

Figure 12. Poly I:C immunization generates cytotoxic Th cells.

(A) Representative flow cytometric analysis of an *in vivo* cytotoxicity assay utilizing CTV to identify 2W peptide-presenting (CTV^{low}) and non-presenting (CTV^{high}) $B220^+$ target cells 20 h after their injection into naïve or 2W peptide/Poly I:C immunized mice. (B) Number of 2W:I-A^{b+} $CD4^+$ T cells and (C) specific cell lysis following an *in vivo* cytotoxicity assay in mice 7 days after immunization with 2W peptide/Poly I:C and after injection of isotype control, CD4, or CD8α depleting antibody (n=5-9/group). The bars in B and C represent the mean for each group. Pooled data from two independent experiments are shown. One-way ANOVA was used to determine significance. ** = $p < 0.01$, **** = $p < 0.0001$.

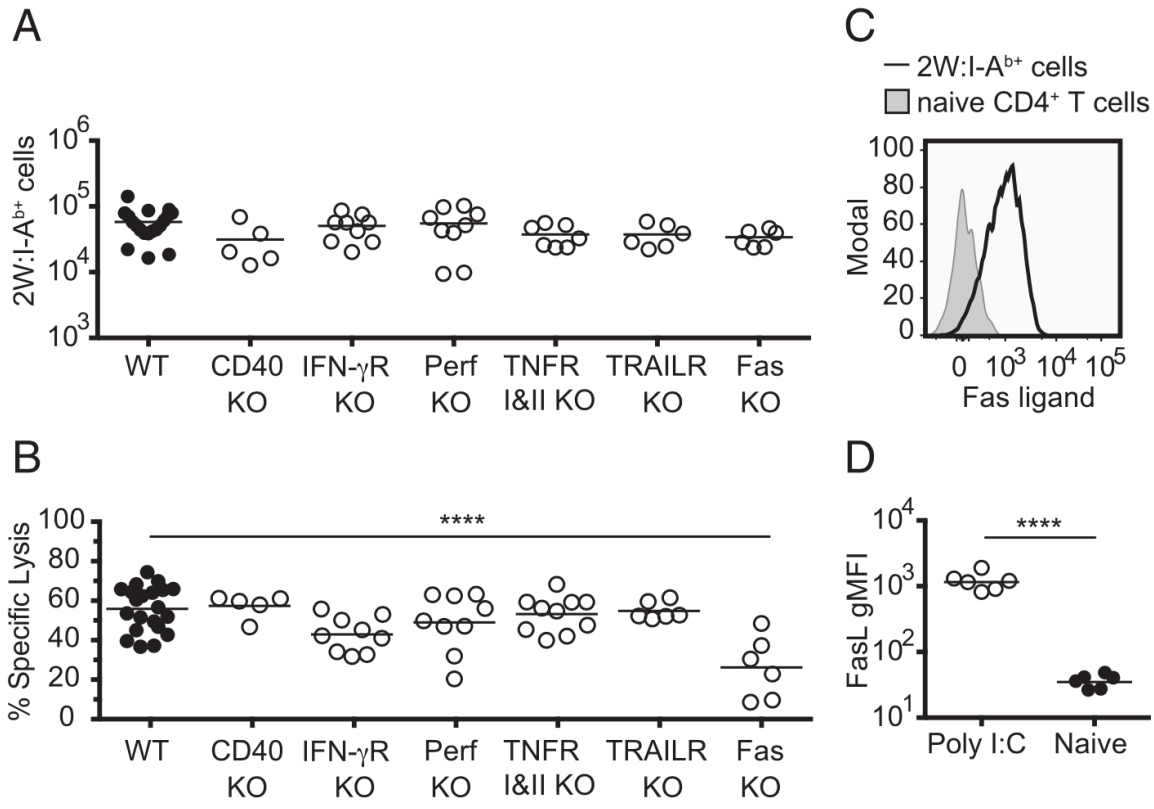

Figure 13. Cytotoxic Th cells generated with Poly I:C primarily utilize the Fas pathway for cytotoxicity.

Mice were examined 7 days after immunization with 2W peptide/Poly I:C. (A) Number of 2W:I-A^{b+} $CD4^+$ T cells and (B) specific cell lysis following an *in vivo* cytotoxicity assay in WT mice that received WT, CD40-deficient, IFN-γ receptor-deficient, TNFα receptor I and II-deficient, TRAIL receptor-deficient or Fas-deficient target cells. Perforin-deficient mice that received WT target cells are also shown (n=5-21/group). (C) Representative flow cytometric analysis of FasL expression by 2W:I-A^{b+} $CD4^+$ T cells (line) or naïve $CD4^+$ T cells (grey). (D) Geometric mean fluorescence intensity of FasL on 2W:I-A^{b+} $CD4^+$ T cells from 2W peptide/Poly I:C immunized or naïve $CD44^{low}$ $CD4^+$ T cells (n=6/group). The bars in A, B, and D represent means. Pooled data from two

independent experiments are shown. One-way ANOVA was used to determine significance for A and B while Student's t test was used for D. **** = $p < 0.0001$.

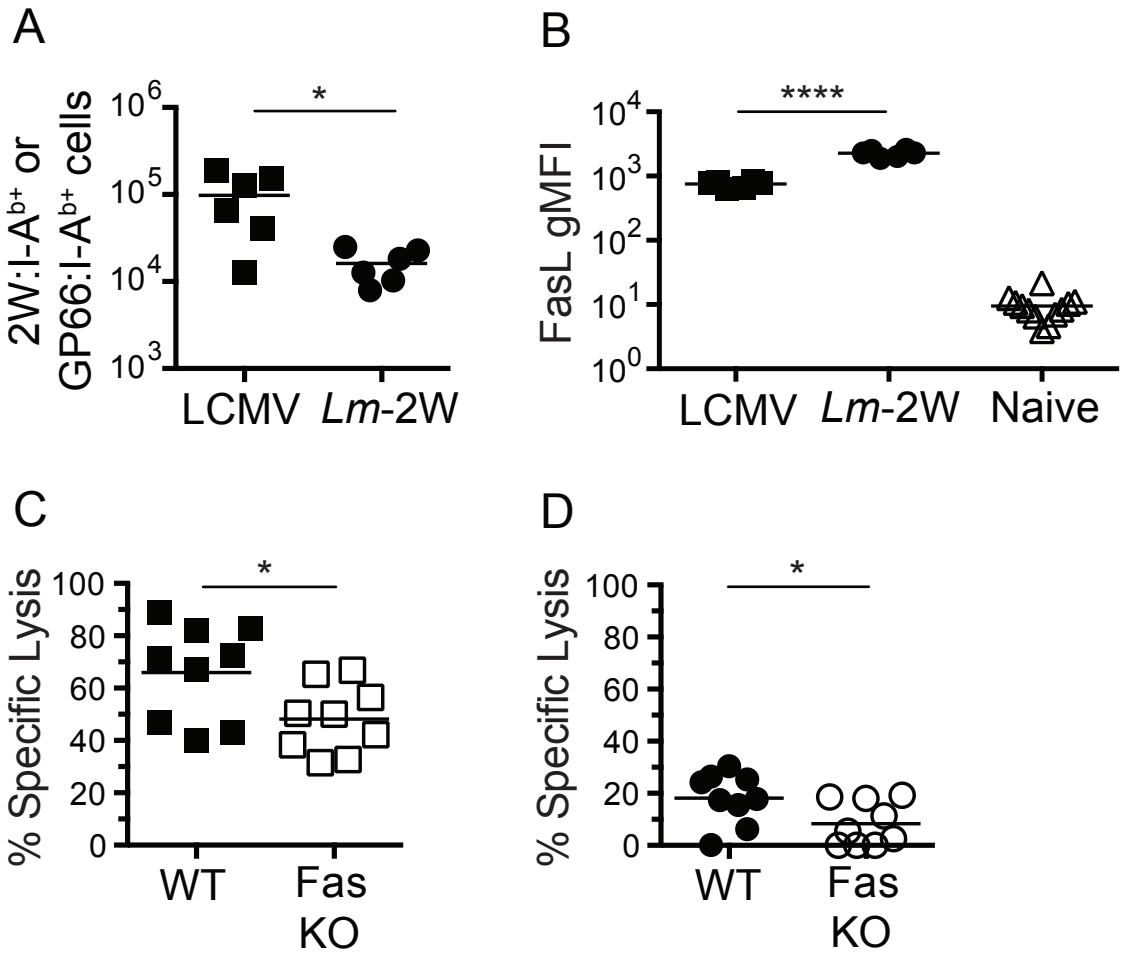

Figure 14. Cytotoxic Th cells primarily utilizing the Fas pathway are induced by LCMV and *Lm* infections.

(A) Number of GP66:I-A^{b+} CD4$^+$ T cells following LCMV infection and 2W:I-A^{b+} CD4$^+$ T cells following *Lm*-2W infection (n = 6/group). (B) Geometric mean fluorescence intensity of FasL on GP66:I-A^{b+} CD4$^+$ T cells from LCMV infected mice, 2W:I-A^{b+} CD4$^+$ T cells from *Lm*-2W infected mice on day 7 post-infection, or naïve CD44^{low} CD4$^+$ T cells (n=6-12/group). Specific cell lysis of WT or Fas-deficient target cells following in mice infected 7 days earlier with (C) LCMV or (D) *Lm*-2W (n=9/group). The bars in A,

B, C, and D represent means. Pooled data from two independent experiments are shown. Student's t-test was used to determine significance. * = $p < 0.05$, **** = $p < 0.0001$.

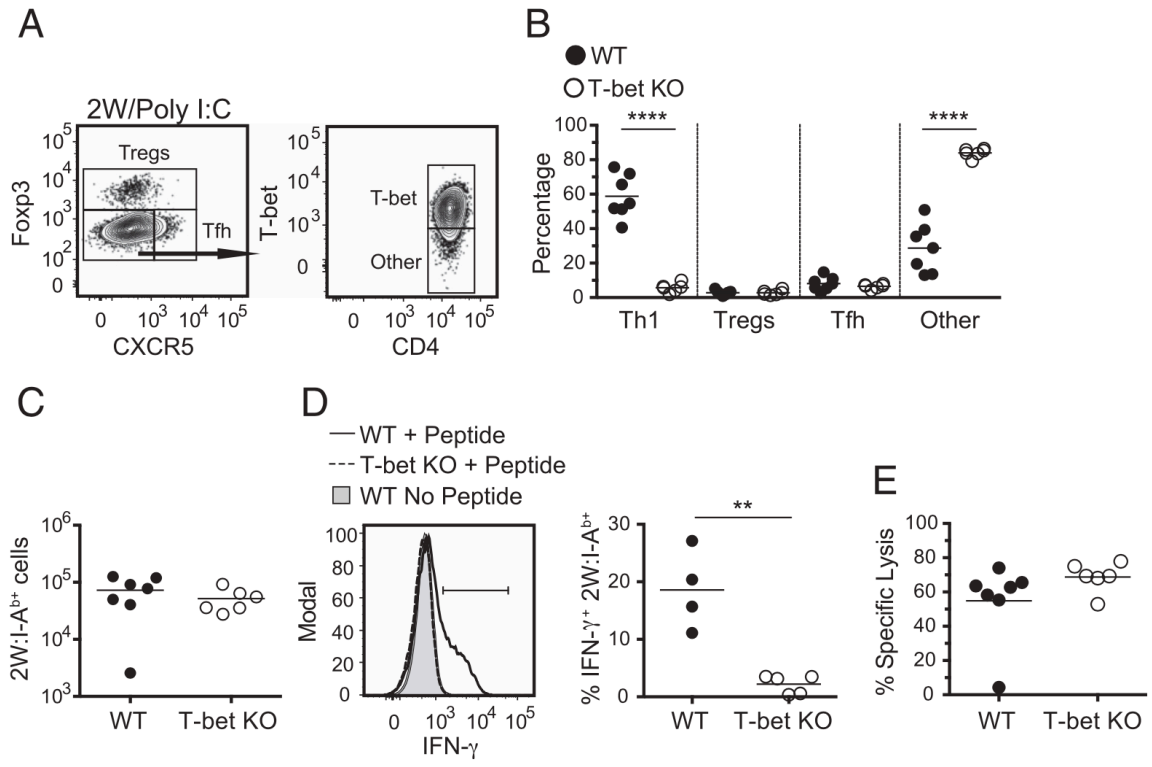

Figure 15. Poly I:C induced CD4$^+$ T cell cytotoxic function is T-bet independent.

2W:I-A^{b+} CD4$^+$ T cells were examined from mice 7 days after immunization with 2W peptide/Poly I:C. (A) Flow cytometric analysis of 2W:I-A^{b+} CD4$^+$ T cell subsets with the gating strategy for Treg, Tfh, Th1, and other cells. (B) Percentage of 2W:I-A^{b+} CD4$^+$ T cells that differentiated into Th1, Treg, Tfh, or other cells in WT or T-bet-deficient mice (n=6-7/group). (C) Number of 2W:I-A^{b+} CD4$^+$ T cells in WT or T-bet-deficient mice (n=6-7/group) after immunization with 2W peptide/Poly I:C. (D) WT and T-bet-deficient mice were immunized with 2W peptide/Poly I:C and injected 7 days later with 2W peptide. The histograms depict IFN-γ production by 2W:I-A^{b+} CD4$^+$ T cells in WT mice (line) or T-bet-deficient mice (dashed line) 2 h after peptide challenge, or WT mice (grey) that were not challenged, with the gate identifying IFN-γ producing cells. The scatterplot shows IFN-γ production in 2W peptide-challenged mice in individual WT or

T-bet-deficient mice (n=4-5/group). (E) Specific cell lysis following an *in vivo* cytotoxicity assay in mice 7 days after immunization with 2W peptide/Poly I:C. The bars in B, C, D, and E represent means. Pooled data from two independent experiments are shown. One-way ANOVA was used to determine significance for B while Student's t test was used for C, D, and E. ** = $p < 0.01$, **** = $p < 0.0001$.

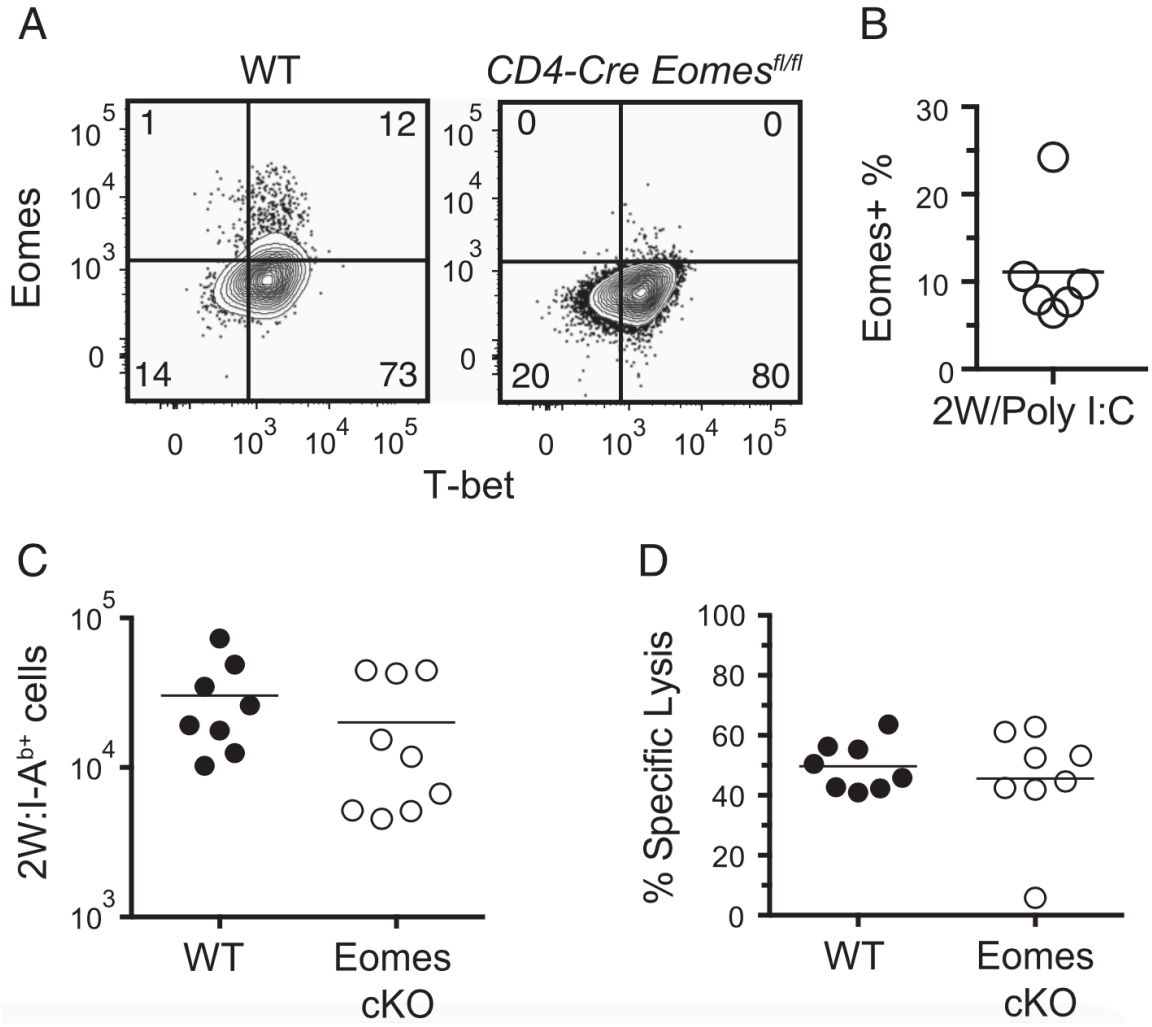

Figure 16. Poly I:C-induced CD4$^+$ T cell cytotoxic function is Eomes independent. 2W:I-A^{b+} CD4$^+$ T cells were examined from mice 7 days after immunization with 2W peptide/Poly I:C. (A) Representative flow cytometric analysis of Eomes and T-bet expression by 2W:I-A^{b+} CD4$^+$ T cells from immunized WT or Eomes conditional knockout mice. (B) Percentage of 2W:I-A^{b+} CD4$^+$ T cells that express Eomes. (C) Number of 2W:I-A^{b+} CD4$^+$ T cells and (D) specific cell lysis following an *in vivo* cytotoxicity assay in WT or Eomes conditional knockout mice (n=8-9/group). The bars in B, C, and D represent means. Pooled data from two independent experiments are shown. Student's t test was used to determine significance for C and D.

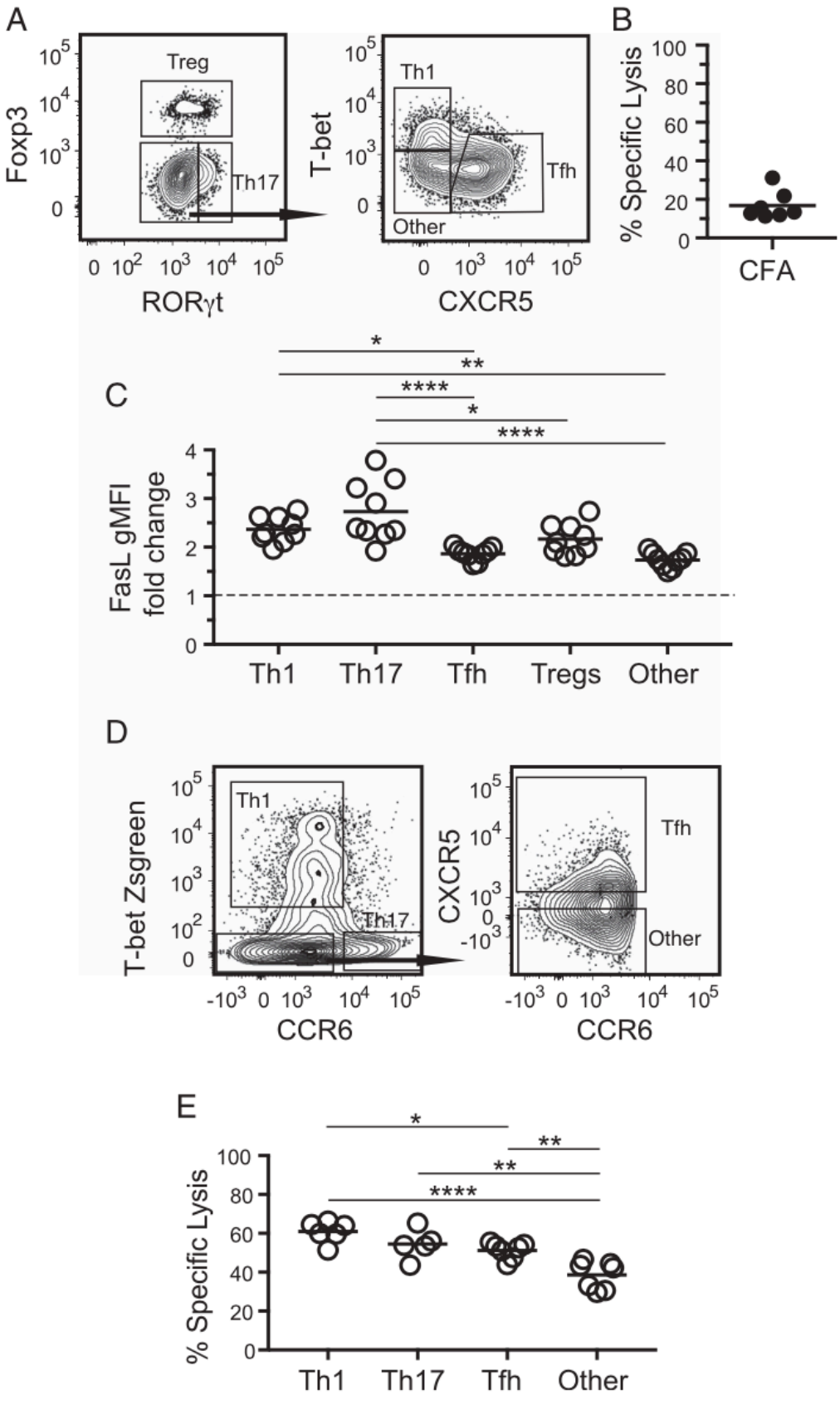
A
Foxp3
Treg
Th17
RORγt
T-bet
Th1
Tfh
Other
CXCR5
B
% Specific Lysis
CFA
C
FasL gMFI fold change
Th1
Th17
Tfh
Tregs
Other
D
T-bet Zsgreen
CCR6
CXCR5
E
% Specific Lysis

Figure 17. FasL expression is conserved across all T helper subsets generated by CFA immunization.

(A) Flow cytometric analysis of 2W:I-A^{b+} $CD4^+$ T cell subsets 7 days after 2W peptide/CFA immunization with the gating strategy for Treg, Th17, Th1, Tfh and other cells. (B) Specific cell lysis following an *in vivo* cytotoxicity assay in mice 7 days after immunization with 2W peptide/CFA (n=7). (C) Fold change in geometric mean fluorescence intensity of FasL on Th1, Th17, Tfh, Treg, or other 2W:I-A^{b+} $CD4^+$ T cells relative to naïve $CD44^{low}$ $CD4^+$ T cells from 2W peptide/CFA immunized mice (n=11/group). (D) Gating strategy for sort-purifying Th1, Th17, Tfh and other SM1 *Tbx21*^{ZsGreen} TCR transgenic $CD4^+$ T cells from adoptive recipient mice 7 days post-immunization with FliC/CFA. (E) Specific cell lysis following an *in vitro* cytotoxicity assay using sort-purified Th1, Th17, Tfh, or other SM1 cells. The bars in B, C, and E represent means. Pooled data from two independent experiments are shown. One-way ANOVA was used to determine significance. * = $p < 0.05$, ** = $p < 0.01$, **** = $p < 0.0001$.

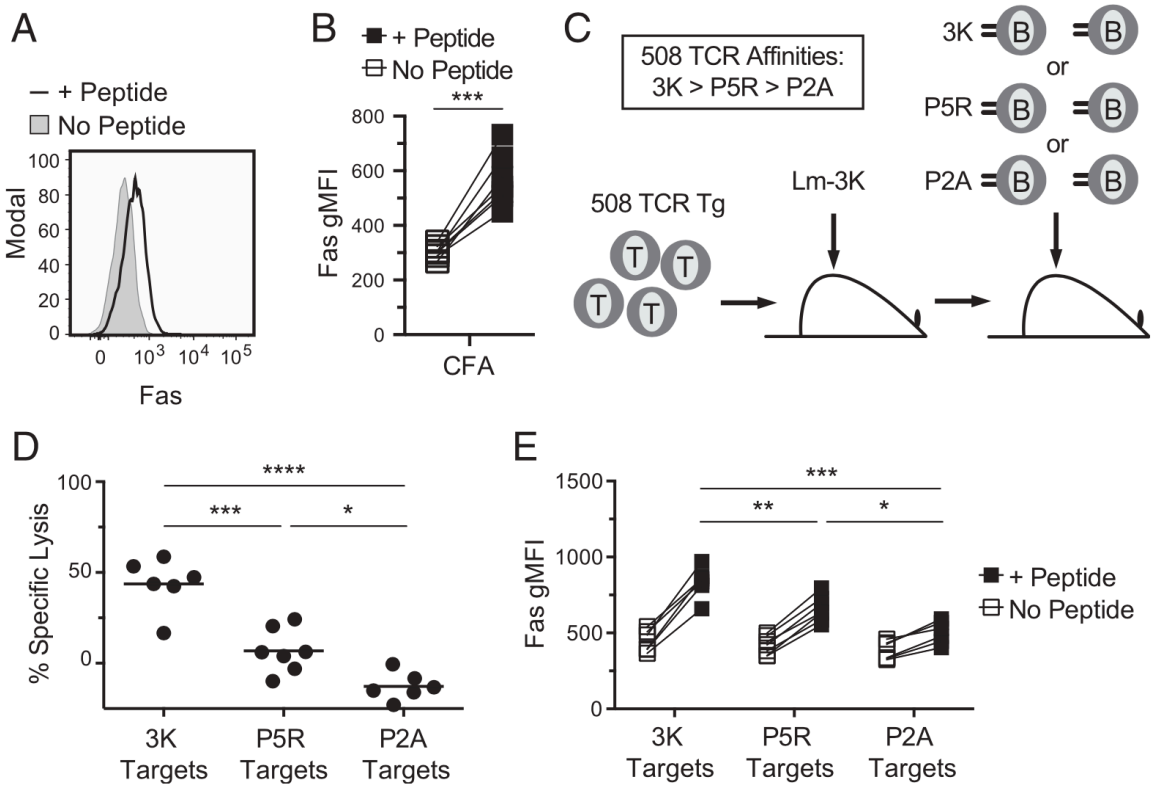

Figure 18. The induction of Fas on target cells correlates with the T cell receptor affinity of responding CD4$^+$ T cells.

(A) Representative flow cytometric analysis of Fas expression and (B) Geometric mean fluorescence intensity of Fas staining on 2W peptide-presenting (line) or non-presenting (grey) target cells after an *in vivo* cytotoxicity assay in 2W peptide/CFA immunized mice. Lines in (B) indicate target cells from the same mouse. (C) Illustration of the adoptive transfer model system for examining the influence of TCR affinity on specific cell lysis and Fas expression. (D) Specific cell lysis following an *in vivo* cytotoxicity assay in mice infected with *Lm*-expressing 3K (n=6-7/group). (E) Fas geometric mean fluorescence intensity on peptide-presenting or non-presenting target cells after an *in vivo* cytotoxicity assay in *Lm*-expressing 3K infected mice. Lines indicate target cells from the same mouse. The bars in D represent means. Pooled data from two independent

experiments are shown. One-way ANOVA was used to determine significance for D and E while Student's t test was used for B. * = $p < 0.05$, ** = $p < 0.01$, *** = $p < 0.001$, **** = $p < 0.0001$.

Chapter 6

Conclusions

The primary focus of my thesis is identifying how TCR affinity for p:MHCII biases helper T cell responses. One of our main interests was identifying the mechanism by which TCR affinity influences the bifurcation of Tfh and non-Tfh differentiation. Due to differences in antigen presentation on MHCII and polarizing cytokine production between the DC subsets, we hypothesized that TCR affinity skewed T cell-DC interactions to favor one DC subset (39, 42). The prediction was that low TCR affinity cells favored SIRPα DCs because of their greater antigen presentation, while high affinity T cells would interact with XCR1 and SIRPα DCs. Thus, the high affinity cells would receive Th1 polarizing signals from XCR1 DCs, while low affinity cells would not.

To test this hypothesis, we developed the image analysis software described in Chapter 3 that substantially expedites analysis of T cell-DC interactions. This software reduced hands-on image analysis time by up to 90% and is compatible with epi-fluorescence, confocal, and two-photon microscopy images. We also described an analysis approach that uses fluorescent signal absorption from surrounding cells to quantify cell localization within tissues. This novel technique accurately quantified T cell localization when compared to a different counting method that directly measured localization. Additionally, this new approach required less steps and time than the direct counting method.

With the improved image analysis pipeline, we sought to identify the mechanism by which TCR affinity regulates T cell differentiation, as presented in Chapter 4. To our surprise, TCR affinity did not bias T cell-DC interactions towards either DC subset, suggesting that TCR affinity influences differentiation in a T cell intrinsic manner. The field has primarily focused on *Irf4* and *Il2ra* as TCR regulated genes that affect differentiation, but it is likely that many genes play a similar role (72, 155). Therefore, we sought to identify novel TCR modulated genes that impact lineage commitment. An in vivo CRISPR/Cas9 screen identified two novel hits, *Eef1e1* and *Gbp2*. *Eef1e1* promoted Th1 differentiation, while *Gbp2* enhanced Tfh differentiation. The expectation for this screen was that only Th1-promoting or Tfh-inhibiting genes would be identified, as higher TCR signaling drives cells towards the Th1 lineage. Positive signals are, however, required for T cells to adopt any fate. For example, low affinity T cells will display signs of activation following antigen exposure but lack expression of lineage defining markers, suggesting they are uncommitted. Thus, for a T cell with medium TCR affinity to adopt the Tfh fate, TCR signaling should induce some Tfh promoting genes, like *Gbp2*.

Chapter 5 also focused on differentiation, but examined cytotoxic function rather than Tfh lineage commitment. Previous work suggested that cytotoxic $CD4^+$ T cells are a unique fate with Eomes as the master transcription factor (78, 82, 86). We identified that many helper T cell subsets have cytotoxic potential via the Fas pathway and Eomes was unnecessary for their cytotoxic function. Additionally, TCR affinity regulated specific cell lysis of target cells with higher TCR affinity correlating to greater Fas expression on target cells.

In summary, TCR affinity influences T cell differentiation by regulating expression of lineage establishing genes. TCR affinity also modifies T cell functions, like cytotoxicity, by directing expression of effector molecules, such as Fas ligand. These findings inform the design of potential vaccines that focus on eliciting a specific pattern of helper T cell differentiation, like a cancer vaccine that seeks to exploit cytotoxic $CD4^+$ T cells to kill MHCII expressing cancer cells.

References

1. Gowans, J. L., G. D. Mc, and D. M. Cowen. 1962. Initiation of immune responses by small lymphocytes. *Nature* 196: 651-655.
2. Miller, J. F. 1961. Immunological function of the thymus. *Lancet* 2: 748-749.
3. Cooper, M. D., R. D. Peterson, and R. A. Good. 1965. Delineation of the Thymic and Bursal Lymphoid Systems in the Chicken. *Nature* 205: 143-146.
4. Mitchell, G. F., and J. F. Miller. 1968. Cell to cell interaction in the immune response. II. The source of hemolysin-forming cells in irradiated mice given bone marrow and thymus or thoracic duct lymphocytes. *J Exp Med* 128: 821-837.
5. Miller, J. F., and G. F. Mitchell. 1968. Cell to cell interaction in the immune response. I. Hemolysin-forming cells in neonatally thymectomized mice reconstituted with thymus or thoracic duct lymphocytes. *J Exp Med* 128: 801-820.
6. Nossal, G. J., A. Cunningham, G. F. Mitchell, and J. F. Miller. 1968. Cell to cell interaction in the immune response. 3. Chromosomal marker analysis of single antibody-forming cells in reconstituted, irradiated, or thymectomized mice. *J Exp Med* 128: 839-853.
7. Zinkernagel, R. M., and P. C. Doherty. 1974. Immunological surveillance against altered self components by sensitised T lymphocytes in lymphocytic choriomeningitis. *Nature* 251: 547-548.
8. Zinkernagel, R. M., and P. C. Doherty. 1974. Restriction of in vitro T cell-mediated cytotoxicity in lymphocytic choriomeningitis within a syngeneic or semiallogeneic system. *Nature* 248: 701-702.
9. Doherty, P. C., and R. M. Zinkernagel. 1975. A biological role for the major histocompatibility antigens. *Lancet* 1: 1406-1409.
10. Reinherz, E. L., S. Meuer, K. A. Fitzgerald, R. E. Hussey, H. Levine, and S. F. Schlossman. 1982. Antigen recognition by human T lymphocytes is linked to surface expression of the T3 molecular complex. *Cell* 30: 735-743.
11. Meuer, S. C., K. A. Fitzgerald, R. E. Hussey, J. C. Hodgdon, S. F. Schlossman, and E. L. Reinherz. 1983. Clonotypic structures involved in antigen-specific human T cell function. Relationship to the T3 molecular complex. *J Exp Med* 157: 705-719.
12. Haskins, K., R. Kubo, J. White, M. Pigeon, J. Kappler, and P. Marrack. 1983. The major histocompatibility complex-restricted antigen receptor on T cells. I. Isolation with a monoclonal antibody. *J Exp Med* 157: 1149-1169.
13. Reinherz, E. L., S. C. Meuer, K. A. Fitzgerald, R. E. Hussey, J. C. Hodgdon, O. Acuto, and S. F. Schlossman. 1983. Comparison of T3-associated 49- and 43-kilodalton cell surface molecules on individual human T-cell clones: evidence for peptide variability in T-cell receptor structures. *Proc Natl Acad Sci U S A* 80: 4104-4108.
14. Meuer, S. C., O. Acuto, R. E. Hussey, J. C. Hodgdon, K. A. Fitzgerald, S. F. Schlossman, and E. L. Reinherz. 1983. Evidence for the T3-associated 90K heterodimer as the T-cell antigen receptor. *Nature* 303: 808-810.
15. Kappler, J., R. Kubo, K. Haskins, J. White, and P. Marrack. 1983. The mouse T cell receptor: comparison of MHC-restricted receptors on two T cell hybridomas. *Cell* 34: 727-737.

16. Chien, Y., D. M. Becker, T. Lindsten, M. Okamura, D. I. Cohen, and M. M. Davis. 1984. A third type of murine T-cell receptor gene. *Nature* 312: 31-35.
17. Patten, P., T. Yokota, J. Rothbard, Y. Chien, K. Arai, and M. M. Davis. 1984. Structure, expression and divergence of T-cell receptor beta-chain variable regions. *Nature* 312: 40-46.
18. Gascoigne, N. R., Y. Chien, D. M. Becker, J. Kavaler, and M. M. Davis. 1984. Genomic organization and sequence of T-cell receptor beta-chain constant- and joining-region genes. *Nature* 310: 387-391.
19. Chien, Y. H., N. R. Gascoigne, J. Kavaler, N. E. Lee, and M. M. Davis. 1984. Somatic recombination in a murine T-cell receptor gene. *Nature* 309: 322-326.
20. Hedrick, S. M., D. I. Cohen, E. A. Nielsen, and M. M. Davis. 1984. Isolation of cDNA clones encoding T cell-specific membrane-associated proteins. *Nature* 308: 149-153.
21. Hedrick, S. M., E. A. Nielsen, J. Kavaler, D. I. Cohen, and M. M. Davis. 1984. Sequence relationships between putative T-cell receptor polypeptides and immunoglobulins. *Nature* 308: 153-158.
22. Yoshikai, Y., D. Anatoniou, S. P. Clark, Y. Yanagi, R. Sangster, P. Van den Elsen, C. Terhorst, and T. W. Mak. 1984. Sequence and expression of transcripts of the human T-cell receptor beta-chain genes. *Nature* 312: 521-524.
23. Clark, S. P., Y. Yoshikai, S. Taylor, G. Siu, L. Hood, and T. W. Mak. 1984. Identification of a diversity segment of human T-cell receptor beta-chain, and comparison with the analogous murine element. *Nature* 311: 387-389.
24. Yanagi, Y., Y. Yoshikai, K. Leggett, S. P. Clark, I. Aleksander, and T. W. Mak. 1984. A human T cell-specific cDNA clone encodes a protein having extensive homology to immunoglobulin chains. *Nature* 308: 145-149.
25. Nikolich-Zugich, J., M. K. Slifka, and I. Messaoudi. 2004. The many important facets of T-cell repertoire diversity. *Nat Rev Immunol* 4: 123-132.
26. Davis, M. M., and P. J. Bjorkman. 1988. T-cell antigen receptor genes and T-cell recognition. *Nature* 334: 395-402.
27. Reinherz, E. L., P. C. Kung, G. Goldstein, and S. F. Schlossman. 1979. Separation of functional subsets of human T cells by a monoclonal antibody. *Proc Natl Acad Sci U S A* 76: 4061-4065.
28. Reinherz, E. L., P. C. Kung, G. Goldstein, and S. F. Schlossman. 1980. A monoclonal antibody reactive with the human cytotoxic/suppressor T cell subset previously defined by a heteroantiserum termed TH2. *J Immunol* 124: 1301-1307.
29. Starr, T. K., S. C. Jameson, and K. A. Hogquist. 2003. Positive and negative selection of T cells. *Annu Rev Immunol* 21: 139-176.
30. Klein, L., B. Kyewski, P. M. Allen, and K. A. Hogquist. 2014. Positive and negative selection of the T cell repertoire: what thymocytes see (and don't see). *Nat Rev Immunol* 14: 377-391.
31. Anderson, M. S., E. S. Venanzi, L. Klein, Z. Chen, S. P. Berzins, S. J. Turley, H. von Boehmer, R. Bronson, A. Dierich, C. Benoist, and D. Mathis. 2002. Projection of an immunological self shadow within the thymus by the aire protein. *Science* 298: 1395-1401.
32. Stritesky, G. L., Y. Xing, J. R. Erickson, L. A. Kalekar, X. Wang, D. L. Mueller, S. C. Jameson, and K. A. Hogquist. 2013. Murine thymic selection quantified using a unique method to capture deleted T cells. *Proc Natl Acad Sci U S A* 110: 4679-4684.

33. Steinman, R. M., and Z. A. Cohn. 1973. Identification of a novel cell type in peripheral lymphoid organs of mice. I. Morphology, quantitation, tissue distribution. *J Exp Med* 137: 1142-1162.
34. Steinman, R. M., and M. D. Witmer. 1978. Lymphoid dendritic cells are potent stimulators of the primary mixed leukocyte reaction in mice. *Proc Natl Acad Sci U S A* 75: 5132-5136.
35. Jenkins, M. K., and R. H. Schwartz. 1987. Antigen presentation by chemically modified splenocytes induces antigen-specific T cell unresponsiveness in vitro and in vivo. *J Exp Med* 165: 302-319.
36. Mueller, D. L., M. K. Jenkins, and R. H. Schwartz. 1989. Clonal expansion versus functional clonal inactivation: a costimulatory signalling pathway determines the outcome of T cell antigen receptor occupancy. *Annu Rev Immunol* 7: 445-480.
37. Guermonprez, P., J. Valladeau, L. Zitvogel, C. Thery, and S. Amigorena. 2002. Antigen presentation and T cell stimulation by dendritic cells. *Annu Rev Immunol* 20: 621-667.
38. Guilliams, M., C. A. Dutertre, C. L. Scott, N. McGovern, D. Sichien, S. Chakarov, S. Van Gassen, J. Chen, M. Poidinger, S. De Prijck, S. J. Tavernier, I. Low, S. E. Irac, C. N. Mattar, H. R. Sumatoh, G. H. L. Low, T. J. K. Chung, D. K. H. Chan, K. K. Tan, T. L. K. Hon, E. Fossum, B. Bogen, M. Choolani, J. K. Y. Chan, A. Larbi, H. Luche, S. Henri, Y. Saeys, E. W. Newell, B. N. Lambrecht, B. Malissen, and F. Ginhoux. 2016. Unsupervised High-Dimensional Analysis Aligns Dendritic Cells across Tissues and Species. *Immunity* 45: 669-684.
39. Dudziak, D., A. O. Kamphorst, G. F. Heidkamp, V. R. Buchholz, C. Trumpfheller, S. Yamazaki, C. Cheong, K. Liu, H. W. Lee, C. G. Park, R. M. Steinman, and M. C. Nussenzweig. 2007. Differential antigen processing by dendritic cell subsets in vivo. *Science* 315: 107-111.
40. Hor, J. L., P. G. Whitney, A. Zaid, A. G. Brooks, W. R. Heath, and S. N. Mueller. 2015. Spatiotemporally Distinct Interactions with Dendritic Cell Subsets Facilitates CD4+ and CD8+ T Cell Activation to Localized Viral Infection. *Immunity* 43: 554-565.
41. Mosmann, T. R., H. Cherwinski, M. W. Bond, M. A. Giedlin, and R. L. Coffman. 1986. Two types of murine helper T cell clone. I. Definition according to profiles of lymphokine activities and secreted proteins. *J Immunol* 136: 2348-2357.
42. Muzaki, A. R., P. Tetlak, J. Sheng, S. C. Loh, Y. A. Setiagani, M. Poidinger, F. Zolezzi, K. Karjalainen, and C. Ruedl. 2016. Intestinal CD103(+)CD11b(-) dendritic cells restrain colitis via IFN-gamma-induced anti-inflammatory response in epithelial cells. *Mucosal Immunol* 9: 336-351.
43. Alexandre, Y. O., S. Ghilas, C. Sanchez, A. Le Bon, K. Crozat, and M. Dalod. 2016. XCR1+ dendritic cells promote memory CD8+ T cell recall upon secondary infections with Listeria monocytogenes or certain viruses. *J Exp Med* 213: 75-92.
44. Fontenot, J. D., M. A. Gavin, and A. Y. Rudensky. 2003. Foxp3 programs the development and function of CD4+CD25+ regulatory T cells. *Nat Immunol* 4: 330-336.
45. Hori, S., T. Nomura, and S. Sakaguchi. 2003. Control of regulatory T cell development by the transcription factor Foxp3. *Science* 299: 1057-1061.
46. Szabo, S. J., S. T. Kim, G. L. Costa, X. Zhang, C. G. Fathman, and L. H. Glimcher. 2000. A novel transcription factor, T-bet, directs Th1 lineage commitment. *Cell* 100: 655-669.
47. Ivanov, II, B. S. McKenzie, L. Zhou, C. E. Tadokoro, A. Lepelley, J. J. Lafaille, D. J. Cua, and D. R. Littman. 2006. The orphan nuclear receptor RORgammat

directs the differentiation program of proinflammatory IL-17+ T helper cells. *Cell* 126: 1121-1133.
48. Johnston, R. J., A. C. Poholek, D. DiToro, I. Yusuf, D. Eto, B. Barnett, A. L. Dent, J. Craft, and S. Crotty. 2009. Bcl6 and Blimp-1 are reciprocal and antagonistic regulators of T follicular helper cell differentiation. *Science* 325: 1006-1010.
49. Lee, H. J., N. Takemoto, H. Kurata, Y. Kamogawa, S. Miyatake, A. O'Garra, and N. Arai. 2000. GATA-3 induces T helper cell type 2 (Th2) cytokine expression and chromatin remodeling in committed Th1 cells. *J Exp Med* 192: 105-115.
50. Zhang, D. H., L. Cohn, P. Ray, K. Bottomly, and A. Ray. 1997. Transcription factor GATA-3 is differentially expressed in murine Th1 and Th2 cells and controls Th2-specific expression of the interleukin-5 gene. *J Biol Chem* 272: 21597-21603.
51. Liu, Z., M. Y. Gerner, N. Van Panhuys, A. G. Levine, A. Y. Rudensky, and R. N. Germain. 2015. Immune homeostasis enforced by co-localized effector and regulatory T cells. *Nature* 528: 225-230.
52. Linehan, J. L., T. Dileepan, S. W. Kashem, D. H. Kaplan, P. Cleary, and M. K. Jenkins. 2015. Generation of Th17 cells in response to intranasal infection requires TGF-beta1 from dendritic cells and IL-6 from CD301b+ dendritic cells. *Proc Natl Acad Sci U S A* 112: 12782-12787.
53. Dileepan, T., J. L. Linehan, J. J. Moon, M. Pepper, M. K. Jenkins, and P. P. Cleary. 2011. Robust antigen specific th17 T cell response to group A Streptococcus is dependent on IL-6 and intranasal route of infection. *PLoS Pathog* 7: e1002252.
54. Yang, J. A., N. J. Tubo, M. D. Gearhart, V. J. Bardwell, and M. K. Jenkins. 2015. Cutting edge: Bcl6-interacting corepressor contributes to germinal center T follicular helper cell formation and B cell helper function. *J Immunol* 194: 5604-5608.
55. Anthony, R. M., L. I. Rutitzky, J. F. Urban, Jr., M. J. Stadecker, and W. C. Gause. 2007. Protective immune mechanisms in helminth infection. *Nat Rev Immunol* 7: 975-987.
56. Pepper, M., J. L. Linehan, A. J. Pagan, T. Zell, T. Dileepan, P. P. Cleary, and M. K. Jenkins. 2010. Different routes of bacterial infection induce long-lived TH1 memory cells and short-lived TH17 cells. *Nat Immunol* 11: 83-89.
57. Korn, T., M. Mitsdoerffer, A. L. Croxford, A. Awasthi, V. A. Dardalhon, G. Galileos, P. Vollmar, G. L. Stritesky, M. H. Kaplan, A. Waisman, V. K. Kuchroo, and M. Oukka. 2008. IL-6 controls Th17 immunity in vivo by inhibiting the conversion of conventional T cells into Foxp3+ regulatory T cells. *Proc Natl Acad Sci U S A* 105: 18460-18465.
58. Nance, J. P., S. Belanger, R. J. Johnston, J. K. Hu, T. Takemori, and S. Crotty. 2015. Bcl6 middle domain repressor function is required for T follicular helper cell differentiation and utilizes the corepressor MTA3. *Proc Natl Acad Sci U S A* 112: 13324-13329.
59. Nance, J. P., S. Belanger, R. J. Johnston, T. Takemori, and S. Crotty. 2015. Cutting edge: T follicular helper cell differentiation is defective in the absence of Bcl6 BTB repressor domain function. *J Immunol* 194: 5599-5603.
60. Yu, D., S. Rao, L. M. Tsai, S. K. Lee, Y. He, E. L. Sutcliffe, M. Srivastava, M. Linterman, L. Zheng, N. Simpson, J. I. Ellyard, I. A. Parish, C. S. Ma, Q. J. Li, C. R. Parish, C. R. Mackay, and C. G. Vinuesa. 2009. The transcriptional repressor Bcl-6 directs T follicular helper cell lineage commitment. *Immunity* 31: 457-468.

61. Hou, J., U. Schindler, W. J. Henzel, S. C. Wong, and S. L. McKnight. 1995. Identification and purification of human Stat proteins activated in response to interleukin-2. *Immunity* 2: 321-329.
62. Gilmour, K. C., R. Pine, and N. C. Reich. 1995. Interleukin 2 activates STAT5 transcription factor (mammary gland factor) and specific gene expression in T lymphocytes. *Proc Natl Acad Sci U S A* 92: 10772-10776.
63. Johnston, R. J., Y. S. Choi, J. A. Diamond, J. A. Yang, and S. Crotty. 2012. STAT5 is a potent negative regulator of TFH cell differentiation. *J Exp Med* 209: 243-250.
64. DiToro, D., C. J. Winstead, D. Pham, S. Witte, R. Andargachew, J. R. Singer, C. G. Wilson, C. L. Zindl, R. J. Luther, D. J. Silberger, B. T. Weaver, E. M. Kolawole, R. J. Martinez, H. Turner, R. D. Hatton, J. J. Moon, S. S. Way, B. D. Evavold, and C. T. Weaver. 2018. Differential IL-2 expression defines developmental fates of follicular versus nonfollicular helper T cells. *Science* 361.
65. Hosken, N. A., K. Shibuya, A. W. Heath, K. M. Murphy, and A. O'Garra. 1995. The effect of antigen dose on CD4+ T helper cell phenotype development in a T cell receptor-alpha beta-transgenic model. *J Exp Med* 182: 1579-1584.
66. Allison, K. A., E. Sajti, J. G. Collier, D. Gosselin, T. D. Troutman, E. L. Stone, S. M. Hedrick, and C. K. Glass. 2016. Affinity and dose of TCR engagement yield proportional enhancer and gene activity in CD4+ T cells. *Elife* 5.
67. Moon, J. J., P. Dash, T. H. Oguin, 3rd, J. L. McClaren, H. H. Chu, P. G. Thomas, and M. K. Jenkins. 2011. Quantitative impact of thymic selection on Foxp3+ and Foxp3- subsets of self-peptide/MHC class II-specific CD4+ T cells. *Proc Natl Acad Sci U S A* 108: 14602-14607.
68. Tubo, N. J., A. J. Pagan, J. J. Taylor, R. W. Nelson, J. L. Linehan, J. M. Ertelt, E. S. Huseby, S. S. Way, and M. K. Jenkins. 2013. Single naive CD4+ T cells from a diverse repertoire produce different effector cell types during infection. *Cell* 153: 785-796.
69. van Panhuys, N., F. Klauschen, and R. N. Germain. 2014. T-cell-receptor-dependent signal intensity dominantly controls CD4(+) T cell polarization In Vivo. *Immunity* 41: 63-74.
70. Fazilleau, N., L. J. McHeyzer-Williams, H. Rosen, and M. G. McHeyzer-Williams. 2009. The function of follicular helper T cells is regulated by the strength of T cell antigen receptor binding. *Nat Immunol* 10: 375-384.
71. Keck, S., M. Schmaler, S. Ganter, L. Wyss, S. Oberle, E. S. Huseby, D. Zehn, and C. G. King. 2014. Antigen affinity and antigen dose exert distinct influences on CD4 T-cell differentiation. *Proc Natl Acad Sci U S A* 111: 14852-14857.
72. Snook, J. P., C. Kim, and M. A. Williams. 2018. TCR signal strength controls the differentiation of CD4(+) effector and memory T cells. *Sci Immunol* 3.
73. Malek, T. R., and I. Castro. 2010. Interleukin-2 receptor signaling: at the interface between tolerance and immunity. *Immunity* 33: 153-165.
74. Latinis, K. M., L. L. Carr, E. J. Peterson, L. A. Norian, S. L. Eliason, and G. A. Koretzky. 1997. Regulation of CD95 (Fas) ligand expression by TCR-mediated signaling events. *J Immunol* 158: 4602-4611.
75. Russell, J. H., and T. J. Ley. 2002. Lymphocyte-mediated cytotoxicity. *Annu Rev Immunol* 20: 323-370.
76. Billings, P., S. Burakoff, M. E. Dorf, and B. Benacerraf. 1977. Cytotoxic T lymphocytes specific for I region determinants do not require interactions with H-2K or D gene products. *J Exp Med* 145: 1387-1392.

77. Wilkinson, T. M., C. K. Li, C. S. Chui, A. K. Huang, M. Perkins, J. C. Liebner, R. Lambkin-Williams, A. Gilbert, J. Oxford, B. Nicholas, K. J. Staples, T. Dong, D. C. Douek, A. J. McMichael, and X. N. Xu. 2012. Preexisting influenza-specific CD4+ T cells correlate with disease protection against influenza challenge in humans. *Nat Med* 18: 274-280.
78. Curran, M. A., T. L. Geiger, W. Montalvo, M. Kim, S. L. Reiner, A. Al-Shamkhani, J. C. Sun, and J. P. Allison. 2013. Systemic 4-1BB activation induces a novel T cell phenotype driven by high expression of Eomesodermin. *J Exp Med* 210: 743-755.
79. Silva, C. L., and D. B. Lowrie. 2000. Identification and characterization of murine cytotoxic T cells that kill Mycobacterium tuberculosis. *Infect Immun* 68: 3269-3274.
80. Martirosyan, A., K. Von Bargen, V. Arce Gorvel, W. Zhao, S. Hanniffy, J. Bonnardel, S. Meresse, and J. P. Gorvel. 2013. In vivo identification and characterization of CD4(+) cytotoxic T cells induced by virulent Brucella abortus infection. *PLoS One* 8: e82508.
81. Brown, D. M., S. Lee, L. Garcia-Hernandez Mde, and S. L. Swain. 2012. Multifunctional CD4 cells expressing gamma interferon and perforin mediate protection against lethal influenza virus infection. *J Virol* 86: 6792-6803.
82. Qui, H. Z., A. T. Hagymasi, S. Bandyopadhyay, M. C. St Rose, R. Ramanarasimhaiah, A. Menoret, R. S. Mittler, S. M. Gordon, S. L. Reiner, A. T. Vella, and A. J. Adler. 2011. CD134 plus CD137 dual costimulation induces Eomesodermin in CD4 T cells to program cytotoxic Th1 differentiation. *J Immunol* 187: 3555-3564.
83. Soghoian, D. Z., H. Jessen, M. Flanders, K. Sierra-Davidson, S. Cutler, T. Pertel, S. Ranasinghe, M. Lindqvist, I. Davis, K. Lane, J. Rychert, E. S. Rosenberg, A. Piechocka-Trocha, A. L. Brass, J. M. Brenchley, B. D. Walker, and H. Streeck. 2012. HIV-specific cytolytic CD4 T cell responses during acute HIV infection predict disease outcome. *Sci Transl Med* 4: 123ra125.
84. Reis, B. S., A. Rogoz, F. A. Costa-Pinto, I. Taniuchi, and D. Mucida. 2013. Mutual expression of the transcription factors Runx3 and ThPOK regulates intestinal CD4(+) T cell immunity. *Nat Immunol* 14: 271-280.
85. Pearce, E. L., A. C. Mullen, G. A. Martins, C. M. Krawczyk, A. S. Hutchins, V. P. Zediak, M. Banica, C. B. DiCioccio, D. A. Gross, C. A. Mao, H. Shen, N. Cereb, S. Y. Yang, T. Lindsten, J. Rossant, C. A. Hunter, and S. L. Reiner. 2003. Control of effector CD8+ T cell function by the transcription factor Eomesodermin. *Science* 302: 1041-1043.
86. Eshima, K., S. Chiba, H. Suzuki, K. Kokubo, H. Kobayashi, M. Iizuka, K. Iwabuchi, and N. Shinohara. 2012. Ectopic expression of a T-box transcription factor, eomesodermin, renders CD4(+) Th cells cytotoxic by activating both perforin- and FasL-pathways. *Immunol Lett* 144: 7-15.
87. Lindquist, R. L., G. Shakhar, D. Dudziak, H. Wardemann, T. Eisenreich, M. L. Dustin, and M. C. Nussenzweig. 2004. Visualizing dendritic cell networks in vivo. *Nat Immunol* 5: 1243-1250.
88. Schaefer, B. C., M. L. Schaefer, J. W. Kappler, P. Marrack, and R. M. Kedl. 2001. Observation of antigen-dependent CD8+ T-cell/ dendritic cell interactions in vivo. *Cell Immunol* 214: 110-122.
89. Grubin, C. E., S. Kovats, P. deRoos, and A. Y. Rudensky. 1997. Deficient positive selection of CD4 T cells in mice displaying altered repertoires of MHC class II-bound self-peptides. *Immunity* 7: 197-208.

90. Huseby, E. S., J. White, F. Crawford, T. Vass, D. Becker, C. Pinilla, P. Marrack, and J. W. Kappler. 2005. How the T cell repertoire becomes peptide and MHC specific. *Cell* 122: 247-260.
91. Ertelt, J. M., J. H. Rowe, T. M. Johanns, J. C. Lai, J. B. McLachlan, and S. S. Way. 2009. Selective priming and expansion of antigen-specific Foxp3- CD4+ T cells during Listeria monocytogenes infection. *J Immunol* 182: 3032-3038.
92. Heaton, N. S., D. Sachs, C. J. Chen, R. Hai, and P. Palese. 2013. Genome-wide mutagenesis of influenza virus reveals unique plasticity of the hemagglutinin and NS1 proteins. *Proc Natl Acad Sci U S A* 110: 20248-20253.
93. Waring, B. M., L. E. Sjaastad, J. K. Fiege, E. J. Fay, I. Reyes, B. Moriarity, and R. A. Langlois. 2018. MicroRNA-Based Attenuation of Influenza Virus across Susceptible Hosts. *J Virol* 92.
94. Moon, J. J., H. H. Chu, J. Hataye, A. J. Pagan, M. Pepper, J. B. McLachlan, T. Zell, and M. K. Jenkins. 2009. Tracking epitope-specific T cells. *Nat Protoc* 4: 565-581.
95. Pepper, M., A. J. Pagan, B. Z. Igyarto, J. J. Taylor, and M. K. Jenkins. 2011. Opposing signals from the Bcl6 transcription factor and the interleukin-2 receptor generate T helper 1 central and effector memory cells. *Immunity* 35: 583-595.
96. Mitchell, J. S., B. J. Burbach, R. Srivastava, B. T. Fife, and Y. Shimizu. 2013. Multistage T cell-dendritic cell interactions control optimal CD4 T cell activation through the ADAP-SKAP55-signaling module. *J Immunol* 191: 2372-2383.
97. Moon, J. J., H. H. Chu, M. Pepper, S. J. McSorley, S. C. Jameson, R. M. Kedl, and M. K. Jenkins. 2007. Naive CD4(+) T cell frequency varies for different epitopes and predicts repertoire diversity and response magnitude. *Immunity* 27: 203-213.
98. Ye, J., G. Coulouris, I. Zaretskaya, I. Cutcutache, S. Rozen, and T. L. Madden. 2012. Primer-BLAST: a tool to design target-specific primers for polymerase chain reaction. *BMC Bioinformatics* 13: 134.
99. Schmittgen, T. D., and K. J. Livak. 2008. Analyzing real-time PCR data by the comparative C(T) method. *Nat Protoc* 3: 1101-1108.
100. Shaner, N. C., G. G. Lambert, A. Chammas, Y. Ni, P. J. Cranfill, M. A. Baird, B. R. Sell, J. R. Allen, R. N. Day, M. Israelsson, M. W. Davidson, and J. Wang. 2013. A bright monomeric green fluorescent protein derived from Branchiostoma lanceolatum. *Nat Methods* 10: 407-409.
101. Ai, H. W., K. L. Hazelwood, M. W. Davidson, and R. E. Campbell. 2008. Fluorescent protein FRET pairs for ratiometric imaging of dual biosensors. *Nat Methods* 5: 401-403.
102. Chen, R., S. Belanger, M. A. Frederick, B. Li, R. J. Johnston, N. Xiao, Y. C. Liu, S. Sharma, B. Peters, A. Rao, S. Crotty, and M. E. Pipkin. 2014. In vivo RNA interference screens identify regulators of antiviral CD4(+) and CD8(+) T cell differentiation. *Immunity* 41: 325-338.
103. Xie, K., B. Minkenberg, and Y. Yang. 2015. Boosting CRISPR/Cas9 multiplex editing capability with the endogenous tRNA-processing system. *Proc Natl Acad Sci U S A* 112: 3570-3575.
104. Xu, L., L. Zhao, Y. Gao, J. Xu, and R. Han. 2017. Empower multiplex cell and tissue-specific CRISPR-mediated gene manipulation with self-cleaving ribozymes and tRNA. *Nucleic Acids Res* 45: e28.
105. Dong, F., K. Xie, Y. Chen, Y. Yang, and Y. Mao. 2017. Polycistronic tRNA and CRISPR guide-RNA enables highly efficient multiplexed genome engineering in human cells. *Biochem Biophys Res Commun* 482: 889-895.

106. Finn, R. D., T. K. Attwood, P. C. Babbitt, A. Bateman, P. Bork, A. J. Bridge, H. Y. Chang, Z. Dosztanyi, S. El-Gebali, M. Fraser, J. Gough, D. Haft, G. L. Holliday, H. Huang, X. Huang, I. Letunic, R. Lopez, S. Lu, A. Marchler-Bauer, H. Mi, J. Mistry, D. A. Natale, M. Necci, G. Nuka, C. A. Orengo, Y. Park, S. Pesseat, D. Piovesan, S. C. Potter, N. D. Rawlings, N. Redaschi, L. Richardson, C. Rivoire, A. Sangrador-Vegas, C. Sigrist, I. Sillitoe, B. Smithers, S. Squizzato, G. Sutton, N. Thanki, P. D. Thomas, S. C. Tosatto, C. H. Wu, I. Xenarios, L. S. Yeh, S. Y. Young, and A. L. Mitchell. 2017. InterPro in 2017-beyond protein family and domain annotations. *Nucleic Acids Res* 45: D190-D199.
107. Cermak, T., S. J. Curtin, J. Gil-Humanes, R. Cegan, T. J. Y. Kono, E. Konecna, J. J. Belanto, C. G. Starker, J. W. Mathre, R. L. Greenstein, and D. F. Voytas. 2017. A Multipurpose Toolkit to Enable Advanced Genome Engineering in Plants. *Plant Cell* 29: 1196-1217.
108. Choi, Y. S., J. A. Yang, I. Yusuf, R. J. Johnston, J. Greenbaum, B. Peters, and S. Crotty. 2013. Bcl6 expressing follicular helper CD4 T cells are fate committed early and have the capacity to form memory. *J Immunol* 190: 4014-4026.
109. Garside, P., E. Ingulli, R. R. Merica, J. G. Johnson, R. J. Noelle, and M. K. Jenkins. 1998. Visualization of specific B and T lymphocyte interactions in the lymph node. *Science* 281: 96-99.
110. Reinhardt, R. L., A. Khoruts, R. Merica, T. Zell, and M. K. Jenkins. 2001. Visualizing the generation of memory CD4 T cells in the whole body. *Nature* 410: 101-105.
111. Gerner, M. Y., W. Kastenmuller, I. Ifrim, J. Kabat, and R. N. Germain. 2012. Histo-cytometry: a method for highly multiplex quantitative tissue imaging analysis applied to dendritic cell subset microanatomy in lymph nodes. *Immunity* 37: 364-376.
112. Moreau, H. D., F. Lemaitre, E. Terriac, G. Azar, M. Piel, A. M. Lennon-Dumenil, and P. Bousso. 2012. Dynamic in situ cytometry uncovers T cell receptor signaling during immunological synapses and kinapses in vivo. *Immunity* 37: 351-363.
113. Brewitz, A., S. Eickhoff, S. Dahling, T. Quast, S. Bedoui, R. A. Kroczek, C. Kurts, N. Garbi, W. Barchet, M. Iannacone, F. Klauschen, W. Kolanus, T. Kaisho, M. Colonna, R. N. Germain, and W. Kastenmuller. 2017. CD8(+) T Cells Orchestrate pDC-XCR1(+) Dendritic Cell Spatial and Functional Cooperativity to Optimize Priming. *Immunity* 46: 205-219.
114. Eickhoff, S., A. Brewitz, M. Y. Gerner, F. Klauschen, K. Komander, H. Hemmi, N. Garbi, T. Kaisho, R. N. Germain, and W. Kastenmuller. 2015. Robust Anti-viral Immunity Requires Multiple Distinct T Cell-Dendritic Cell Interactions. *Cell* 162: 1322-1337.
115. Gerner, M. Y., P. Torabi-Parizi, and R. N. Germain. 2015. Strategically localized dendritic cells promote rapid T cell responses to lymph-borne particulate antigens. *Immunity* 42: 172-185.
116. Im, S. J., M. Hashimoto, M. Y. Gerner, J. Lee, H. T. Kissick, M. C. Burger, Q. Shan, J. S. Hale, J. Lee, T. H. Nasti, A. H. Sharpe, G. J. Freeman, R. N. Germain, H. I. Nakaya, H. H. Xue, and R. Ahmed. 2016. Defining CD8+ T cells that provide the proliferative burst after PD-1 therapy. *Nature* 537: 417-421.
117. Gerner, M. Y., K. A. Casey, W. Kastenmuller, and R. N. Germain. 2017. Dendritic cell and antigen dispersal landscapes regulate T cell immunity. *J Exp Med* 214: 3105-3122.

118. Lee, Y. J., H. Wang, G. J. Starrett, V. Phuong, S. C. Jameson, and K. A. Hogquist. 2015. Tissue-Specific Distribution of iNKT Cells Impacts Their Cytokine Response. *Immunity* 43: 566-578.
119. Ruscher, R., R. L. Kummer, Y. J. Lee, S. C. Jameson, and K. A. Hogquist. 2017. CD8alphaalpha intraepithelial lymphocytes arise from two main thymic precursors. *Nat Immunol* 18: 771-779.
120. Gao, X., Y. Cui, R. M. Levenson, L. W. Chung, and S. Nie. 2004. In vivo cancer targeting and imaging with semiconductor quantum dots. *Nat Biotechnol* 22: 969-976.
121. Pengo, T., A. Munoz-Barrutia, I. Zudaire, and C. Ortiz-de-Solorzano. 2013. Efficient blind spectral unmixing of fluorescently labeled samples using multi-layer non-negative matrix factorization. *PLoS One* 8: e78504.
122. Jung, S., D. Unutmaz, P. Wong, G. Sano, K. De los Santos, T. Sparwasser, S. Wu, S. Vuthoori, K. Ko, F. Zavala, E. G. Pamer, D. R. Littman, and R. A. Lang. 2002. In vivo depletion of CD11c+ dendritic cells abrogates priming of CD8+ T cells by exogenous cell-associated antigens. *Immunity* 17: 211-220.
123. Zack, G. W., W. E. Rogers, and S. A. Latt. 1977. Automatic measurement of sister chromatid exchange frequency. *J Histochem Cytochem* 25: 741-753.
124. Li, W., R. N. Germain, and M. Y. Gerner. 2017. Multiplex, quantitative cellular analysis in large tissue volumes with clearing-enhanced 3D microscopy (Ce3D). *Proc Natl Acad Sci U S A* 114: E7321-E7330.
125. Coutu, D. L., K. D. Kokkaliaris, L. Kunz, and T. Schroeder. 2018. Multicolor quantitative confocal imaging cytometry. *Nat Methods* 15: 39-46.
126. Loschko, J., H. A. Schreiber, G. J. Rieke, D. Esterhazy, M. M. Meredith, V. A. Pedicord, K. H. Yao, S. Caballero, E. G. Pamer, D. Mucida, and M. C. Nussenzweig. 2016. Absence of MHC class II on cDCs results in microbial-dependent intestinal inflammation. *J Exp Med* 213: 517-534.
127. Heath, W. R., and F. R. Carbone. 2009. Dendritic cell subsets in primary and secondary T cell responses at body surfaces. *Nat Immunol* 10: 1237-1244.
128. Mempel, T. R., S. E. Henrickson, and U. H. Von Andrian. 2004. T-cell priming by dendritic cells in lymph nodes occurs in three distinct phases. *Nature* 427: 154-159.
129. Katzman, S. D., W. E. O'Gorman, A. V. Villarino, E. Gallo, R. S. Friedman, M. F. Krummel, G. P. Nolan, and A. K. Abbas. 2010. Duration of antigen receptor signaling determines T-cell tolerance or activation. *Proc Natl Acad Sci U S A* 107: 18085-18090.
130. Hildner, K., B. T. Edelson, W. E. Purtha, M. Diamond, H. Matsushita, M. Kohyama, B. Calderon, B. U. Schraml, E. R. Unanue, M. S. Diamond, R. D. Schreiber, T. L. Murphy, and K. M. Murphy. 2008. Batf3 deficiency reveals a critical role for CD8alpha+ dendritic cells in cytotoxic T cell immunity. *Science* 322: 1097-1100.
131. Persson, E. K., H. Uronen-Hansson, M. Semmrich, A. Rivollier, K. Hagerbrand, J. Marsal, S. Gudjonsson, U. Hakansson, B. Reizis, K. Kotarsky, and W. W. Agace. 2013. IRF4 transcription-factor-dependent CD103(+)CD11b(+) dendritic cells drive mucosal T helper 17 cell differentiation. *Immunity* 38: 958-969.
132. Schlitzer, A., N. McGovern, P. Teo, T. Zelante, K. Atarashi, D. Low, A. W. Ho, P. See, A. Shin, P. S. Wasan, G. Hoeffel, B. Malleret, A. Heiseke, S. Chew, L. Jardine, H. A. Purvis, C. M. Hilkens, J. Tam, M. Poidinger, E. R. Stanley, A. B. Krug, L. Renia, B. Sivasankar, L. G. Ng, M. Collin, P. Ricciardi-Castagnoli, K. Honda, M. Haniffa, and F. Ginhoux. 2013. IRF4 transcription factor-dependent

CD11b+ dendritic cells in human and mouse control mucosal IL-17 cytokine responses. *Immunity* 38: 970-983.
133. Mestas, J., and C. C. Hughes. 2004. Of mice and not men: differences between mouse and human immunology. *J Immunol* 172: 2731-2738.
134. Mebius, R. E., and G. Kraal. 2005. Structure and function of the spleen. *Nat Rev Immunol* 5: 606-616.
135. Kohyama, M., W. Ise, B. T. Edelson, P. R. Wilker, K. Hildner, C. Mejia, W. A. Frazier, T. L. Murphy, and K. M. Murphy. 2009. Role for Spi-C in the development of red pulp macrophages and splenic iron homeostasis. *Nature* 457: 318-321.
136. Cyster, J. G., S. B. Hartley, and C. C. Goodnow. 1994. Competition for follicular niches excludes self-reactive cells from the recirculating B-cell repertoire. *Nature* 371: 389-395.
137. Austyn, J. M., and S. Gordon. 1981. F4/80, a monoclonal antibody directed specifically against the mouse macrophage. *Eur J Immunol* 11: 805-815.
138. Coffman, R. L., and I. L. Weissman. 1981. B220: a B cell-specific member of th T200 glycoprotein family. *Nature* 289: 681-683.
139. Coffman, R. L., and I. L. Weissman. 1981. A monoclonal antibody that recognizes B cells and B cell precursors in mice. *J Exp Med* 153: 269-279.
140. Bonecchi, R., G. Bianchi, P. P. Bordignon, D. D'Ambrosio, R. Lang, A. Borsatti, S. Sozzani, P. Allavena, P. A. Gray, A. Mantovani, and F. Sinigaglia. 1998. Differential expression of chemokine receptors and chemotactic responsiveness of type 1 T helper cells (Th1s) and Th2s. *J Exp Med* 187: 129-134.
141. Sallusto, F., D. Lenig, C. R. Mackay, and A. Lanzavecchia. 1998. Flexible programs of chemokine receptor expression on human polarized T helper 1 and 2 lymphocytes. *J Exp Med* 187: 875-883.
142. Ansel, K. M., L. J. McHeyzer-Williams, V. N. Ngo, M. G. McHeyzer-Williams, and J. G. Cyster. 1999. In vivo-activated CD4 T cells upregulate CXC chemokine receptor 5 and reprogram their response to lymphoid chemokines. *J Exp Med* 190: 1123-1134.
143. Shulman, Z., A. D. Gitlin, S. Targ, M. Jankovic, G. Pasqual, M. C. Nussenzweig, and G. D. Victora. 2013. T follicular helper cell dynamics in germinal centers. *Science* 341: 673-677.
144. Govern, C. C., M. K. Paczosa, A. K. Chakraborty, and E. S. Huseby. 2010. Fast on-rates allow short dwell time ligands to activate T cells. *Proc Natl Acad Sci U S A* 107: 8724-8729.
145. Cahalan, M. D., I. Parker, S. H. Wei, and M. J. Miller. 2002. Two-photon tissue imaging: seeing the immune system in a fresh light. *Nat Rev Immunol* 2: 872-880.
146. Miller, M. J., S. H. Wei, I. Parker, and M. D. Cahalan. 2002. Two-photon imaging of lymphocyte motility and antigen response in intact lymph node. *Science* 296: 1869-1873.
147. Gardner, J. M., J. J. Devoss, R. S. Friedman, D. J. Wong, Y. X. Tan, X. Zhou, K. P. Johannes, M. A. Su, H. Y. Chang, M. F. Krummel, and M. S. Anderson. 2008. Deletional tolerance mediated by extrathymic Aire-expressing cells. *Science* 321: 843-847.
148. Smith, K., F. Piccinini, T. Balassa, K. Koos, T. Danka, H. Azizpour, and P. Horvath. 2018. Phenotypic Image Analysis Software Tools for Exploring and Understanding Big Image Data from Cell-Based Assays. *Cell Syst* 6: 636-653.

149. Carpenter, A. E., T. R. Jones, M. R. Lamprecht, C. Clarke, I. H. Kang, O. Friman, D. A. Guertin, J. H. Chang, R. A. Lindquist, J. Moffat, P. Golland, and D. M. Sabatini. 2006. CellProfiler: image analysis software for identifying and quantifying cell phenotypes. *Genome Biol* 7: R100.
150. Dao, D., A. N. Fraser, J. Hung, V. Ljosa, S. Singh, and A. E. Carpenter. 2016. CellProfiler Analyst: interactive data exploration, analysis and classification of large biological image sets. *Bioinformatics* 32: 3210-3212.
151. Sommer, C. S., C. ; Köthe, U.; Hamprecht, F. A. 2011. ilastik: Interactive Learning and Segmentation Toolkit. *IEEE International Symposium on Biomedical Imaging: From Nano to Macro*: pp. 230-233.
152. Bürglin, T. R. H., J. 2017. FACSanadu: Graphical user interface for rapid visualization and quantification of flow cytometry data. *bioRxiv*.
153. van Panhuys, N. 2016. TCR Signal Strength Alters T-DC Activation and Interaction Times and Directs the Outcome of Differentiation. *Front Immunol* 7: 6.
154. Meredith, M. M., K. Liu, G. Darrasse-Jeze, A. O. Kamphorst, H. A. Schreiber, P. Guermonprez, J. Idoyaga, C. Cheong, K. H. Yao, R. E. Niec, and M. C. Nussenzweig. 2012. Expression of the zinc finger transcription factor zDC (Zbtb46, Btbd4) defines the classical dendritic cell lineage. *J Exp Med* 209: 1153-1165.
155. Krishnamoorthy, V., S. Kannanganat, M. Maienschein-Cline, S. L. Cook, J. Chen, N. Bahroos, E. Sievert, E. Corse, A. Chong, and R. Sciammas. 2017. The IRF4 Gene Regulatory Module Functions as a Read-Write Integrator to Dynamically Coordinate T Helper Cell Fate. *Immunity* 47: 481-497 e487.
156. Choi, Y. S., R. Kageyama, D. Eto, T. C. Escobar, R. J. Johnston, L. Monticelli, C. Lao, and S. Crotty. 2011. ICOS receptor instructs T follicular helper cell versus effector cell differentiation via induction of the transcriptional repressor Bcl6. *Immunity* 34: 932-946.
157. Tkach, K. E., D. Barik, G. Voisinne, N. Malandro, M. M. Hathorn, J. W. Cotari, R. Vogel, T. Merghoub, J. Wolchok, O. Krichevsky, and G. Altan-Bonnet. 2014. T cells translate individual, quantal activation into collective, analog cytokine responses via time-integrated feedbacks. *Elife* 3: e01944.
158. Voisinne, G., B. G. Nixon, A. Melbinger, G. Gasteiger, M. Vergassola, and G. Altan-Bonnet. 2015. T Cells Integrate Local and Global Cues to Discriminate between Structurally Similar Antigens. *Cell Rep* 11: 1208-1219.
159. Ballesteros-Tato, A., B. Leon, B. A. Graf, A. Moquin, P. S. Adams, F. E. Lund, and T. D. Randall. 2012. Interleukin-2 inhibits germinal center formation by limiting T follicular helper cell differentiation. *Immunity* 36: 847-856.
160. Briseno, C. G., A. T. Satpathy, J. T. t. Davidson, S. T. Ferris, V. Durai, P. Bagadia, K. W. O'Connor, D. J. Theisen, T. L. Murphy, and K. M. Murphy. 2018. Notch2-dependent DC2s mediate splenic germinal center responses. *Proc Natl Acad Sci U S A*.
161. Kearney, E. R., K. A. Pape, D. Y. Loh, and M. K. Jenkins. 1994. Visualization of peptide-specific T cell immunity and peripheral tolerance induction in vivo. *Immunity* 1: 327-339.
162. Breitfeld, D., L. Ohl, E. Kremmer, J. Ellwart, F. Sallusto, M. Lipp, and R. Forster. 2000. Follicular B helper T cells express CXC chemokine receptor 5, localize to B cell follicles, and support immunoglobulin production. *J Exp Med* 192: 1545-1552.
163. Forster, R., T. Emrich, E. Kremmer, and M. Lipp. 1994. Expression of the G-protein--coupled receptor BLR1 defines mature, recirculating B cells and a subset of T-helper memory cells. *Blood* 84: 830-840.

164. Schaerli, P., K. Willimann, A. B. Lang, M. Lipp, P. Loetscher, and B. Moser. 2000. CXC chemokine receptor 5 expression defines follicular homing T cells with B cell helper function. *J Exp Med* 192: 1553-1562.
165. Bachem, A., E. Hartung, S. Guttler, A. Mora, X. Zhou, A. Hegemann, M. Plantinga, E. Mazzini, P. Stoitzner, S. Gurka, V. Henn, H. W. Mages, and R. A. Kroczek. 2012. Expression of XCR1 Characterizes the Batf3-Dependent Lineage of Dendritic Cells Capable of Antigen Cross-Presentation. *Front Immunol* 3: 214.
166. Tussiwand, R., W. L. Lee, T. L. Murphy, M. Mashayekhi, W. Kc, J. C. Albring, A. T. Satpathy, J. A. Rotondo, B. T. Edelson, N. M. Kretzer, X. Wu, L. A. Weiss, E. Glasmacher, P. Li, W. Liao, M. Behnke, S. S. Lam, C. T. Aurthur, W. J. Leonard, H. Singh, C. L. Stallings, L. D. Sibley, R. D. Schreiber, and K. M. Murphy. 2012. Compensatory dendritic cell development mediated by BATF-IRF interactions. *Nature* 490: 502-507.
167. Li, J., E. Lu, T. Yi, and J. G. Cyster. 2016. EBI2 augments Tfh cell fate by promoting interaction with IL-2-quenching dendritic cells. *Nature* 533: 110-114.
168. Krishnaswamy, J. K., U. Gowthaman, B. Zhang, J. Mattsson, L. Szeponik, D. Liu, R. Wu, T. White, S. Calabro, L. Xu, M. A. Collet, M. Yurieva, S. Alsen, P. Fogelstrand, A. Walter, W. R. Heath, S. N. Mueller, U. Yrlid, A. Williams, and S. C. Eisenbarth. 2017. Migratory CD11b(+) conventional dendritic cells induce T follicular helper cell-dependent antibody responses. *Sci Immunol* 2.
169. Brustle, A., S. Heink, M. Huber, C. Rosenplanter, C. Stadelmann, P. Yu, E. Arpaia, T. W. Mak, T. Kamradt, and M. Lohoff. 2007. The development of inflammatory T(H)-17 cells requires interferon-regulatory factor 4. *Nat Immunol* 8: 958-966.
170. Huber, M., A. Brustle, K. Reinhard, A. Guralnik, G. Walter, A. Mahiny, E. von Low, and M. Lohoff. 2008. IRF4 is essential for IL-21-mediated induction, amplification, and stabilization of the Th17 phenotype. *Proc Natl Acad Sci U S A* 105: 20846-20851.
171. Man, K., M. Miasari, W. Shi, A. Xin, D. C. Henstridge, S. Preston, M. Pellegrini, G. T. Belz, G. K. Smyth, M. A. Febbraio, S. L. Nutt, and A. Kallies. 2013. The transcription factor IRF4 is essential for TCR affinity-mediated metabolic programming and clonal expansion of T cells. *Nat Immunol* 14: 1155-1165.
172. Mahnke, J., V. Schumacher, S. Ahrens, N. Kading, L. M. Feldhoff, M. Huber, J. Rupp, F. Raczkowski, and H. W. Mittrucker. 2016. Interferon Regulatory Factor 4 controls TH1 cell effector function and metabolism. *Sci Rep* 6: 35521.
173. Fassett, M. S., W. Jiang, A. M. D'Alise, D. Mathis, and C. Benoist. 2012. Nuclear receptor Nr4a1 modulates both regulatory T-cell (Treg) differentiation and clonal deletion. *Proc Natl Acad Sci U S A* 109: 3891-3896.
174. Caton, A. J., E. Kropf, D. M. Simons, M. Aitken, K. A. Weissler, and M. S. Jordan. 2014. Strength of TCR signal from self-peptide modulates autoreactive thymocyte deletion and Foxp3(+) Treg-cell formation. *Eur J Immunol* 44: 785-793.
175. Hondowicz, B. D., D. An, J. M. Schenkel, K. S. Kim, H. R. Steach, A. T. Krishnamurty, G. J. Keitany, E. N. Garza, K. A. Fraser, J. J. Moon, W. A. Altemeier, D. Masopust, and M. Pepper. 2016. Interleukin-2-Dependent Allergen-Specific Tissue-Resident Memory Cells Drive Asthma. *Immunity* 44: 155-166.
176. Zhu, J., J. Cote-Sierra, L. Guo, and W. E. Paul. 2003. Stat5 activation plays a critical role in Th2 differentiation. *Immunity* 19: 739-748.

177. Cote-Sierra, J., G. Foucras, L. Guo, L. Chiodetti, H. A. Young, J. Hu-Li, J. Zhu, and W. E. Paul. 2004. Interleukin 2 plays a central role in Th2 differentiation. *Proc Natl Acad Sci U S A* 101: 3880-3885.
178. Liao, W., D. E. Schones, J. Oh, Y. Cui, K. Cui, T. Y. Roh, K. Zhao, and W. J. Leonard. 2008. Priming for T helper type 2 differentiation by interleukin 2-mediated induction of interleukin 4 receptor alpha-chain expression. *Nat Immunol* 9: 1288-1296.
179. Tao, Y., P. Fang, S. Kim, M. Guo, N. L. Young, and A. G. Marshall. 2017. Mapping the contact surfaces in the Lamin A:AIMP3 complex by hydrogen/deuterium exchange FT-ICR mass spectrometry. *PLoS One* 12: e0181869.
180. Oh, Y. S., D. G. Kim, G. Kim, E. C. Choi, B. K. Kennedy, Y. Suh, B. J. Park, and S. Kim. 2010. Downregulation of lamin A by tumor suppressor AIMP3/p18 leads to a progeroid phenotype in mice. *Aging Cell* 9: 810-822.
181. Toribio-Fernandez, R., V. Zorita, V. Rocha-Perugini, S. Iborra, G. Martinez Del Hoyo, R. Chevre, B. Dorado, D. Sancho, F. Sanchez-Madrid, V. Andres, and J. M. Gonzalez-Granado. 2018. Lamin A/C augments Th1 differentiation and response against vaccinia virus and Leishmania major. *Cell Death Dis* 9: 9.
182. Matsui-Hasumi, A., Y. Sato, A. Uto-Konomi, S. Yamashita, J. Uehori, A. Yoshimura, M. Yamashita, H. Asahara, S. Suzuki, and M. Kubo. 2017. E3 ubiquitin ligases SIAH1/2 regulate hypoxia-inducible factor-1 (HIF-1)-mediated Th17 cell differentiation. *Int Immunol* 29: 133-143.
183. Ray, J. P., M. M. Staron, J. A. Shyer, P. C. Ho, H. D. Marshall, S. M. Gray, B. J. Laidlaw, K. Araki, R. Ahmed, S. M. Kaech, and J. Craft. 2015. The Interleukin-2-mTORc1 Kinase Axis Defines the Signaling, Differentiation, and Metabolism of T Helper 1 and Follicular B Helper T Cells. *Immunity* 43: 690-702.
184. Park, B. J., J. W. Kang, S. W. Lee, S. J. Choi, Y. K. Shin, Y. H. Ahn, Y. H. Choi, D. Choi, K. S. Lee, and S. Kim. 2005. The haploinsufficient tumor suppressor p18 upregulates p53 via interactions with ATM/ATR. *Cell* 120: 209-221.
185. Bagley, J., G. Singh, and J. Iacomini. 2007. Regulation of oxidative stress responses by ataxia-telangiectasia mutated is required for T cell proliferation. *J Immunol* 178: 4757-4763.
186. Zhang, J., Y. Zhang, W. Wu, F. Wang, X. Liu, G. Shui, and C. Nie. 2017. Guanylate-binding protein 2 regulates Drp1-mediated mitochondrial fission to suppress breast cancer cell invasion. *Cell Death Dis* 8: e3151.
187. Hagenbuchner, J., A. V. Kuznetsov, P. Obexer, and M. J. Ausserlechner. 2013. BIRC5/Survivin enhances aerobic glycolysis and drug resistance by altered regulation of the mitochondrial fusion/fission machinery. *Oncogene* 32: 4748-4757.
188. Salabei, J. K., and B. G. Hill. 2013. Mitochondrial fission induced by platelet-derived growth factor regulates vascular smooth muscle cell bioenergetics and cell proliferation. *Redox Biol* 1: 542-551.
189. Guido, C., D. Whitaker-Menezes, Z. Lin, R. G. Pestell, A. Howell, T. A. Zimmers, M. C. Casimiro, S. Aquila, S. Ando, U. E. Martinez-Outschoorn, F. Sotgia, and M. P. Lisanti. 2012. Mitochondrial fission induces glycolytic reprogramming in cancer-associated myofibroblasts, driving stromal lactate production, and early tumor growth. *Oncotarget* 3: 798-810.
190. Oestreich, K. J., K. A. Read, S. E. Gilbertson, K. P. Hough, P. W. McDonald, V. Krishnamoorthy, and A. S. Weinmann. 2014. Bcl-6 directly represses the gene program of the glycolysis pathway. *Nat Immunol* 15: 957-964.

191. Topham, D. J., R. A. Tripp, and P. C. Doherty. 1997. CD8+ T cells clear influenza virus by perforin or Fas-dependent processes. *J Immunol* 159: 5197-5200.
192. Ratner, A., and W. R. Clark. 1993. Role of TNF-alpha in CD8+ cytotoxic T lymphocyte-mediated lysis. *J Immunol* 150: 4303-4314.
193. Koguchi, Y., A. C. Buenafe, T. J. Thauland, J. L. Gardell, E. R. Bivins-Smith, D. B. Jacoby, M. K. Slifka, and D. C. Parker. 2012. Preformed CD40L is stored in Th1, Th2, Th17, and T follicular helper cells as well as CD4+ 8- thymocytes and invariant NKT cells but not in Treg cells. *PLoS One* 7: e31296.
194. Koguchi, Y., T. J. Thauland, M. K. Slifka, and D. C. Parker. 2007. Preformed CD40 ligand exists in secretory lysosomes in effector and memory CD4+ T cells and is quickly expressed on the cell surface in an antigen-specific manner. *Blood* 110: 2520-2527.
195. Stout, R. D., and K. Bottomly. 1989. Antigen-specific activation of effector macrophages by IFN-gamma producing (TH1) T cell clones. Failure of IL-4-producing (TH2) T cell clones to activate effector function in macrophages. *J Immunol* 142: 760-765.
196. Heusinkveld, M., P. J. de Vos van Steenwijk, R. Goedemans, T. H. Ramwadhdoebe, A. Gorter, M. J. Welters, T. van Hall, and S. H. van der Burg. 2011. M2 macrophages induced by prostaglandin E2 and IL-6 from cervical carcinoma are switched to activated M1 macrophages by CD4+ Th1 cells. *J Immunol* 187: 1157-1165.
197. Marshall, H. D., A. Chandele, Y. W. Jung, H. Meng, A. C. Poholek, I. A. Parish, R. Rutishauser, W. Cui, S. H. Kleinstein, J. Craft, and S. M. Kaech. 2011. Differential expression of Ly6C and T-bet distinguish effector and memory Th1 CD4(+) cell properties during viral infection. *Immunity* 35: 633-646.
198. Sakai, S., K. D. Kauffman, J. M. Schenkel, C. C. McBerry, K. D. Mayer-Barber, D. Masopust, and D. L. Barber. 2014. Cutting edge: control of Mycobacterium tuberculosis infection by a subset of lung parenchyma-homing CD4 T cells. *J Immunol* 192: 2965-2969.
199. Nanki, T., T. Imai, K. Nagasaka, Y. Urasaki, Y. Nonomura, K. Taniguchi, K. Hayashida, J. Hasegawa, O. Yoshie, and N. Miyasaka. 2002. Migration of CX3CR1-positive T cells producing type 1 cytokines and cytotoxic molecules into the synovium of patients with rheumatoid arthritis. *Arthritis Rheum* 46: 2878-2883.
200. Hu, Z., M. A. Blackman, K. M. Kaye, and E. J. Usherwood. 2015. Functional heterogeneity in the CD4+ T cell response to murine gamma-herpesvirus 68. *J Immunol* 194: 2746-2756.
201. Pachnio, A., M. Ciaurriz, J. Begum, N. Lal, J. Zuo, A. Beggs, and P. Moss. 2016. Cytomegalovirus Infection Leads to Development of High Frequencies of Cytotoxic Virus-Specific CD4+ T Cells Targeted to Vascular Endothelium. *PLoS Pathog* 12: e1005832.
202. Weiskopf, D., D. J. Bangs, J. Sidney, R. V. Kolla, A. D. De Silva, A. M. de Silva, S. Crotty, B. Peters, and A. Sette. 2015. Dengue virus infection elicits highly polarized CX3CR1+ cytotoxic CD4+ T cells associated with protective immunity. *Proc Natl Acad Sci U S A* 112: E4256-4263.
203. Jellison, E. R., S. K. Kim, and R. M. Welsh. 2005. Cutting edge: MHC class II-restricted killing in vivo during viral infection. *J Immunol* 174: 614-618.
204. Quezada, S. A., T. R. Simpson, K. S. Peggs, T. Merghoub, J. Vider, X. Fan, R. Blasberg, H. Yagita, P. Muranski, P. A. Antony, N. P. Restifo, and J. P. Allison. 2010. Tumor-reactive CD4(+) T cells develop cytotoxic activity and eradicate

large established melanoma after transfer into lymphopenic hosts. *J Exp Med* 207: 637-650.
205. Fang, M., N. A. Siciliano, A. R. Hersperger, F. Roscoe, A. Hu, X. Ma, A. R. Shamsedeen, L. C. Eisenlohr, and L. J. Sigal. 2012. Perforin-dependent CD4+ T-cell cytotoxicity contributes to control a murine poxvirus infection. *Proc Natl Acad Sci U S A* 109: 9983-9988.
206. Brown, D. M., A. M. Dilzer, D. L. Meents, and S. L. Swain. 2006. CD4 T cell-mediated protection from lethal influenza: perforin and antibody-mediated mechanisms give a one-two punch. *J Immunol* 177: 2888-2898.
207. Hua, L., S. Yao, D. Pham, L. Jiang, J. Wright, D. Sawant, A. L. Dent, T. J. Braciale, M. H. Kaplan, and J. Sun. 2013. Cytokine-dependent induction of CD4+ T cells with cytotoxic potential during influenza virus infection. *J Virol* 87: 11884-11893.
208. Marshall, N. B., A. M. Vong, P. Devarajan, M. D. Brauner, Y. Kuang, R. Nayar, E. A. Schutten, C. H. Castonguay, L. J. Berg, S. L. Nutt, and S. L. Swain. 2017. NKG2C/E Marks the Unique Cytotoxic CD4 T Cell Subset, ThCTL, Generated by Influenza Infection. *J Immunol* 198: 1142-1155.
209. Rees, W., J. Bender, T. K. Teague, R. M. Kedl, F. Crawford, P. Marrack, and J. Kappler. 1999. An inverse relationship between T cell receptor affinity and antigen dose during CD4(+) T cell responses in vivo and in vitro. *Proc Natl Acad Sci U S A* 96: 9781-9786.
210. Longhi, M. P., C. Trumpfheller, J. Idoyaga, M. Caskey, I. Matos, C. Kluger, A. M. Salazar, M. Colonna, and R. M. Steinman. 2009. Dendritic cells require a systemic type I interferon response to mature and induce CD4+ Th1 immunity with poly IC as adjuvant. *J Exp Med* 206: 1589-1602.
211. Coler, R. N., T. Hudson, S. Hughes, P. W. Huang, E. A. Beebe, and M. T. Orr. 2015. Vaccination Produces CD4 T Cells with a Novel CD154-CD40-Dependent Cytolytic Mechanism. *J Immunol* 195: 3190-3197.
212. Kayagaki, N., N. Yamaguchi, M. Nakayama, A. Kawasaki, H. Akiba, K. Okumura, and H. Yagita. 1999. Involvement of TNF-related apoptosis-inducing ligand in human CD4+ T cell-mediated cytotoxicity. *J Immunol* 162: 2639-2647.
213. Gromkowski, S. H., J. Yagi, and C. A. Janeway, Jr. 1989. Elevated temperature regulates tumor necrosis factor-mediated immune killing. *Eur J Immunol* 19: 1709-1714.
214. Stalder, T., S. Hahn, and P. Erb. 1994. Fas antigen is the major target molecule for CD4+ T cell-mediated cytotoxicity. *J Immunol* 152: 1127-1133.
215. Khattri, R., T. Cox, S. A. Yasayko, and F. Ramsdell. 2003. An essential role for Scurfin in CD4+CD25+ T regulatory cells. *Nat Immunol* 4: 337-342.
216. Szabo, S. J., B. M. Sullivan, C. Stemmann, A. R. Satoskar, B. P. Sleckman, and L. H. Glimcher. 2002. Distinct effects of T-bet in TH1 lineage commitment and IFN-gamma production in CD4 and CD8 T cells. *Science* 295: 338-342.
217. Malhotra, D., J. L. Linehan, T. Dileepan, Y. J. Lee, W. E. Purtha, J. V. Lu, R. W. Nelson, B. T. Fife, H. T. Orr, M. S. Anderson, K. A. Hogquist, and M. K. Jenkins. 2016. Tolerance is established in polyclonal CD4(+) T cells by distinct mechanisms, according to self-peptide expression patterns. *Nat Immunol* 17: 187-195.
218. McSorley, S. J., S. Asch, M. Costalonga, R. L. Reinhardt, and M. K. Jenkins. 2002. Tracking salmonella-specific CD4 T cells in vivo reveals a local mucosal response to a disseminated infection. *Immunity* 16: 365-377.

219. Zhu, J., D. Jankovic, A. J. Oler, G. Wei, S. Sharma, G. Hu, L. Guo, R. Yagi, H. Yamane, G. Punkosdy, L. Feigenbaum, K. Zhao, and W. E. Paul. 2012. The transcription factor T-bet is induced by multiple pathways and prevents an endogenous Th2 cell program during Th1 cell responses. *Immunity* 37: 660-673.
220. Acosta-Rodriguez, E. V., L. Rivino, J. Geginat, D. Jarrossay, M. Gattorno, A. Lanzavecchia, F. Sallusto, and G. Napolitani. 2007. Surface phenotype and antigenic specificity of human interleukin 17-producing T helper memory cells. *Nat Immunol* 8: 639-646.
221. Takeuchi, A., S. Badr Mel, K. Miyauchi, C. Ishihara, R. Onishi, Z. Guo, Y. Sasaki, H. Ike, A. Takumi, N. M. Tsuji, Y. Murakami, T. Katakai, M. Kubo, and T. Saito. 2016. CRTAM determines the CD4+ cytotoxic T lymphocyte lineage. *J Exp Med* 213: 123-138.
222. Mucida, D., M. M. Husain, S. Muroi, F. van Wijk, R. Shinnakasu, Y. Naoe, B. S. Reis, Y. Huang, F. Lambolez, M. Docherty, A. Attinger, J. W. Shui, G. Kim, C. J. Lena, S. Sakaguchi, C. Miyamoto, P. Wang, K. Atarashi, Y. Park, T. Nakayama, K. Honda, W. Ellmeier, M. Kronenberg, I. Taniuchi, and H. Cheroutre. 2013. Transcriptional reprogramming of mature CD4(+) helper T cells generates distinct MHC class II-restricted cytotoxic T lymphocytes. *Nat Immunol* 14: 281-289.
223. Mutis, T., Y. E. Cornelisse, and T. H. Ottenhoff. 1993. Mycobacteria induce CD4+ T cells that are cytotoxic and display Th1-like cytokine secretion profile: heterogeneity in cytotoxic activity and cytokine secretion levels. *Eur J Immunol* 23: 2189-2195.
224. Vignaux, F., E. Vivier, B. Malissen, V. Depraetere, S. Nagata, and P. Golstein. 1995. TCR/CD3 coupling to Fas-based cytotoxicity. *J Exp Med* 181: 781-786.
225. Armitage, R. J., W. C. Fanslow, L. Strockbine, T. A. Sato, K. N. Clifford, B. M. Macduff, D. M. Anderson, S. D. Gimpel, T. Davis-Smith, C. R. Maliszewski, and et al. 1992. Molecular and biological characterization of a murine ligand for CD40. *Nature* 357: 80-82.
226. Jaiswal, A. I., C. Dubey, S. L. Swain, and M. Croft. 1996. Regulation of CD40 ligand expression on naive CD4 T cells: a role for TCR but not co-stimulatory signals. *Int Immunol* 8: 275-285.
227. Rathmell, J. C., S. E. Townsend, J. C. Xu, R. A. Flavell, and C. C. Goodnow. 1996. Expansion or elimination of B cells in vivo: dual roles for CD40- and Fas (CD95)-ligands modulated by the B cell antigen receptor. *Cell* 87: 319-329.
228. Stranges, P. B., J. Watson, C. J. Cooper, C. M. Choisy-Rossi, A. C. Stonebraker, R. A. Beighton, H. Hartig, J. P. Sundberg, S. Servick, G. Kaufmann, P. J. Fink, and A. V. Chervonsky. 2007. Elimination of antigen-presenting cells and autoreactive T cells by Fas contributes to prevention of autoimmunity. *Immunity* 26: 629-641.
229. Acosta-Rodriguez, E. V., A. Craxton, D. W. Hendricks, M. C. Merino, C. L. Montes, E. A. Clark, and A. Gruppi. 2007. BAFF and LPS cooperate to induce B cells to become susceptible to CD95/Fas-mediated cell death. *Eur J Immunol* 37: 990-1000.
230. Rothstein, T. L., J. K. Wang, D. J. Panka, L. C. Foote, Z. Wang, B. Stanger, H. Cui, S. T. Ju, and A. Marshak-Rothstein. 1995. Protection against Fas-dependent Th1-mediated apoptosis by antigen receptor engagement in B cells. *Nature* 374: 163-165.
231. Verma, S., D. Weiskopf, A. Gupta, B. McDonald, B. Peters, A. Sette, and C. A. Benedict. 2015. Cytomegalovirus-Specific CD4 T Cells Are Cytolytic and Mediate Vaccine Protection. *J Virol* 90: 650-658.

232. Slutter, B., L. L. Pewe, S. M. Kaech, and J. T. Harty. 2013. Lung airway-surveilling CXCR3(hi) memory CD8(+) T cells are critical for protection against influenza A virus. *Immunity* 39: 939-948.
233. Matloubian, M., R. J. Concepcion, and R. Ahmed. 1994. CD4+ T cells are required to sustain CD8+ cytotoxic T-cell responses during chronic viral infection. *J Virol* 68: 8056-8063.
234. Hildemann, S. K., J. Eberlein, B. Davenport, T. T. Nguyen, F. Victorino, and D. Homann. 2013. High efficiency of antiviral CD4(+) killer T cells. *PLoS One* 8: e60420.
235. Hildeman, D., D. Yanez, K. Pederson, T. Havighurst, and D. Muller. 1997. Vaccination against persistent viral infection exacerbates CD4+ T-cell-mediated immunopathological disease. *J Virol* 71: 9672-9678.